Nanoscale Surface Modification of Ramie Fibres by Plasma Treatment for Polymer Composite Applications

By:

Sameer Falih Hamad

A thesis submitted in partial fulfilment of the requirements for the degree of Doctor of Philosophy

The University of Sheffield
Faculty of Engineering
Department of Materials Science and Engineering

Submitted October 2019

Acknowledgements

First and foremost, I would like to deeply express my thanks to my supervisor Dr. Cornelia Rodenburg for her supervision, tremendous guidance, support, kindness, motivation and encouragement throughout my PhD study. Secondly, I would like to thank Dr. Joel P. Foreman and Dr. Simon A. Hayes for their valuable feedback and valuable suggestions during the development of my project, especially with the experiments.

I would like also to express my thanks to my sponsor (Ministry of Higher Education and Scientific Research in Iraq and its representative in the UK, the Iraqi Cultural Attaché). I also grateful acknowledge the College of Engineering, University of Misan for giving me this opportunity to do my PhD study.

A big thank goes to my group mates, Rob, Quan, Alaa, Kerry, Nicola, Vikas, and Nicholas for their friendship, valuable feedback, and helpful advice throughout the las four years.

Thanks as well to my friends Noori, Haider, Mohammed, and Nassar for their friendship and support throughout the last four years.

Finally, I would like to express my gratitude and appreciation to my family (father, mother, sisters and brothers) for the encouragement, and support during my PhD study. I would like also to express my special thanks to my wife, Sura for her support, patience, care, and love. I also would like to thank my lovely daughter, Mina, who was born during my PhD study.

Abstract

Natural plant fibres have recently received a great attention as potential alternative replacement for synthetic fibres, as reinforcement of different polymer matrices for various engineering applications. This is due to their desirable properties such as low density and high specific mechanical properties, at the same time they are sustainable, renewable, and eco-friendly. However, one of the main issues that has limited the applications of plant fibres in polymer composites is their incompatibility with polymer matrices. This have resulted in poor interfacial bonding between the fibres and matrix, and consequently reduction in the mechanical properties of the composites. Therefore, surface modification of plant fibres is necessary to modify the fibre surface characteristics and to improve their surface adhesion properties. Chemical treatments are commonly used in modifying the surface characteristics of plant fibres, however, these treatments have some disadvantages such as consuming substantial volumes of liquids and chemicals as well as the treatment time could be hours and sometimes days. As an alternative, plasma treatment has attracted more attention in recent years, as it is simple, dry (solvent-free), environmentally friendly, and time-saving (reduces energy consumption). However, the efficiency of plasma surface treatments depend on several factors such as the nature of the substrate and the plasma operating conditions, that could affect the fibre main properties.

Therefore, in this study, plasma treatment as a prospective tool for simple and efficient fibre surface modification was used with the goal of improving the surface adhesion properties of ramie plant fibres without adversely affecting the fibre mechanical properties. The results reveal nanostructures at the fibre surface including microfibrils and elementary fibrils after plasma treatment, and their importance for fibre surface wettability, fibre-thermoset polymer interlocking, and fibre mechanical properties. All these peak at short treatment times. In addition, the problem of lack of adhesion between natural plant fibres and polymer matrices

can be minimised if phenolic thermoset resin is used as a matrix for plant fibres. This is because some degree of interaction is expected to exist between the hydrophilic natural fibres and polar hydroxyl groups present in the structure of phenolic resins. However, the presence of microvoids in the structure of cured phenolic resins adversely affect the mechanical properties. The conventional approach to overcome this challenge and to produce void free structure is via utilising long heating cure cycles (3-4 days), which is not favourable for most industries due to time and energy consumption issues. Therefore, in this study, the tailoring of void size and distribution in the phenolic resins was introduced as an alternative approach to achieve a better balance between processing time and mechanical properties. For this purpose, two different catalysts (slow and fast action acid catalysts) and a short cure cycle (4 hrs) were used to alter the void size and distributions in the structure of phenolic resins. Long heat cure cycle (4 days) was also used to obtain void free phenolic structure without the addition of any catalyst and used as a reference sample in terms of flexural properties. The flexural fractured surfaces of all materials were investigated using low voltage scanning electron microscopy (LV-SEM), Fourier-transform infrared spectroscopy (FTIR). Results are compared to finite element modelling that confirmed the effects of different void size and distributions on the mechanical properties.

Finally, the effects of plasma treatment and cure cycle conditions on the properties of random short ramie fibres reinforced phenolic composites were investigated. A new method for making mats of short fibres was developed and used for the fabrication of composites containing plasma treated fibres. The results indicated clear effects for the plasma treatment and cure cycle conditions on the fibre-matrix interfacial bonding, and consequently the flexural properties of the composites.

Publications

[1] S. F. Hamad, N. Stehling, C. Holland, J. P. Foreman, and C. Rodenburg, "Low-Voltage SEM of Natural Plant Fibers: Microstructure Properties (Surface and Cross-Section) and their Link to the Tensile Properties," in *Procedia Engineering*, vol. 200, 2017. **Published.**

[2] S. F. Hamad, N. Stehling, S. A. Hayes, J. P. Foreman, and C. Rodenburg, "Exploiting Plasma Exposed, Natural Surface Nanostructures in Ramie Fibers for Polymer Composite Applications," *Materials*, vol. 12, pp. 1–15, 2019. **Published.**

[3] S. F. Hamad, N. Farr, T. Fei, N. F. Shukor, J. S. Dean, S. A. Hayes, J. P. Foreman, and C. Rodenburg, "Optimizing size and distribution of voids in phenolic resins through the choice of catalyst types," *J. Appl. Polym. Sci.*, vol. 48249, pp. 1–10, 2019. **Published.**

[4] S. F. Hamad, T. Fei, S. A. Hayes, J.P. Foreman, and C. Rodenburg, "Interfacial bonding between ramie fibres and phenolic resins: effects of plasma treatment and cure cycle,". *Polymer composites*. **Under review, October 2019.**

Conference Presentations

1. Sheffield Doctoral Academy Conference, Sheffield, UK, June 2016.
   Natural Fibres Reinforced Polymer Composites **(Poster presentation).**
2. ICNF 2017: the 3rd International Conference on Natural Fibres (ICNF), Braga, Portugal, June 2017.
   Low-Voltage SEM of natural plant fbres: Microstructure Properties (Surface and cross section) and their link to the tensile properties **(Oral presentation).**
3. N.I.C.E. 2018: the 4th International Conference on Bioinspired and Biobased Chemistry & Materials (Symposium on Plasma and Laser Processing of Bioinspired and Biobased Materials (PLASMAT 2018), Nice, France, October 2018.
   Low Voltage-SEM insights into Nanoscale Surface Modification of Ramie Plant Fibers by Plasma Treatment **(Oral presentation).**

Award

Best oral communication in the Symposium of Plasma and Laser Processing of Bioinspired and Biobased Materials (PLASMAT 2018), Nice, France, October 2018.

Table of Contents

List of Figures

List of Tables

Chapter 1: Introduction

Fibres reinforced polymer composites represent an interesting group of engineering materials due to their unique characteristics such as high strength to weight ratio, high fracture toughness, non-corrosive property, electrical resistance, and fire resistance, as well as their flexibility in design and ease of fabrication [1]–[3]. Composite materials reinforced by high strength synthetic fibres such as carbon, aramid, and glass fibres are widely used in various applications including automotive parts, aerospace structures, sporting goods, and building materials [4]–[6]. However, these materials have serious drawbacks such as no-recyclability, health hazards, high density, high energy consumption and environmental issues [3][6]. Therefore, the research in fibre-composite materials has recently been directed at using environmentally friendly materials instead of synthetic fibres [7]–[9]. Natural plant fibres are eco-friendly, renewable, biodegradable, lightweight, strong, and cheap. Therefore, they are increasingly attracting more attention in recent years as a viable alternative to synthetic fibres [6][10][11].

Natural plant fibres such as ramie, flax, jute, hemp, and sisal are the most commonly used fibres in the field of natural fibre-polymer composites because of their wide availability, low cost, low density as well as their high specific mechanical properties [12]–[14]. However, these fibres are characterised by the complex cell wall structure and organisation, with semi-crystalline cellulose microfibrils embedded in an amorphous matrix of lignin and hemicellulose [15][16]. Therefore, one of the issues of these fibres is the large scatter of their mechanical properties [17]. This is partly due to the variations of the fibre internal structure, crystal structure, fibre diameter, microfibril angles, and defects [18][19], but some of the variation in tensile properties commonly reported in the literature are likely due to inaccurate cross-sectional area measurements of single fibres [19][20]. Therefore, in chapter 4 of this thesis, the microstructure of different natural plant fibres (flax, jute, ramie, and sisal) was

investigated using low voltage scanning electron microscopy (LV-SEM) and link between the fibre microstructure and property variations was also investigated.

Among the various plant fibre, ramie fibre has unique characteristics such as the high crystallinity, commercial availability, and one of the strongest fine textile fibres [14][21][22]. Therefore, it could play a very important role as a reinforcement in polymer matrix composites [23]. Nonetheless, ramie fibres have some disadvantage such as poor wettability, incompatibility with some types of polymer matrices, and low moisture resistance [24]. However, it is possible to overcome these challenges through the surface modification of the fibres [22]. In recent years, some efficient new energy techniques have been developed in cellulose surface modification, among which plasma techniques have attracted more attention as a clean and efficient surface modification technologies [24][25].

Plasma treatment has been efficiently used to modify the surface characteristics of various polymers without affecting or changing the original bulk properties of the polymers [26]. This is due to the very limited penetration depth of plasma species. However, in the case of plant fibres and fibrils, this is not necessarily true because of the penetration depth will be much larger [22][27]. Most of the previous studies on surface modification of plant fibres have focused on using plasma treatment for the purpose of surface cleaning, modifying the fibre surface microroughness, and producing hydrophilic or hydrophobic surfaces [14][22][25][28]. Whereas, very limited studies can be found in the literature [29][30] that have exploited plasma treatment to produce nanoscale surface structures for plant fibres which can modify the fibre surface without affecting the fibre bulk properties. Therefore, in chapter 5 of this thesis, low pressure plasma treatment was exploited to expose nanoscale surface structures for ramie fibres, to roughen the fibre surface without affecting the fibre mechanical properties (strength and modulus). The link between those nanostructures and fibre mechanical properties in the case of single ramie fibres was investigated. Moreover,

the link between exposed nanostructures and surface wettability with the use of resole phenolic resin as a potential polymer matrix was also investigated.

Phenolic resins are amongst the oldest thermosetting polymer matrices which characterised by the excellent ablative properties, high chemical resistance and thermal stability as well as the low smoke density [31]–[33]. Polymer composites based on phenolic resin as a matrix yield low levels of combustion products and smoke under both smouldering and flaming fire conditions, and is superior in terms of other flammability properties compared to epoxy, polyester, and vinyl ester-based composites [34]. However, the applications of phenolic resins are still limited due to their slow crosslinking rate and high curing temperature [35]. In addition, the mechanical properties of these resins can be compromised by porosity and the process on how to control it to a desired level still poses a scientific and industrial challenge [36]. This is due to the long and complex polymerisation process together with the generation of water and formaldehyde as by-products. Void free structure of phenolic usually requires long heating cure cycles [37][38], which not only takes a long time to cure but their production is also energy-intensive. Therefore, in chapter 6 of this thesis, an investigation on how to minimise any reduction in mechanical properties as a result of implementing a short curing cycle was carried out.

Finally, short fibre reinforced polymer composites are becoming very attractive materials with many advantages including the simplicity of fabrication, economically, as well as the ability to fabricate complex structural parts due to the high ductility in all directions [39]–[41]. However, the process of mixing short fibres into the thermosetting resins has generally been based on mechanical stirring or blending, a process which has the tendency to cause fibre damage and fibre agglomeration, as well as the high possibility of forming air-bubbles [42]. To overcome this challenge, a method was reported in chapter 7 of this thesis, in which the effect of plasma treatment can also be utilised to hold the short ramie fibres together as

a mat after compacting. Furthermore, the fibre-matrix interface was optimised for the prepared composites in terms of structural and mechanical properties.

This thesis is an alternative format thesis with a permission for submission in this format. The main body of this thesis contains 4 result chapters: one conference paper (chapter 4), two journal papers (chapters 5 and 6), and one original chapter (chapter 7).

Section 1.1: References

[1] D. M. Matoke, G. M.; Owido, S.F.; Nyaanga, "Effect of Production Methods and Material Ratios on Physical Properties of the Composites," *Am. Int. J. Contemp. Res.*, vol. 2, no. 2, pp. 208–213, 2012.

[2] A. Ticoalu, T. Aravinthan, and F. Cardona, "A review of current development in natural fiber composites for structural and infrastructure applications," in *Southern Region Engineering Conference*, 2010, no. November, pp. 1–5.

[3] H. Cheung, M. Ho, K. Lau, F. Cardona, and D. Hui, "Natural fibre-reinforced composites for bioengineering and environmental engineering applications," *Compos. Part B*, vol. 40, no. 7, pp. 655–663, 2009.

[4] C. Unterweger, O. Bruggemann, and C. Furst, "Synthetic Fibers and Thermoplastic Short-Fiber-Reinforced Polymers: Properties and Characterization," *Polym. Compos.*, pp. 227–236, 2014.

[5] A. Manikandan and R. Rajkumar, "Evaluation of mechanical properties of synthetic fiber reinforced polymer composites by mixture design analysis," *Polym. Polym. Compos.*, vol. 24, no. 7, pp. 455–462, 2016.

[6] K. Begum and M. . Islam, "Natural Fiber as a substitute to Synthetic Fiber in Polymer Composites : A Review," *Res. J. Eng. Sci.*, vol. 2, no. 3, pp. 46–53, 2013.

[7] L. Mohammed, M. N. M. Ansari, G. Pua, M. Jawaid, and M. S. Islam, "A Review on Natural Fiber Reinforced Polymer Composite and Its Applications," *Int. J. ofPolymer Sci. fibers.*, pp. 1–15, 2015.

[8] S. H. Aziz and M. P. Ansell, "The effect of alkalization and fibre alignment on the

mechanical and thermal properties of kenaf and hemp bast fibre composites: Part 2 - cashew nut shell liquid matrix," *Compos. Sci. Technol.*, vol. 64, no. 9, pp. 1231–1238, 2004.

[9] U. S. Bongarde and V. D. Shinde, "Review on natural fiber reinforcement polymer composites," *Int. J. Eng. Sci. Innov. Technol.*, vol. 3, no. 2, pp. 431–436, 2014.

[10] D. N. Saheb and J. P. Jog, "Natural Fiber Polymer Composites: A Review," *J. Adv. Polym. Technol.*, vol. 18, no. 4, pp. 351–363, 1999.

[11] M. J. Mochane *et al.*, "Recent progress on natural fiber hybrid composites for advanced applications: A review," *Express Polym. Lett.*, vol. 13, no. 2, pp. 159–198, 2019.

[12] R. Lalit, P. Mayank, and K. Ankur, "Natural fibers and biopolymers characterization: A future potential composite material," *J. Mech. Eng. – Strojnícky časopis*, vol. 68, no. 1, pp. 33–50, 2018.

[13] R. Mohamad *et al.*, "Potential Use of Plant Fibres and their Composites for Biomedical Applications," *BioResources*, vol. 9, no. 3, pp. 1–19, 2014.

[14] Q. Zhang, Y. Jiang, L. Yao, Q. Jiang, and Y. Qiu, "Hydrophobic surface modification of ramie fibers by plasma-induced addition polymerization of propylene," *J. Adhes. Sci. Technol.*, vol. 29, no. 8, pp. 691–704, 2015.

[15] A. Célino, S. Fréour, F. Jacquemin, and P. Casari, "The hygroscopic behavior of plant fibers: a review," *Front. Chem.*, vol. 1, pp. 1–12, 2014.

[16] K. Oksman, A. P. Mathew, R. Långström, B. Nyström, and K. Joseph, "The influence of fibre microstructure on fibre breakage and mechanical properties of natural fibre reinforced polypropylene," *Compos. Sci. Technol.*, vol. 69, pp. 1847–1853, 2009.

[17] P. Peças, H. Carvalho, H. Salman, and M. Leite, "Natural Fibre Composites and Their Applications: A Review," *J. Compos. Sci.*, vol. 2, no. 66, pp. 1–20, 2018.

[18] R. Ahmad, R. Hamid, and S. A. Osman, "Physical and Chemical Modifications of Plant Fibres for Reinforcement in Cementitious Composites," *Adv. Civ. Eng.*, pp. 1–18, 2019.

[19] N. M. Everitt, N. T. Aboulkhair, and M. J. Clifford, “Looking for Links between Natural Fibres’ Structures and Their Physical Properties,” in *Conference Papers in Materials Science*, 2013, pp. 1–10.

[20] J. L. Thomason, J. Carruthers, J. Kelly, and G. Johnson, “Fibre cross-section determination and variability in sisal and flax and its effects on fibre performance characterisation,” *Compos. Sci. Technol.*, vol. 71, no. 7, pp. 1008–1015, 2011.

[21] Y. Tang *et al.*, “Correlation Analysis of Lignin Accumulation and Expression of Key Genes Involved in Lignin,” *Genes (Basel).*, vol. 10, no. 389, pp. 1–13, 2019.

[22] X. Liu and L. Cheng, “Influence of plasma treatment on properties of ramie fiber and the reinforced composites,” *J. Adhes. Sci. Technol.*, vol. 31, no. 15, pp. 1723–1734, 2017.

[23] G. Koronis, A. Silva, and A. P. Soares Dias, “Development of green composites reinforced with ramie fabrics: Effect of aging on mechanical properties of coated and uncoated specimens,” *Fibers Polym.*, vol. 15, no. 12, pp. 2618–2624, 2014.

[24] Y. Li, S. Manolache, Y. Qiu, and M. Sarmadi, “Effect of atmospheric pressure plasma treatment condition on adhesion of ramie fibers to polypropylene for composite,” *Appl. Surf. Sci.*, vol. 364, pp. 294–301, 2016.

[25] Y. Il Huh, M. Bismark, S. Kim, H. K. Lee, and C. Nah, “Effects of Plasma Treatment on Mechanical Properties of Jute Fibers and Their Composites with Polypropylene,” *Elastomers Compos.*, vol. 47, no. 4, pp. 310–317, 2013.

[26] S. Yoshida, K. Hagiwara, T. Hasebe, and A. Hotta, “Surface modification of polymers by plasma treatments for the enhancement of biocompatibility and controlled drug release,” *Surf. Coatings Technol.*, vol. 233, pp. 99–107, 2013.

[27] A. Vesel, M. Mozetic, S. Strnad, Z. Peršin, K. Stana-Kleinschek, and N. Hauptman, “Plasma modification of viscose textile,” *Vacuum*, vol. 84, no. 1, pp. 79–82, 2010.

[28] E. Bozaci *et al.*, “Effects of the atmospheric plasma treatments on surface and mechanical properties of flax fiber and adhesion between fiber-matrix for composite materials,” *Compos. Part B Eng.*, vol. 45, no. 1, pp. 565–572, 2013.

[29] B. Balu, V. Breedveld, and D. W. Hess, “Fabrication of ‘roll-off’ and ‘sticky’

superhydrophobic cellulose surfaces-via plasma processing," *Langmuir*, vol. 24, no. 9, pp. 4785–4790, 2008.

[30] L. Jiang, K. J. Park-Lee, R. M. Clinton, Z. Tang, V. Breedveld, and D. W. Hess, "Mechanical durability of liquid repellent coatings," *Surf. Coatings Technol.*, vol. 328, pp. 182–191, 2017.

[31] J. Wang and Y. F. Zhang, "Chemical Structure and Curing Characteristics of Phenol Formaldehyde Resins Catalyzed with Calcium Oxide," *Polym. - Plast. Technol. Eng.*, vol. 51, no. 12, pp. 1213–1217, 2012.

[32] H. Der Wu, M. S. Lee, Y. D. Wu, Y. F. Su, and C. C. M. Ma, "Pultruded Fiber-Reinforced Polyurethane-Toughened Phenolic Resin. 11. Mechanical Properties, Thermal Properties, and Flame Resistance," *J. Appl. Polym. Sci.*, vol. 62, pp. 227–234, 1996.

[33] J. Wang, H. Jiang, and N. Jiang, "Study on the pyrolysis of phenol-formaldehyde (PF) resin and modified PF resin," *Thermochim. Acta*, vol. 496, no. 1–2, pp. 136–142, 2009.

[34] J. Brown and Z. Mathys, "Plasma surface modification of advanced organic fibres: Part V Part V Effects on themechanical properties of aramid/phenolic composites," *J. Mater. Sci.*, vol. 32, pp. 2599–2604, 1997.

[35] J. Li *et al.*, "Curing properties of high-Ortho phenol-formaldehyde resins with co-catalysis," *J. Appl. Polym. Sci.*, vol. 136, no. 12, pp. 1–9, 2019.

[36] C. Pupin, A. Ross, C. Dubois, J. C. Rietsch, and E. Ruiz, "Predicting porosity formation in phenolic resins for RTM manufacturing: The porosity map," *Compos. Part A Appl. Sci. Manuf.*, vol. 100, pp. 294–304, 2017.

[37] M. Natali, J. Kenny, and L. Torre, "Phenolic matrix nanocomposites based on commercial grade resols: Synthesis and characterization," *Compos. Sci. Technol.*, vol. 70, no. 4, pp. 571–577, 2010.

[38] C. Kaynak and C. C. Tasan, "Effects of production parameters on the structure of resol type phenolic resin/layered silicate nanocomposites," *Eur. Polym. J.*, vol. 42, pp. 1908–1921, 2006.

[39] S. Y. Fu, B. Lauke, E. Mäder, C. Y. Yue, and X. Hu, “Tensile properties of short-glass-fiber- and short-carbon-fiber-reinforced polypropylene composites,” *Compos. Part A Appl. Sci. Manuf.*, vol. 31, no. 10, pp. 1117–1125, 2000.

[40] T. Flemming, G. Kress, and M. Flemming, “A new aligned short-carbon-fiber-reinforced thermoplastic prepreg,” *Adv. Compos. Mater.*, vol. 5, no. 2, pp. 151–159, 1996.

[41] H. Yu, K. D. Potter, and M. R. Wisnom, “A novel manufacturing method for aligned discontinuous fibre composites (High Performance-Discontinuous Fibre method),” *Compos. Part A Appl. Sci. Manuf.*, vol. 65, pp. 175–185, 2014.

[42] I. M. Low, J. Somers, H. S. Kho, I. J. Davies, and B. A. Latella, “Fabrication and properties of recycled cellulose fibre-reinforced epoxy composites,” *Compos. Interfaces*, vol. 16, no. 7–9, pp. 659–669, 2009.

Chapter 2: Literature review

Section 2.1: Introduction

A comprehensive literature review about the structure, chemical composition, physical and mechanical properties of natural plant fibres and their limitations in the context of polymer composites is presented in this chapter. Surface modification of plant fibres and its influences on fibre-matrix interfacial bonding were also considered. Special emphasis was given on the use of plasma treatment to modify the surface of natural fibres. Phenolic resin as a matrix for natural fibre-polymer composites were reviewed and discussed in this chapter as well. In the final part of this chapter the properties, characterisations and applications of natural plant fibres reinforced polymer composites are discussed.

Section 2.2: Natural fibres

In general, any fibres that are not man-made or synthetic fibres are called natural fibres. These fibres can be categorized depending on their origins into animal, mineral, and cellulose or plant fibres (Figure 2-1) [1][2]. Animal fibres such as silk, hair, and wool fibres are mostly made from proteins and mainly used in textile applications. Recently, bioengineering applications have started to use animal fibres in various applications, for instance in biomedical and biodegradable applications [3]. Geological materials are the main source of mineral fibres such as asbestos and quartz. These fibres are highly temperature resistance and hard, therefore their applications in high temperature gaskets and ceiling tiles [4]. Natural plant fibres are mainly made from cellulose as well as other components such as hemicellulose, pectin, and lignin. Plant fibres can be classified based on their part from plant into leaf fibres (pineapple, agave, and banana), grass fibres (corn, wheat, and rice), seed fibres (kapok, cotton, and coir), bast fibres (ramie, flax, jute, and hemp) as shown in Figure 2-1 [2][5][6][7]. Among these fibres, bast and leaf fibres are the hardest and the most commonly used as a reinforcement in the composite applications [6].

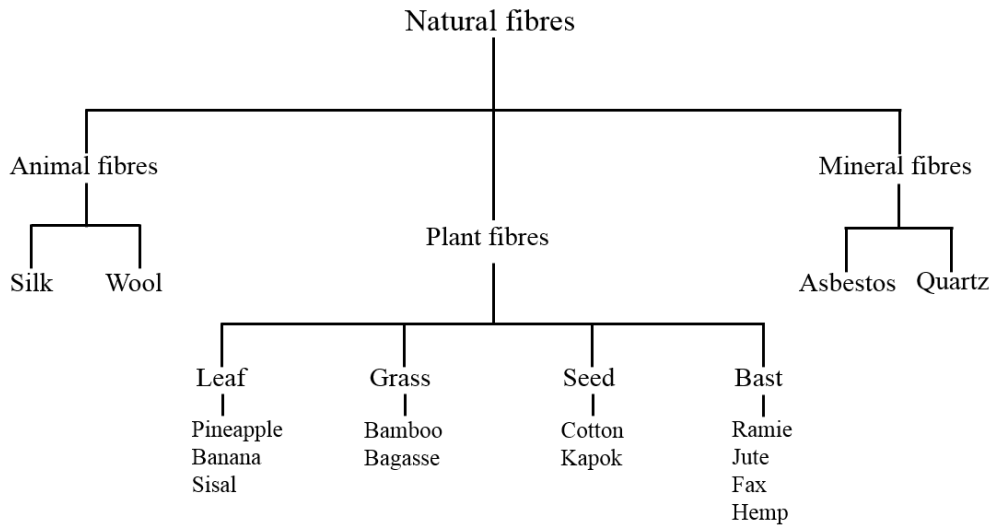

Figure 2-1: *Classification of natural fibres. Adapted from [1].*

Section 2.2.1: Structure of natural plant fibres

Natural plant fibres are characterized by their complex structure and organization. A hollow central canal or lumen surrounded by a thick cell wall is the typical structure of the single plant fibres. These fibres are linked together by means of middle lamellae, which mainly consist of hemicellulose, lignin, and pectin as shown in Figure 2-2. The cell wall is formed of two main layers: a very thin primary wall, and the secondary wall. The secondary wall is subdivided into three layers S1, S2, and S3, from the primary wall towards the lumen as shown in Figure 2-2 [6][8]. Each layer of the cell wall can be considered as a natural nanocomposite material that consists of semi-crystalline cellulose microfibrils with a diameters ranging from 10 to 30 nm [8] embedded in an amorphous matrix of lignin and noncellulosic compounds like hemicellulose and pectin (Figure 2-2) [9]. The high tensile strength microfibrils form the fundamental structural unit of the cell wall and provide mechanical strength to the fibre [10]. They are made up of 30-100 of cellulose molecules in the form of an extended chain [8] with characteristic orientations (microfibrils angle) to the fibre axis. Figure 2-3 shows the arrangement of the microfibrils and cellulose molecules in the cell wall of the plant fibre [11]. The microfibrils orientation varies as a function of the

cell wall layer and plant type [12]. Therefore, the properties of the plant fibres vary depending on the structure, microfibrils angle, dimensions and the chemical composition of the cell [13][14].

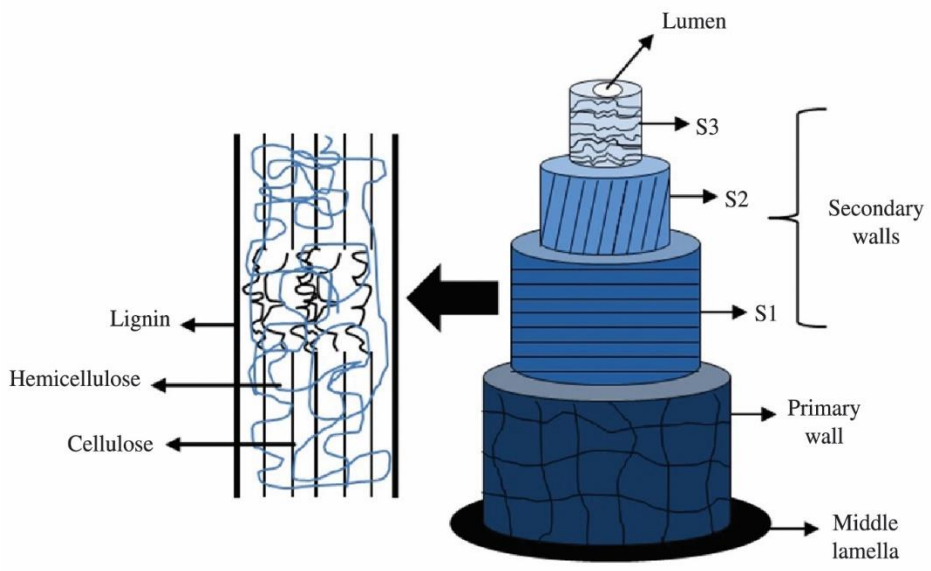

Figure 2-2: *Cell wall structure of single plant fibres. Adapted from [15].*

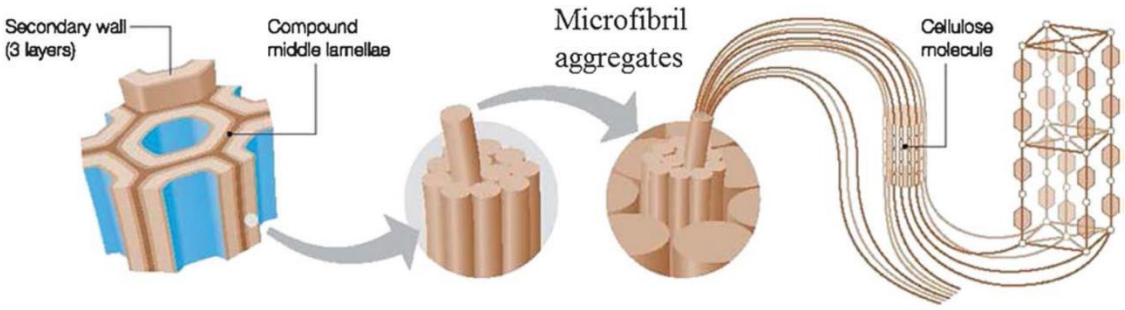

Figure 2-3: *Arrangement of microfibrils and cellulose molecules in the cell wall of the plant fibres. Adapted from [11].*

Section 2.2.2: Chemical composition of natural plant fibres

The cell wall of plant fibres is mainly made from cellulose and other non-cellulosic compounds such as hemicellulose, lignin, waxes, pectin, and water soluble compounds [16][17]. The cellulose, hemicellulose and lignin are the main constituents and they are responsible for the physical properties of the plant fibres [18]. However, the percentage of each component differs from plant to another (Table 2-1) depends on the plant age, growth

rate, geographic locations, climate, and soil conditions and could also vary in different parts within the same plant [19][20].

Table 2-1: *Chemical composition of some commonly used plant fibres. Adapted from [21].*

Fiber	Cellulose (Wt %)	Hemicellulose (Wt %)	Lignin (Wt %)	Waxes (Wt %)
Ramie	68.6-76.2	13-16	0.6-0.7	0.3
Flax	71	18.6-20.6	2.2	1.5
Jute	61-71	14-20	12-13	0.5
Hemp	68	15	10	0.8
Kenaf	72	20.3	9	-
Nettle	53-86	4-10	3.5-9.4	3.1-4.2
Sisal	65	12	9.9	2
Pineapple	81	-	12.7	-

(a) Cellulose

Cellulose is the most important component in the plant fibres due to its mechanical and physical properties. Cellulose's name is suggested by Anselme Payen in 1838, he observed that a large part of the cell wall for all plant fibres have the same substance [22][23]. Cellulose is a natural polymer with a degree of polymerization around 10,000. Cellulose is forming from repeating units of D-anhydroglucose with the formula $C_6H_{11}O_5$ and linked together by linkages of 1, 4-β-D-glycosidic at two positions which are C1 and C4 as shown in Figure 2-4 [23]. Three groups of hydroxyl are contained in each repeating unit. The cellulose properties such as crystalline packing and physical properties are mainly controlled by the hydroxyl groups and the ability to form hydrogen bond [24]. Solid cellulose is formed of microcrystalline structure with high order crystalline regions and low order amorphous regions. Cellulose have a very strong resistance to alkali and oxidizing agents whereas it can be hydrolysed into water and sugar by acids [14].

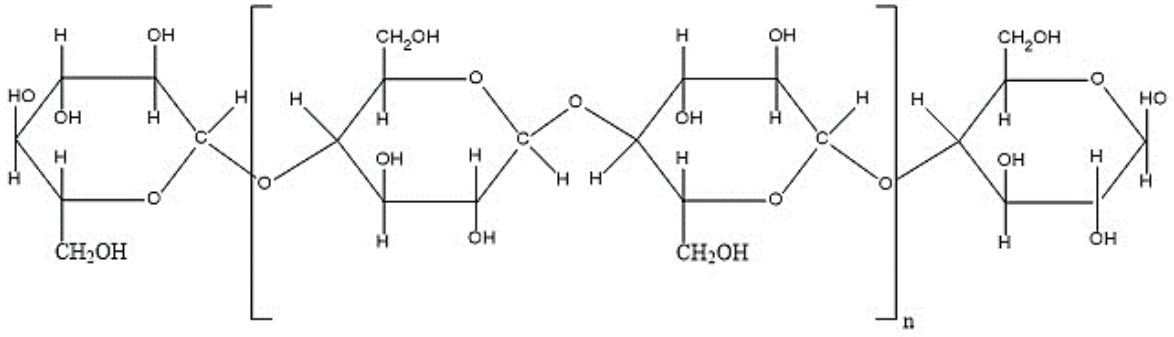

Figure 2-4: *Chemical structure of cellulose. Adapted from [25].*

(b) Hemicellulose

Hemicellulose is the second most important component in the plant fibres and mostly concentrated in the secondary walls [26]. Hemicellulose with lignin act as a matrix for microcrystalline cellulose microfibrils [14]. The chemical structure of hemicellulose is shown in Figure 2-5. It does not have the same form of cellulose, however, they are different in three points. The first point is that hemicellulose contains various sugar units, while 1, 4-β-d-glucopyranose units are only found in the cellulose. Secondly, the non-crystalline nature of hemicellulose provides chain branching in contrast to the linear crystalline polymer exhibited by cellulose. Lastly, hemicellulose have a degree of polymerization between 50 and 300, whereas cellulose is around 10,000 which means higher in 10 to 100 times. Hemicellulose also have a hydrophilic nature and it can be hydrolysed by acids, and can be dissolved in alkali [14][22].

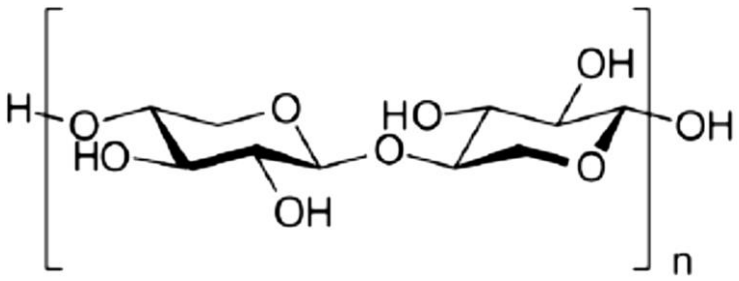

Figure 2-5: *Chemical structure of hemicellulose. Adapted from [27].*

(c) Lignin

Lignin is a kind of thermoplastic polymer with amorphous structure and it provides rigidity to the fibre. It is a complex hydrocarbon polymer with both aromatic and aliphatic constituents which are insoluble in most solvents and also cannot be broken down to monomeric units. Figure 2-6 shows the chemical structure of lignin. The three dimensional carbonyl, hydroxyl, and methoxyl groups of aromatic and aliphatic with high molecular weight have led to very complex structure of lignin. Five groups of methoxyl and five groups of hydroxyl have been observed in each building unit of lignin [14]. The glass transition and melting temperature of lignin are about 90 °C and 170 °C respectively. Lignin cannot be hydrolysed by acids, but it is dissolvable in hot alkali. It is easily condensable with phenol, and readily oxidized [28].

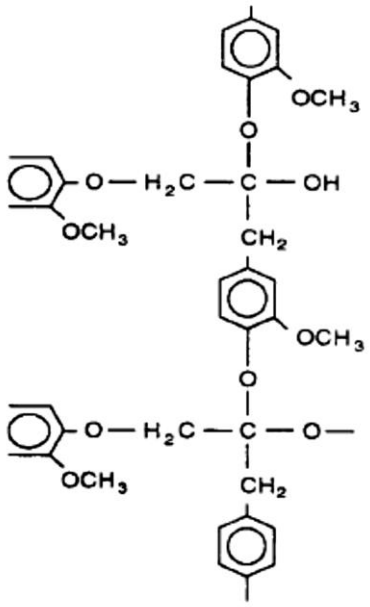

Figure 2-6: *Chemical structure of lignin. Adapted from [22].*

(d) Pectins and waxes

The fibres flexibility are provided by pectins, which are mostly made from polygalacturon acids. The neutralisation of lignin by ammonium hydroxide or alkali can help to dissolve

pectin in water. Waxes represent the outer layers of fibres which contain various types of alcohols. Waxes are resistant to water and also to many acids [8].

Section 2.2.3: Physical and mechanical properties of natural plant fibres

Many reports can be found in the literature that present the physical and mechanical properties of different plant fibres. The properties of the plant fibres vary from one fibre to another depending on the plant type, chemical composition, cell wall structure, and growth conditions [29]. Table 2-2 represents the physical properties of some commonly used plant fibres. It can be seen that ramie, flax, and nettle fibres have the highest density while isora and kenaf fibres have the lowest density. The longest and one of the thickest elementary fibre can be found is the ramie fibre whereas hemp fibre show the longest technical fibre [30].

Table 2-2: *Physical properties of some commonly used plant fibres. Adapted from* [30].

Fiber	Density (g/cm^3)	Diameter (μm)	Length technical fibres (m)	Length elementary fibres (mm)
Ramie	1.51-1.55	40-60	0.1-1.8	120-150
Flax	1.50	17-20	0.2-1.4	13-40
Jute	1.44-1.49	14-20	0.15-0.4	2-3
Hemp	1.48-1.49	15-30	1.0-3.0	15-25
Isora	1.2-1.3	-	-	-
Kenaf	1.2	14-33	0.9-1.8	1.5-11
Nettle	1.51	20-80	0.02-0.08	5.5

1.1.1

The mechanical properties of plant fibres are strongly affected by the composition and the structure of the cell wall. Due to the excellent mechanical properties of crystalline cellulose such as stiffness and strength, the higher content of cellulose results in better mechanical strength. The elasticity properties of plant fibres are highly affected by the micro-fibril angle. For instance, the ductility will increase if the micro-fibrils angle are helically oriented with fibre axis whereas the highest tensile strength is observed when the micro-fibrils angle are parallel oriented with fibre axis [24][31].

Table 2-3 represents the mechanical properties of some commonly used plant fibres and E-glass fibre. Amongst all the plant fibres, it can be seen that ramie, hemp, and fax fibres have the highest tensile strengths and specific Young's modulus. However, the observed large variation in the tensile properties is typical for the plant fibres due to the above factors. Some variations can be also added by the experimental testing methods such as fibre cross sectional area measurements. In relation to synthetic fibres, tensile strengths of E-glass fibres are generally higher than those of plant fibres but the stiffness can be comparable especially for ramie, flax, and hemp fibres. However, the specific Young's modulus for plant fibres can be higher than those of E-glass fibres and also the specific tensile strength of some plant fibres compare well with the lower specific strength of E-glass fibres as shown in Table 2-3 [32][33].

Table 2-3: *Mechanical properties of some commonly used plant fibres and E-glass fibre. Adapted from [33][34].*

Fiber	Tensile strength (MPa)	Young's modulus (GPa)	Specific strength (MPa/g cm^{-3})	Specific modulus (GPa/g cm^{-3})	Elongation at break (%)
Ramie	400-938	44-128	270-620	29-85	2.0-3.8
Flax	345-1830	27-80	230-1220	18-53	1.2-3.2
Jute	393-800	10-55	300-610	7.1-39	1.5-1.8
Hemp	550-1110	58-70	370-740	39-47	1.6
Kenaf	930	53	-	-	1.5
Nettle	650	38	-	-	1.7
Sisal	507-855	9.4-28	362-610	6.7-20	2.0-2.5
E-glass	2000-3000	70	800-1400	29	2.5

Section 2.2.4: Surface characteristics of natural plant fibres

As mentioned earlier in this chapter, most of the natural plant fibres have a hollow structure (lumen) surrounded by a thick cell wall as well as nodes at irregular distances along the fibre which divide the fibre into individual cells. Although the semi-crystalline cellulose microfibrils represent the main structural components of the fibre cell wall, the non-cellulosic compounds such as hemicellulose, lignin, pectin, and waxes also highly influence

the fibre surface properties [35][36]. In polymer composites, the presence of the non-cellulosic compounds on the fibre surface contribute enormously to ineffective interfacial bonding between the fibres and polymer matrices [37]. Furthermore, the existence of the water soluble substances and hydroxyl groups, particularly in the amorphous regions, deteriorates the capability of plant fibres to develop the surface adhesive characteristics with most polymer materials [38]. Also, the fibre surface roughness which is highly controlled by the surface chemical composition play a major role in determining the compatibility of the fibres with the matrix [37]. The poor fibre/matrix interfacial bonding results in a weak load transfer from the matrix to the fibre, leading to a low fibre reinforcement effect [36]. This has limited the applications of plant fibres in polymer composites significantly. Consequently, surface modifications of plant fibres are suggested to improve the fibre surface characteristics and hence a better compatibility of plant fibres with polymer matrices.

Section 2.2.5: Ramie plant fibres

Ramie fibre is a member of the nettle family and represents one of the oldest textile plant fibres in the world [39][40][41]. It is a bast fibre extracted from the inner bark (phloem) of the ramie plant stem [42]. The process of obtaining ramie fibres from the stem as follows: first wetting the stem by water; fibres then stripped from the stem in the form of ribbons; finally, degumming the ribbons using either microbiological or chemical treatments [43]. Figure 2-7 shows the longitudinal and cross sectional views of ramie fibres [44]. Ramie fibres among all plant fibres are characterised to be the strongest, longest, and silkiest fibres [40][43]. In addition, they possess good corrosion resistance, good resistance to atmospheric conditions, good ventilation, and good durability, as well as the commercial availability [40][45]. Such characteristics make ramie fibres suitable for various applications. Polymer composite is one of the most widely used fields of ramie fibres [46].

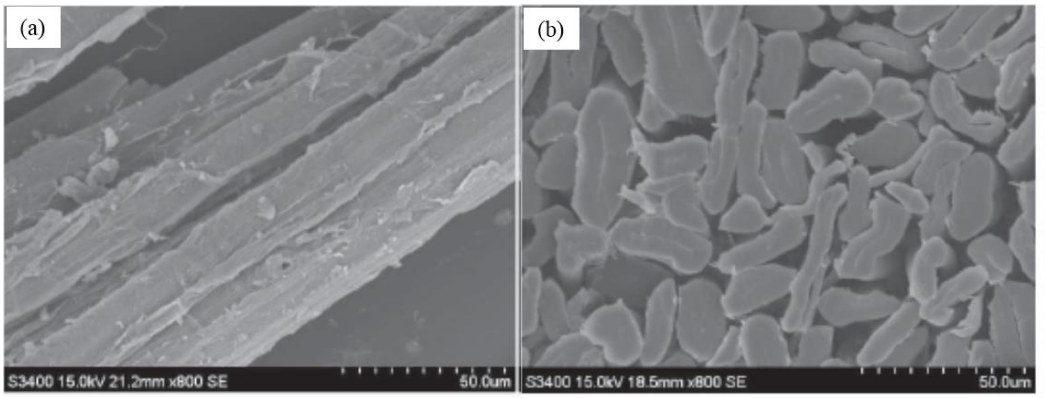

Figure 2-7: *SEM micrographs of ramie fibre, (a) longitudinal view and (b) cross sectional view. Adapted from [44].*

Section 2.2.6: Surface modification of plant fibres

Surface treatments of plant fibres are very important in order to improve the surface characteristics such as surface roughness and surface adhesion properties. Therefore, various methods have been developed and applied in the field of surface modifications. Chemical and physical treatments are the most effective methods that have been used to treat the fibre surface. Chemical treatments such as alkali treatment, silane treatment, acetylation, peroxide treatment, etc. have been used for a long time to treat different cellulose fibres [47][48]. They have provided desirable modification for the fibre surface by improving the moisture resistance and adhesion properties and hence improving the fibre/matrix interfacial bonding [38][49][50]. However, the large quantities of liquids and chemicals that are usually used in chemical methods as well as the high cost and energy consumption have restricted their applications in recent years [51]. Physical methods such as plasma treatments, corona treatment, and electron beam irradiation have been used as well to enhance the surface properties of different cellulose fibres [52]. Among these, plasma technology is the most effective process, and it has advantages like simplicity, low energy consumption, low cost, and no need for chemicals or liquids and therefore reduced effects on the environment [53]. Moreover, plasma treatment provides desirable surfaces properties (wettability,

hydrophobicity, chemical reactivity, and moisture resistance) without affecting the bulk properties [52][53].

Section 2.2.6.1: Plasma process

Plasma can be defined as the fourth state of matter which it is basically a partially ionized gas with a high energy. Plasma can be classified according to the temperature into thermal and non-thermal plasma. The non-thermal plasma also known as low temperature plasma (LTP) is more suitable for surface modification of textile materials and heat surface sensitive polymers [54]. This kind of plasma can be generated by creating an electrical field over two electrodes with a gas in between or by inducing radio frequency (RF) resonant current in a coil [54][55]. This can be done either in a closed vessel under reduced pressure (referred to as low pressure plasma) or at atmospheric pressure (referred to as atmospheric pressure plasma) [54][56]. However, the required power to generate low pressure plasma is lower than those of atmospheric plasma. Normally, 60 to 100 W is the required power to generate low pressure plasma, whereas atmospheric plasma is generated at around 10 kW [57]. The generated plasma contains the mixture of many reactive species such as highly excited atomic, ionic, molecular, and radical species with free electrons and photons as shown in Figure 2-8 [58][59]. Free electrons gain energy from the imposed radio frequency electric field, colliding with neutral gas molecules and transferring energy dissociating the molecules to form numerous reactive species. The primary process in the generation of activated species, especially ions, involves electron impact and photoionization. Photoionization occurs when a photon is emitted, due to the energy falling of an electron from a higher level to a lower one, hitting a gas molecule with high enough energy. Ionization also takes place via collisions of metastable species. Free radicals may also be generated by electron impact, thermally and by photolysis. The impact with a monomer can lead to its excitation and dissociation, generating free radicals [60].

The interaction of these excited species with the surface of a substrate placed in the plasma reactors which results in the physical and chemical modification of the material surface [58]. Changes in the surface occur when the excited and energetic electrons, radicals, and ions are bombarded onto the material surface. This can bring out two types of interactions with the surface depending on the gas type: (1) surface cleaning, etching or activation, when non-polymerizing gases like air, oxygen, helium, and nitrogen are used and; (2) plasma induced polymerisation or grafting, which is carried out by using various polymerising gases and precursors like hydrocarbons, fluorocarbons, and silicon containing monomers [37]. Therefore, the surface changes and interaction depth induced by plasma are controlled by several factors such as the gas type, power, pressure, frequency, and treatment duration as well as the nature of the substrate [54].

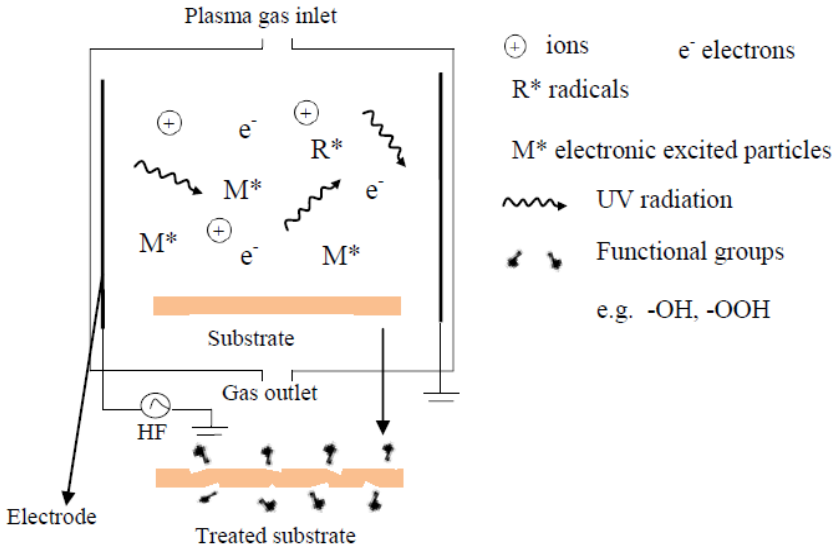

Figure 2-8: *describes the principle of plasma treatment. Adapted from [60].*

Section 2.2.6.2: Plasma treatment of plant fibres

Plasma techniques have gained much attention from researchers and industries in recent years due to the high efficiency in modifying most of the polymer surfaces as well as the simplicity, cheap, and low environmental impacts [61]. Surface characteristics of different

polymers can be effectively improved by low temperature plasma without affecting or changing the main properties such as toughness, strength, and biodegradability [62]. Surface cleaning and surface coating were the most common applications of plasma in the past. In recent years, plasma techniques have been applied to enhance surface wettability, dyeability, printability, bond ability, surface hardness and surface adhesion properties of both natural and synthetic fibres [63][64]. In terms of natural plant fibres, low pressure plasma and atmospheric pressure plasma are the most two effective techniques that have been used to modify plant fibres [57].

Several researchers have investigated the effects of plasma treatments on the surface characteristics of different plant fibres and their impacts on the polymer composites. For instance, low pressure plasma has been used to modify the surface characteristics of sisal fibres and wood fibres, using two different gases (argon and air) in order to improve the compatibility between fibres and polypropylene composites [65][66]. The results showed that the plasma treatments of both fibres (sisal and wood fibres) have a positive impact on the fibre surface characteristics such as surface roughness and surface chemistry. This resulted in a higher mechanical properties such as flexural strength and flexural modulus, tensile strength and tensile modulus, and the storage modulus for the plasma treated fibre composites in comparison to those of untreated fibre composites. Jute fibres were also treated using low pressure plasma with argon as a treated gas at three different times (5, 10, and 15 min) and then processed for composites with unsaturated polyester resin [67]. It was found that with the long-time of plasma treatment the fibre surface became rougher and also the formation of pits on the surface was observed especially after 15 min of plasma treatment. As a result of this, the jute fibre/unsaturated polyester adhesion properties were improved which resulted in a better composite flexural properties when compared to the untreated fibre composite properties. It has been shown that the flexural strength of composites reinforced

with 10 min plasma treated fibres is higher by ~14% than those of untreated fibre composites. However, composites reinforced with 15 min plasma treated fibres showed a lower flexural strength which they attributed to the degradation of the fibre surface caused by long-time of plasma treatment.

Atmospheric pressure plasmas techniques were also used to modify the surface characteristics of flax fibres in order to improve the interfacial adhesion properties between flax fibres and high density polyethylene (HDPE) and unsaturated polyester composites [52]. In this study, two different gases (argon and air) with three different powers (100, 200, 300 W) were used to treat the flax fibre for 2 min. As a result of using three different plasma powers, cracks and longitudinal grooves were observed on the fibre surface with increasing plasma power due to the high etching effect of plasma treatments which resulted in a loss in the fibre strength. However, in terms of the composites, it has been shown that the interfacial adhesion between the argon treated flax fibre and HDPE matrix is superior to those of untreated and air treated flax fibres. This is in contrast, in the case of using polyester as a matrix, the air plasma treatment is more effective than argon plasma treatment. However, the reported interfacial shear strength (IFSS) for both plasma treated composites were higher than those of untreated flax fibre composites.

Although of the all studies that have been done so far in this field (plasma treatment of plant fibres), an extensive investigation and a deep understanding of the effects of plasma treatment on the surface characteristics of plant fibres is still needed. This might help to rise up the usefulness of those fibres as environmentally reinforcing materials for polymer composites and to gain more insights about the interfacial bonding between these materials. To cover this, a detail investigation of the surface topography and single fibre mechanical testing of ramie fibres under different durations of plasma treatment is presented in chapter 5.

Section 2.3: Composite materials

The composite material can be defined as a combination of two or more different phases in a microscopic scale. They are joined together by a recognizable interface to give overall properties different from their individual properties [68]. The strongest phase is known as reinforcement or filler material, whereas the weakest phase is called matrix material. Therefore, reinforcement material supports the composite material by rigidity and strength [29]. The excellent structural properties of composite material have attracted the attention of scientist to use it in a various applications such as thermal, electrical, tribological, constructional, and environmental applications [68].

Section 2.3.1: Matrix phase

The continuous phase in composite materials is known as matrix. The purpose of this phase in fibre reinforced composite materials are: (1) keeping the fibres in place and transferring the mechanical stresses in between the fibres, (2) Protecting the fibres from environmental effects like chemical liquids and moistures, and (3) Protecting the fibre surface from mechanical abrasion. Therefore, the matrix phase is very important in determining the overall composite properties such as compressive, in plane shear, and interlaminar shear properties.

In many cases under compressive loading, the matrix phase provides support against the possibility of fibre buckling that influencing the compressive strength of the fibre composite material. The in plane shear strength is also an important design consideration for structures under torsional loads whereas the interlaminar shear strength is important under bending loads. Such properties are highly affected by the quality of the interfacial bonding between the fibres and the matrix. In addition, the process characteristics of the matrix is also responsible for the processing and the presence of the defects in the composites [69].

Section 2.3.2: Classifications of composite materials based on matrix phase

Depending on the matrix compositions, three groups of composite materials are being classified. They are: metal-matrix composites, ceramic-matrix composites, and polymer matrix composites [68].

(a) Metal matrix composites (MMCs)

Metals are the matrix phase of these composites such as aluminium, titanium, and magnesium. The most common fibres have been used as a reinforcement for metal matrices are silicon carbide, titanium carbide, and carbon. The elasticity and strength of metals can be enhanced by using fibres as a reinforcement. However, the thermal expansion coefficient, electrical and thermal conductivity of metals could be decreased by introducing fibres as a reinforcement material like silicon carbide fibres [29].

(b) Ceramic matrix composites (CMCs)

Ceramic matrices can be categorized into four groups: (1) glasses like alumina silicates and borosilicate which are recognized by low melting temperature and hence easy to design, (2) traditional ceramics like alumina and zirconia are normally fully crystalline materials and having a high melting temperature, (3) cements and (4) carbon ceramic matrices. Generally, ceramic materials are characterised by having high hardness and strength, high service temperature, and low density. Ceramic composites provide excellent properties especially for high temperature applications. However, the fabrication of ceramic composites are not easy due to the brittleness of ceramics, as well as the starting materials usually in the powder form [29].

(c) Polymer matrix composites (PMCs)

Polymer matrix composites are the most common advanced materials due to their properties such as high mechanical properties (strength and stiffness), easy to fabricate, and low cost.

Polymer matrices weather thermosetting or thermoplastic polymers can be reinforced by natural and synthetic fibres. Such composite provides excellent strength and stiffness properties with high corrosion resistance [29]. Therefore, most of the composite materials utilised in the industry are based on polymer matrices.

Section 2.3.3: Polymers

Polymers can be defined as a long molecular chains containing one or more repeating units of atoms linked together with strong covalent bonds as shown in Figure 2-9. The chemical structure of the polymer molecules are similar but they are different in their length. These molecules in the solid state of polymers are frozen in space in the form of either randomly distributed such as in amorphous polymers or a combination of both randomly and orderly distributed such as in semicrystalline polymers as presented in Figure 2-10 [69].

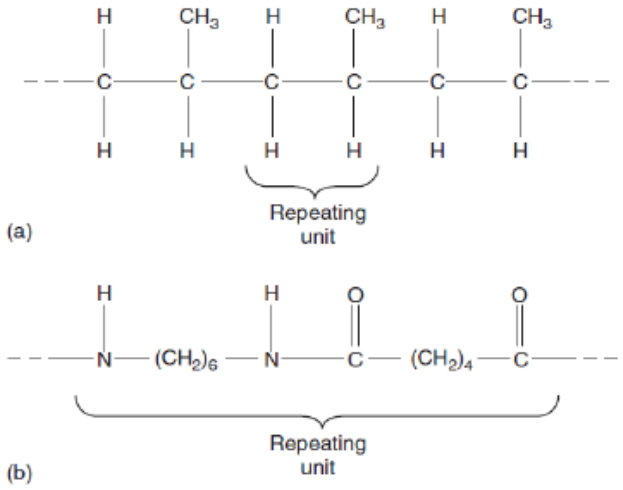

Figure 2-9: *(a) Repeating units of polypropylene molecule. (b) Repeating units of nylon 6 molecule. Adapted from [69].*

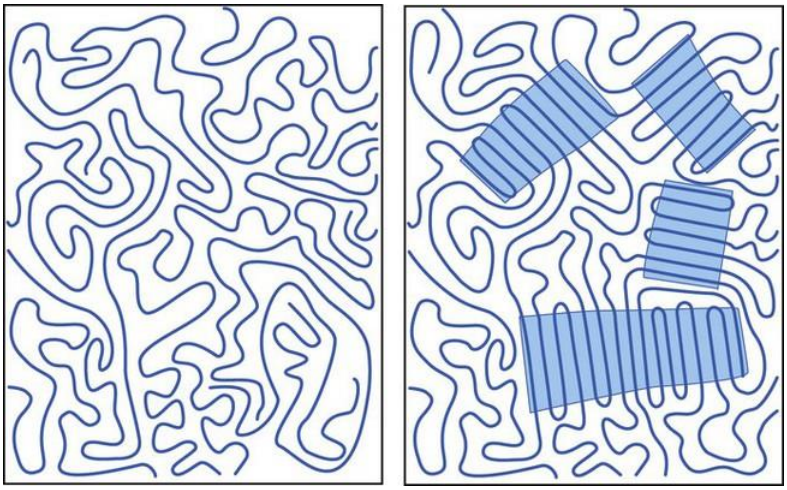

Figure 2-10: *Amorphous (left) and semicrystalline (right) structure of polymers. Shaded area represents the crystalline region. Adapted from [70].*

Section 2.3.3.1: Types of polymer

Thermoplastics and thermosets are the main two types of polymers. Thermoplastics such as polyethylene, polypropylene, poly (vinyl chloride), etc. are differ from thermosets in their chemical and physical structure, for instance, molecules in thermoplastic polymers are bonded together by weak secondary bonds or intermolecular forces such as hydrogen bonds and van der Waals bonds (Figure 2-11a). These bonds can be easily broken by applying heat on the solid thermoplastics polymer and hence the polymer molecules can be freely moved and form a new shape when cooled. Therefore, thermoplastics polymer are characterized by the ability to reshape and reuse as many times as required. The most applicable thermoplastic polymers for natural fibres are those with processing temperature no more than 230 °C [29][69]. In contrast, thermoset molecules are chemically linked to each other by cross links of covalent bonds (Figure 2-11b), which cannot be melted or broken by heating like in thermoplastics. Compered with thermoplastic polymers, thermosets are recognized by higher strength, higher hardness, better stability, higher electrical resistance, as well as higher resistance to chemicals and solvents [69]. The most common thermosets polymers that have been used as a matrix for natural fibres are unsaturated polyester resins, polyimide resins, epoxy resins, and phenolic resins [69][71]. Among all types of thermoset resins,

phenolics keep hold of industrial and commercial interest due to their excellent properties such as high strength and modulus as well as better chemical and thermal resistance [72].

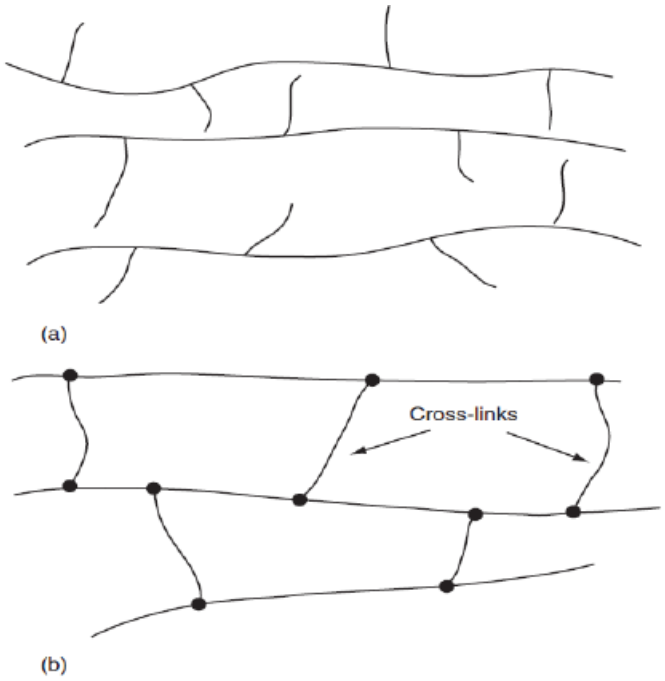

Figure 2-11: *Polymer structure of (a) thermoplastic, and (b) thermoset. Adapted from [69].*

Section 2.3.3.2: Phenolic resin

Phenolic resins also known as phenol-formaldehyde resins can be considered as the first synthetic thermosetting polymers, produced from simple compounds with a low molecular weight [73][74]. Since 1930 when the phenolic resins where first used as binders in plywood and particle boards, these resins have become one of the most important thermosetting matrices in the industry of wood composites, particularly for exterior applications [75]. Such resins continue to be used in a broad range of applications such as in the aerospace and automotive industries as well as in the semiconductor devices [76][77]. Moreover, phenolic foams are being developed to be used in various applications such as building structural materials and passenger and military aircraft [78][79][80]. Furthermore, phenolics have been successfully utilised as a matrix material for composite applications in the sport and construction industries due to their capability of withstanding highly corrosive environments

[72][81][82]. The wide variety of phenolic resins applications are mainly due to their properties such as excellent ablative properties, low smoke density, high chemical resistance, thermal stability with low flammability, structural integrity, and easily processability as well as their excellent mechanical properties [83]. Table 2-4 represents the typical properties of cast phenolic resins [84][85].

Table 2-4: *Typical properties of phenolic resins. Adapted from* [84][85].

Properties	Values
Density, g/cm^3	1.19
Tensile strength, MPa	34-62
Flexural strength, MPa	75-117
Compressive strength, MPa	82-103
Elongation at break (%)	1.5-2.0

Section 2.3.3.3: Reaction mechanism of phenol-formaldehyde resin

The initial compounds of phenolic resins are a group of aromatic compounds which are linked directly with the hydroxyl groups as shown in Figure 2-12 [72]. Such resins are synthesised from the polycondensation reaction of the phenol and formaldehyde. Based on the phenol/formaldehyde ratios and curing conditions (basic or acidic), two types of phenolic resins can be produced, novolac and resole resins [86][87], as presented in Figure 2-12. Generally, both types (novolac and resole) are almost identical in terms of mechanical properties and chemical resistance [88]. Novolacs are prepared in the existence of an acid catalysts such as sulfuric acid, oxalic acid, aromatic sulfuric acids, formic acid, and hydrochloric acid [72], with an excess of phenol to formaldehyde ratio (Figure 2-12). Such resin does not react further without curing agent. Hence, curing agent such as hexamethylenetramine (HMTA) must be added in order produce a crosslinked structure of novolac phenolic resins [88]. However, the resin of interest for liquid moulding and also for fibre composites is resole resin [89][90]. Resoles are synthesised in the presence of alkaline catalyst with an excess of formaldehyde to phenol ratio (Figure 2-12), producing a soluble

and fusible pre-polymer. Resole structure contains reactive hydroxymethyl groups and hence it can be catalysed either by heating, acid-base, or special ester conditions [90].

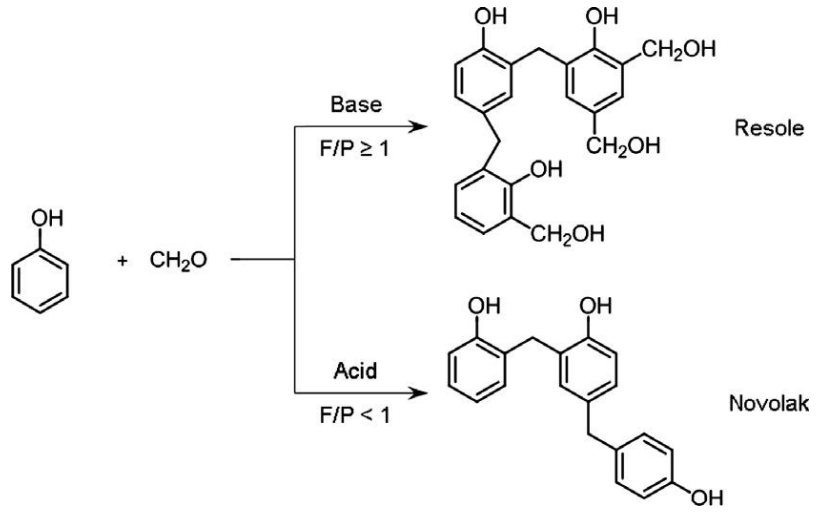

Figure 2-12: *Synthesis of resole and novolac phenolic resins. Adapted from [90]*.

However, the polymerisation process of phenol/formaldehyde resin is characterized by a long process with the generation of water and formaldehyde as by-products [91]. The release of these products become very difficult as the resin viscosity rises during the curing reaction [83]. Consequently, the presence of these products in the cured resin leads to microvoids (8-10 μm in size), which adversely affects the properties of the final cured resin [89]. Therefore, there have been many attempts from different researches to reduce or control the voids content in the final cured resin. It has been found that the resin viscosity and the cure cycle are the main two factors that highly influence the voids content in the crosslinked resin. For instance, [89] used ethylene glycol as a diluent in order to replace the water loss during curing process and also to reduce the resin viscosity. They noticed a significant reduction in the void content (Figure 2-13) and increase in the density as well as an improvements in the fracture toughness and flexural modulus of the cured resin. They attributed this to the reduced viscosity of the resin caused by ethylene glycol which have resulted in a more and easy release of water during curing processing, before the crosslinking stage.

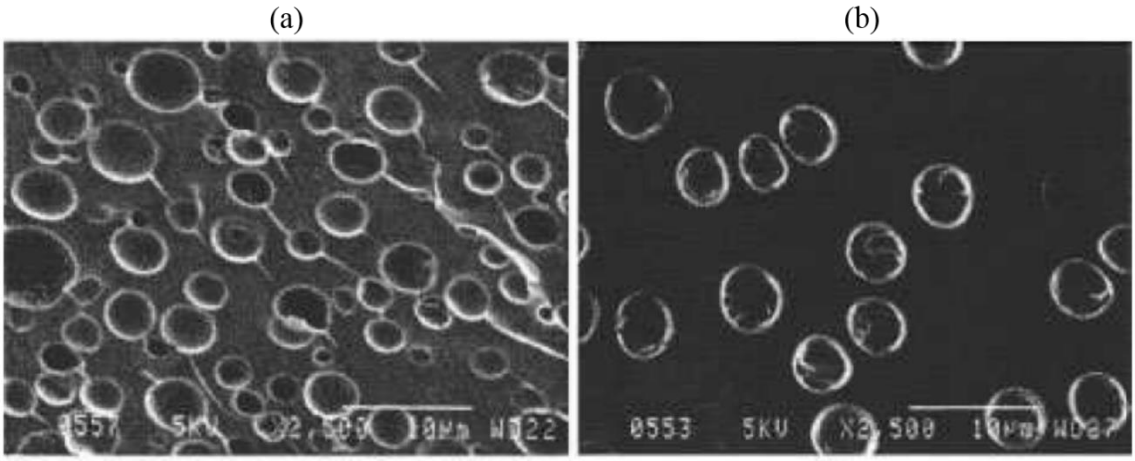

Figure 2-13: *SEM micrographs of cured phenolic resins (BPJ2027L). (a) Original cured resin; and (b) diluted (ethylene glycol) cured resin. Adapted from* [89].

Wolfrun and Ehrenstein [92] investigated the influence of the hardener concentrations and the curing temperatures on the structure of two phenolic resin systems (phenolic resin DW247 and phenolic resin N). It was found that the hardener amount highly influences the void size and void diameter distribution in the cured resin. With an increase in the hardener concentration from 2% to 15%, the average void diameter in the case of phenolic resin system N was decreased from 4.60 μm to 0.25 μm, respectively. Similarly, in the case of phenolic resin system DW247, the average void diameter was decreased from 1.80 μm to 0.25 μm with the increase of the hardener concentration from 7% to 17%, respectively. A linear relationship between the hardener concentration and the void dimeter were clearly observed as presented in Figure 2-14a. Moreover, the cure temperature was shown to have similar effects as the hardener concentration effects on the void diameter. The average void diameter in the case of phenolic system N, was decreased from 2.40 μm to 1.60 μm with the increase of curing temperature from 40 °C to 80 °C, respectively. Similarly, the average void dimeter in the case of phenolic system DW247, was decreased from 1.80 μm to 1.50 μm with the increase of curing temperature from 40 °C to 80 °C, respectively, as shown in Figure 2-14b. However, it can be clearly seen that the hardener concentrations influence the average void diameter more than the curing temperatures.

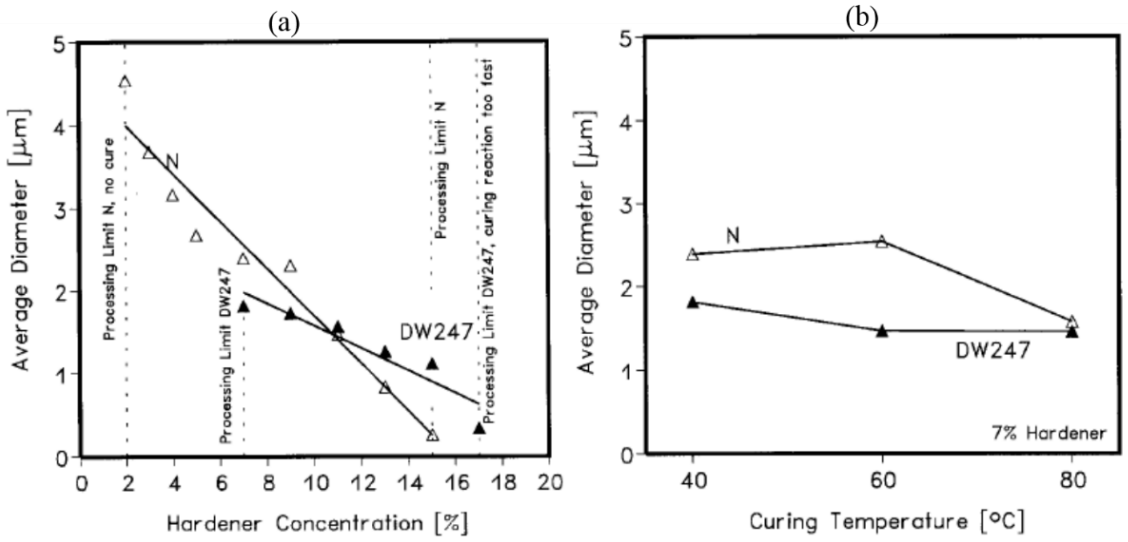

Figure 2-14: *(a) the relationship between the hardener concentrations and the average void diameter for both phenolic resin systems (DW274 and N); (b) the relationship between the curing temperatures and the average void diameter for both phenolic resin systems (DW274 and N). Adapted from [92].*

Kaynak and Tasan [93], studied the effects of using two different curing methods on the morphology of the cured resole phenolic resins. They considered the ability of resole phenolic resin to be crosslinked either with the application of heat only without curing agents or with the use of curing agents. It was found that a void free microstructure of resole phenolic resin can be achieved if the resin gelation time is kept long enough for the slow water vapour to be released. This approach required a very long heat cure cycle (3 days) without the use of any curing agents. In contrast, microvoids were observed in the case of using short cure cycle with the use of acid curing agent. This was attributed to the faster crosslinking rate than the water vapour release rate and hence the resin gelation happened earlier than the release of water vapour.

However, the long cure cycle is not favourable for most industries due to time and energy consumption issues. Moreover, so far no existing approaches allow void free microstructures to be achieved with a short cure cycle, therefore, a novel approach to optimise the voids size and distribution in fast curing process for better mechanical properties at minimum processing time is proposed as an alternative. This will be discussed in detail in chapter 6.

Section 2.4: Natural plant fibres reinforced polymer composites

In recent times, natural plant fibres like ramie, flax, jute, hemp, kenaf, and sisal have gained much attention to be used as a reinforcement for polymer matrices in various applications. This is because of their excellent properties such as low density, easy availability with low cost, renewability, and good mechanical characteristics like flexibility, high specific strength and modulus, as well as high toughness [94][95][96]. Moreover, the environmental issues and consumer requirements have pushed many scientist and engineers to find new materials (renewable, cheap, and environmental friendly) to substitute the conventional (non-renewable) materials like glass, aramid, and carbon fibres. Polymer matrices reinforced by natural plant fibres are eco-friendly composites and represent a suitable alternative to traditional polymer composites in many applications such as automotive, constructions, and packaging applications [97][98]. For instance, it has been reported in the literature that in automotive applications the natural fibre components require 83% less energy and 40% less expensive than that of glass fibre components [99]. Moreover, the hollow structure of plant fibres results in better sound insulation and damping properties when combined with specific types of polymer matrices [100][101]. Therefore, nowadays, natural plant fibres reinforced polymer matrix composites represent one of the fastest growing industries.

Section 2.4.1: Theoretical properties prediction for natural fibre composite

In fibre reinforced polymer composite materials, the intrinsic mechanical properties of the matrix are improved by the addition of the reinforcing fibres. This occurs by transferring the stresses from the matrix to the fibres via the fibre-matrix interface. Thus, the final mechanical properties of fibre composite materials depend on the properties of the individual components (fibres and matrix) and their interfacial bonding, as well as the amount of reinforcing material and its geometrical arrangement within the matrix [102]. The amount of reinforcements and their arrangement are determined by the composite fabrication process. To understand how the manufacturing process affects the finished product

properties, one needs a model which relates the above-mentioned characteristics of composites to their mechanical properties. A number of theoretical models have been put forward to model the mechanical properties of fibre composites [103]. Although they are very different, they all use the same basic assumptions [103]:

(1) Both fibres and matrix are linearly elastic, the fibres are either isotropic or transversely isotropic and the matrix is isotropic.

(2) The perfect interfacial bonding between the fibres and matrix, and remain that way during the deformation.

(3) The fibres are axisymmetric and identical in shape.

Section 2.4.1.1: Rule of mixture

The rule of mixture model was first proposed by Kelly and Tyson [104] to predict the modulus and strength of the continuous uniaxial fibre composites. In fibre direction with assuming perfect bonding between fibres and matrix, the obtained properties are:

$$E_L = E_f V_f + E_m V_m \qquad (2.1)$$

$$\sigma_c = \sigma_f V_f + \sigma_m V_m \qquad (2.2)$$

Where:

$$V_m = 1 - V_f \qquad (2.3)$$

such that E_L and σ_c are the modulus and strength of composites, respectively. E_f and E_m are the modulus of the fibres and matrix, respectively. V_f and V_m are the volume fractions of the fibres and matrix, respectively. σ_f and σm are the stresses in the fibres and matrix respectively, at fibre failure [104].

Compared to the continuous fibre composites, the modelling of discontinuous fibres composites is more complex due to the complicated fibre orientation and fibre length distribution. To estimate the properties of these composites, the effects of fibre orientation and fibre length need to be considered [105].

Section 2.4.1.2: Shear lag models

Shear lag model is one of the earliest models developed by Cox et al. [106] for short fibre composites. It is usually completed by combining the average stress in the fibre with an average stress in the matrix to produce a modified rule of mixtures [103]. According to Cox et al. [106] in shear lag models, the main aspects of controlling the mechanical properties of fibre composites are the critical length of the fibre and the interfacial shear strength between fibres and matrix. In the case of composites containing short fibres, the applied load is transferred to the fibres by means of shear forces at the fibre-matrix interface, and high shear stresses are experienced at the fibre ends [104]. Therefore, the composite failure mechanisms are administrating by fibre length and sub-critical length fibres ($L<L_c$) cannot be fully stressed and will finally deboned and be pulled out of the matrix. Critical length fibres ($L=L_c$) can only be fully stressed at a very small location in the middle of the fibre, whereas supercritical length fibres (L>Lc) can be stressed over a much greater proportion of the fibre. Once the stress in the fibre reaches the fibre strength, fibre fracture occurs. The critical fibre length (L_c) is defined as:

$$\frac{L_c}{d} = \frac{\sigma_{fu}}{2\tau_y} \qquad (2.4)$$

where d is the fibre diameter, τ_y is the shear stress on the cylindrical fibre-matrix interface, σ_{fu} is the maximum permissible fibre stress.

Kelly and Tyson [104] modified the rule of mixtures model Equation 2.2 by replacing the mean fibre strength (σ_f) with the average stress along the fibre. The average stress of a sub-critical length fibre is given by the area under the curve in Figure 2-15a divided by the fibre length, and the average stress of a critical length fibre or super-critical length fibre is given by the area under the curve in Figure 2-15b divided by the fibre length.

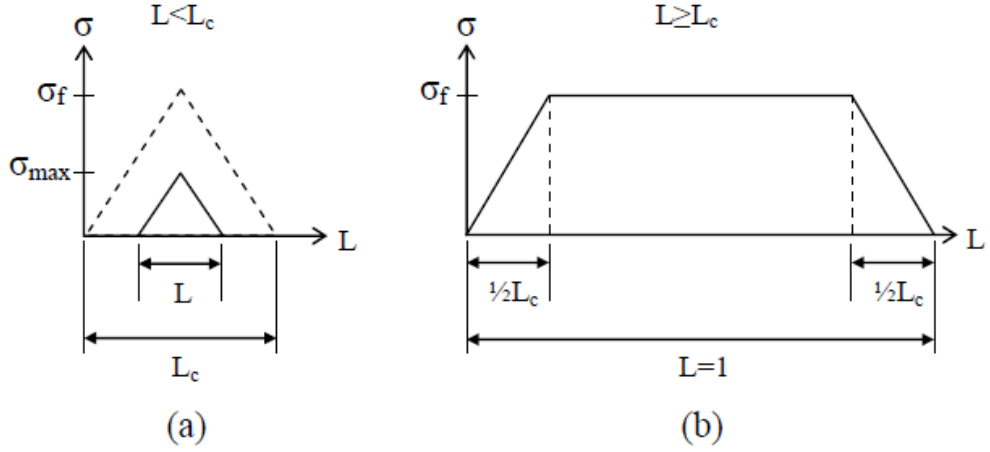

Figure 2-15: *Linear build up of stress inside the fibre, (a) $L < L_c$, (b) $L \geq L_c$. Adapted from [107].*

Thus, the tensile strength of composites (σ_c) containing fibres shorter than critical fibres length (L_c) is given by:

$$\sigma_c = V_f\, \sigma_f \left(\frac{L}{2\, L_c}\right) + V_m\, \sigma_m \qquad For\ L < L_c \qquad (2.5)$$

and the tensile strength of composites containing fibres longer than critical fibres length (L_c) is given by:

$$\sigma_c = V_f\, \sigma_f \left(1 - \frac{L}{2\, L_c}\right) + V_m\, \sigma_m \qquad For\ L \geq L_c \qquad (2.6)$$

Equations 2.5 and 2.6 can be combined into the following equation to determine the composite tensile strength:

$$\sigma_C = K_2\, V_f \sigma_f + V_m \sigma_m \qquad (2.7)$$

where K_2 is the fibre length factor, which can be determined by:

$$K_2 = \frac{L}{2L_c} \qquad For\ L < L_c \qquad (2.8)$$

$$K_2 = 1 - \left(\frac{L}{2L_c}\right) \qquad For L \geq L_c \qquad (2.9)$$

However, these theories assume that the reinforcing fibres are isotropic in nature, and this is unlikely for natural plant fibres as they are expected to be weaker in the transvers direction than the axial direction. These models also assume that the fibres are cylindrically shaped,

but the actual shape of the ramie fibre is not cylindrical due to surface irregularities. Moreover, these models only consider the in-plane failure of fibre composites, and do not consider the large fibre strength distributions that are associated with natural plant fibres. In addition, each model is based on the assumption that the produced composite is void-free, and do not incorporate a factor that accounts for the presence of voids. This may lead to strength prediction inaccuracies, as microvoids formed during the composite fabrication can influence the composite properties. All of these factors can account for deviations in composite experimental properties from the theoretical predictions.

Section 2.4.2: Properties of natural plant fibres reinforced polymer composites

Generally, the performance of natural fibre-composite materials depend on several factors such as fibre type, fibre volume fraction, adhesion properties between fibre and matrix, fibre dispersion in matrix, physical and mechanical properties of fibre and matrix, fibre orientation, and fibre length [33]. Therefore, there have been many attempts to investigate the effects of different plant fibres on the properties of polymer composite materials.

E. Rojo et al., [108] have investigated the influence of cellulose fibre content on the properties of resole phenolic composites. The cellulosic fibres were obtained from eucalyptus wood. In order to improve the fibre-matrix adhesion properties, alkali and silane treatments were used to modify the fibre surface characteristics. Then, four different fibre ratios (1, 3, 5, and 7 wt%) were used to reinforce the phenolic resin. It was reported that the maximum tensile and flexural properties of the composites were found at 3 wt% fibre loading. The results also showed that the silane treatment of fibres improved the thermal stability as well as the flexural and tensile properties of the composites. In contrast, it has been found that alkali fibres treatments resulted in reducing the tensile properties of the composites due to the weakening of the fibres and also the poor adhesion between fibre and matrix.

As a function of fibre length and fibre loading, the mechanical properties of short sisal fibres reinforced phenolic composites have been investigated by M. G. Maya et al., [109]. Chopped sisal fibres with different lengths (10, 20, 30, 40, and 50 mm) were used to reinforce the resole phenolic resin, using the simple hand lay-up technique followed by compression moulding. The composites were prepared with different fibre loading: 38, 46, 54 and 70 wt%. It was found that the tensile and impact properties of phenolic resin were significantly improved by incorporating chopped sisal fibres. However, the maximum tensile and impact properties of the composites were noticed at 50 mm fibre length as presented in Table 2-5. Moreover, in the case of varying the fibre loading, the maximum properties were at 54 wt% fibre loading as presented in Table 2-6. The best balance between fibre length and fibre loading in terms of mechanical properties were found in the composites reinforced with 40 mm fibre length and 54 wt% fibre content. It was also found that composites with 54 wt% fibre content show less water uptake when compared with other composite samples. The authors attributed this to the better adhesion properties between sisal fibre and phenolic matrix in the case of containing 54 wt% fibre.

Table 2-5: *Mechanical properties of sisal fibre reinforced phenolic composites as a function of fibre length. Fibre content 54 wt%. Adapted from [109].*

Fiber length (mm)	Tensile strength (MPa)	Tensile modulus (MPa)	Elongation at break (%)	Impact strength (kJ/m^2)
10	30	450	2.8	9.5
20	47	525	3.7	10
30	53	650	6.1	11.1
40	62	920	4.8	12
50	84	1300	5.9	12.7

Table 2-6: *Mechanical properties of sisal fibre reinforced phenolic composites as a function of fibre loading. Fibre length 40 mm. Adapted from [109].*

Fiber loading (wt%)	Tensile strength (MPa)	Tensile modulus (MPa)	Elongation at break (%)	Impact strength (kJ/m^2)
0	10	380	2	6.2
38	45	560	4.4	7.5
46	53	915	4	9
54	60	1100	3.8	9.6
70	51	700	-	14

The tensile, flexural, and impact properties of pseudo stem banana fibre-epoxy composites were investigated by M. Maleque et al., [110]. The composite was fabricated using the simple hand lay-up method. The results showed that the woven fabric of pseudo stem banana fibre increased the ultimate tensile strength and Young's modulus of epoxy composites by 90% and 36% respectively. Moreover, the flexural strength and flexural modulus were increased from 53.38 MPa and 1563.00 MPa to 73.58 MPa and 1834.00 MPa respectively, when the woven fabric used as a reinforcement. Also, the impact strength of the banana woven fabric-epoxy composite was improved by approximately 40% when compared to unreinforced epoxy resin.

S. Josepha et al., [111] have investigated the differences in mechanical properties between phenolic composites reinforced with banana fibres and glass fibres. The composites were prepared using the hand lay-up and compression moulding techniques with changing fibre length and fibre content. The results revealed that the interfacial shear strength (ISS) of single banana fibre pull out test is much higher (44 MPa) than that of single glass fibre (17 MPa), indicating the strong interfacial bond between banana fibre and phenolic resin. Moreover, in terms of mechanical properties, the optimum fibre length for banana fibre/phenolic composites was found to be 30 mm whereas it was 40 mm for glass fibre/phenolic composites due to the better adhesion properties of banana fibres. The authors concluded that the banana fibre/phenolic composites can be used as structural materials due

to their excellent specific properties which could be compared well with glass fibre/phenolic composites.

Section 2.4.3: Characterisation of natural plant fibres reinforced polymer composites

Structural and morphological characterisations of natural plant fibres reinforced polymer composites are very important for the deep understanding of the effects of natural fibres in polymer matrices. Scanning Electron Microscopy (SEM), Fourier Transform Infrared (FTIR) spectroscopy, X-ray diffraction (XRD), and differential scanning calorimetry (DSC) are the most used techniques in characterising plant fibre polymer composites. For instance, Z. Zhou et al., [112] used SEM and X-ray photoelectron spectroscopy to investigate the surface structural and compositional changes of ramie fibres before and after plasma treatment with ethanol pre-treatment. The purpose of the treatment was to improve the adhesion properties of ramie fibres to polypropylene composites. Ramie fibres were first soaked in ethanol for 10 min and then plasma treated for 8, 16, and 24 s. A relatively smooth surface was observed by the SEM images for the untreated ramie fibres with distinguishing longitudinal striations and some impurities on the fibre surface as shown in Figure 2-16a. However, after ethanol pre-treatment and 16 s of plasma treatment, a rougher surface was observed (Figure 2-16b). With increase of the plasma treatment time to 24 s, a large number of pits, cracks, and corrugations were observed on the fibre surface as shown in Figure 2-16c. Moreover, the analysis of X-ray photoelectron spectroscopy of the untreated and plasma treated fibres indicated an increase in the carbon contents from 67.4% to 74.8% when the ramie fibre pre-treated with ethanol and then plasma treated for 16 s. As a results of the fibre surface changes, it was found that after ethanol and plasma treatments, the interfacial shear strength of the ramie fibres to the polypropylene increased by up to 50% compared to the untreated fibre.

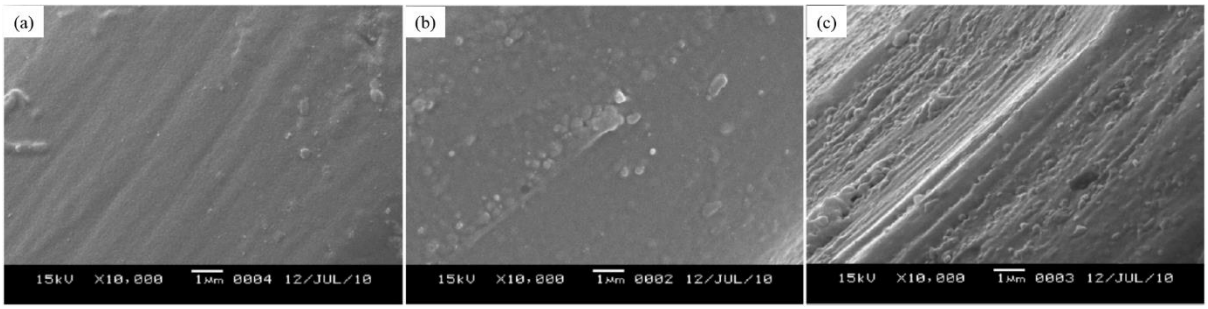

Figure 2-16: *SEM micrographs of untreated and treated ramie fibres: (a) raw ramie fibre, (b) ethanol pre-treatment with plasma treatment for 16 s, and (c) ethanol pre-treatment with plasma treatment for 24 s. Adapted from [112].*

L. Y. Mwaikambo et al., [113] investigated the surface morphology, chemical reactivity, crystallinity index, and thermal characteristics of untreated and alkali treated fibres (hemp, jute, sisal, and kapok) using SEM, FTIR, wide angle X-ray diffraction (WAXRD), and DSC, respectively. SEM micrographs of all untreated fibres revealed a relatively smooth surfaces, however, rougher surfaces were observed after alkali treatment for all different fibres. FTIR results of the treated fibres showed that the most reactive fibre was kapok whereas jute, sisal, and hemp fibres were less reactivity. In terms of crystallinity index, XRD results showed that there was a slight increase in the crystallinity index of jute, sisal, and kapok fibres after alkali treatment while a marginal drop in the crystallinity of hemp fibres. The DSC analysis of all fibres after alkali treatment with NaOH concentration between 0.8 and 8% showed a rapid cellulose degradation, beyond which degradation was found to be marginal. Based on the above results, authors concluded that such changes in the fibre surface properties will effectively improve the fibre-matrix interfacial energy and hence better mechanical and thermal properties of the produced composites.

T.P. Sathishkumar et al., [114] investigated the tensile fracture surface of snake grass fibres reinforced polyester composites using SEM. The SEM micrograph of the fractured composite clearly indicated the pulled out fibres and also some cracks running through the

matrix and fibre-matrix interface as shown in Figure 2-17. This was attributed by the authors to the poor interfacial bonding between fibres and matrix.

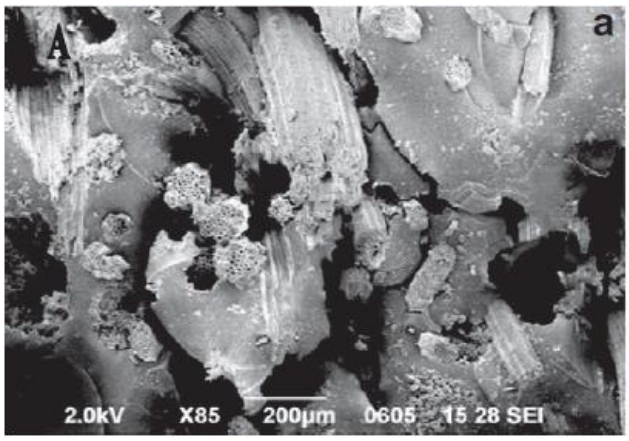

Figure 2-17: *SEM micrograph of the tensile fractured sample of snake grass fibres polyester composite. Adapted from [114].*

X. Yuan, [65] carried out SEM observations on the tensile fracture surface of untreated and plasma treated sisal fibre reinforced polypropylene composites. The SEM micrograph of the untreated fibre polypropylene composite revealed cracks along the fibre matrix interface, indicating the poor adhesion properties between sisal fibre and polypropylene as shown in Figure 2-18a. This is in contrast a better adhesion with no clear interfacial gaps between sisal fibre and matrix was observed for the plasma treated fibre polypropylene composite as shown in Figure 2-18b. This was attributed to the effects of plasma treatment on the fibre surface such as surface roughness and surface chemical composition.

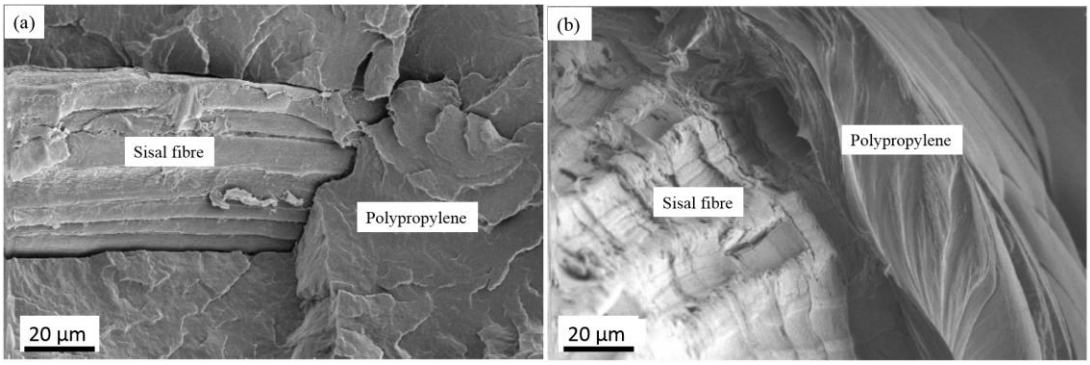

Figure 2-18: *SEM micrographs of the tensile fractured samples of (a) untreated sisal fibres reinforced polypropylene composite and (b) plasma treated sisal fibre reinforced polypropylene composite. Adapted from [65].*

Section 2.4.4: Applications of natural plant fibre composites

The applications of natural plant fibre composites in several engineering fields are growing rapidly nowadays mainly due to their excellent properties such as low specific weight, low production cost, totally biodegradable, relatively good mechanical properties, available and renewable sources when compared to synthetic fibres [115]. The automotive industry is one of the fields where are most widely used of natural plant fibre composites [116]. Natural plant fibre composite components are mainly used in internal parts of automotive such as door panels, dashboards, seat backs, and trunk liners [116]. Moreover, plant fibres have also been utilised in exterior composite components such as engine covers of a Mercedes-Benz Travego [105]. It has been reported that natural plant fibre composites are used in more than 1.5 million vehicles in the USA. Moreover, the marketing of natural plant fibre composites in Europe and North America was reached 685,000 tonnes for the year 2002, which valued at 775 million US dollar [116]. The widespread use of plant fibres composites by automotive industries is not only motivated by reductions in cost, but also by issues related to environmental awareness. For instance, the legislations in Europe & USA have issued a specific directive regarding the deposition fraction of each vehicle at the end-of-life. This directive predetermines 15% the deposition fraction for each vehicle for the year 2005 and then should be gradually reduced to only 5% in the year 2015 [116]. Such regulations have motivated the automotive industries to rely more on natural fibre composite components.

Moreover, the use of natural fibre composite components is not only limited to the automotive industries, but also they have been used in aircraft industry for interior panelling [34]. Also, they have been used in different applications such as structural components, sports, machinery office products, packing, and construction, as well as in electrical and electronic industries [34][117].

Section 2.5: Summary

Natural plant fibres reinforced polymer composites represent an important group of materials for several applications due to their excellent properties. Therefore, these materials are becoming an interest of many researches in the last few years. According to the literature, several studies have been published on investigating the physical, thermal, and mechanical properties of untreated and chemical/physical treated plant fibres reinforced both thermoplastic and thermosetting polymer composites.

However, regarding the fibres, very few studies can be found in the literature have used plasma treatment as a method to produce nanoscale structures for plant fibres which can roughen the fibre surface without affecting or changing the bulk properties. Therefore, we investigated and quantified the effect of plasma surface modification on ramie plant fibres as a potential tool for simple and efficient surface modification and subsequently investigate the relationship between exposed nanostructures, surface wettability, fibre-matrix interlocking, and single fibre mechanical properties

Moreover, amongst thermosetting polymer matrices, phenolic resins present an attractive material for natural plant fibre composites due to their chemical resistance and thermo-mechanical properties. Although of the all studies that have been done so far on phenolic resins, still no existing approaches allow void free microstructures to be achieved with a short cure cycle. Therefore, a novel approach to optimise the microvoids size and distribution in fast curing process for better mechanical properties at minimum processing time is proposed as an alternative here.

Finally, very limited studies can be found in the literature that used ramie fibres as a reinforcement for phenolic resin polymers. Therefore, we presented here a detailed

investigation of the morphological and mechanical properties of untreated and plasma treated ramie fibres reinforced phenolic resin composites.

Section 2.6: References

[1] S. Thomas, S. A. Paul, L. A. Pothan, and B. Deepa, "Natural Fibres: Structure, Properties and Applications," in *Cellulose Fibers: Bio- and Nano-Polymer Composites*, Verlag Berlin Heidelberg, 2011, pp. 3–42.

[2] A. Ticoalu, T. Aravinthan, and F. Cardona, "A review of current development in natural fiber composites for structural and infrastructure applications," in *Southern Region Engineering Conference*, 2010, no. November, pp. 1–5.

[3] H. Cheung, M. Ho, K. Lau, F. Cardona, and D. Hui, "Natural fibre-reinforced composites for bioengineering and environmental engineering applications," *Compos. Part B*, vol. 40, no. 7, pp. 655–663, 2009.

[4] B. Yeoman and L. Paisley, "Out , Out , Brown Spot ; or , Ceiling Tile Alternatives," *Nabe J.*, pp. 16–17, 2005.

[5] U. S. Bongarde and V. D. Shinde, "Review on natural fiber reinforcement polymer composites," *Int. J. Eng. Sci. Innov. Technol.*, vol. 3, no. 2, pp. 431–436, 2014.

[6] S. Kalia, B. S. Kaith, and I. Kaur, "Pretreatments of natural fibers and their application as reinforcing material in polymer composites-a review," *Polym. Eng. Sci.*, vol. 49, no. 7, pp. 1253–1272, 2009.

[7] L. Mohammed, M. N. M. Ansari, G. Pua, M. Jawaid, and M. S. Islam, "A Review on Natural Fiber Reinforced Polymer Composite and Its Applications," *Int. J. ofPolymer Sci. fibers.*, pp. 1–15, 2015.

[8] M. J. John and R. D. Anandjiwala, "Recent Developments in Chemical Modification and Characterization of Natural Fiber-Reinforced Composites," *Polym. Compos.*, vol. 116, no. 1, pp. 187–207, 2008.

[9] L. H. Thomas *et al.*, "Structure of Cellulose Microfibrils in Primary Cell Walls from Collenchyma," *Plant Physiol.*, vol. 161, no. 1, pp. 465–476, 2013.

[10] Y. Nishiyama, U. J. Kim, D. Y. Kim, K. S. Katsumata, R. P. May, and P. Langan,

"Periodic disorder along ramie cellulose microfibrils," *Biomacromolecules*, vol. 4, no. 4, pp. 1013–1017, 2003.

[11] P. Tingaut, T. Zimmermann, and G. Sèbe, "Cellulose nanocrystals and microfibrillated cellulose as building blocks for the design of hierarchical functional materials," *J. Mater. Chem.*, vol. 22, no. 38, pp. 20105–20111, 2012.

[12] D. Klemm, B. Heublein, H. P. Fink, and A. Bohn, "Cellulose: Fascinating biopolymer and sustainable raw material," *Angew. Chemie - Int. Ed.*, vol. 44, no. 22, pp. 3358–3393, 2005.

[13] M. Sorieul, A. Dickson, S. J. Hill, and H. Pearson, *Plant fibre: Molecular structure and biomechanical properties, of a complex living material, influencing its deconstruction towards a biobased composite*, vol. 9, no. 8. 2016.

[14] M. J. John and S. Thomas, "Biofibres and biocomposites," *Carbohydr. Polym.*, vol. 71, no. 3, pp. 343–364, Feb. 2008.

[15] M. Z. Rong, M. Q. Zhang, Y. Liu, G. C. Yang, and H. M. Zeng, "The effect of fiber treatment on the mechanical properties of unidirectional sisal-reinforced epoxy composites," *Compos. Sci. Technol.*, vol. 61, no. 10, pp. 1437–1447, 2001.

[16] A. Komuraiah, N. S. Kumar, and D. Prasad, "Chemical Composition of Natural Fibers and its Influence on Their Mechanical Properties," *Mech. Compos. Mater.*, vol. 50, no. 3, pp. 359–376, 2014.

[17] D. Puglia, C. Santulli, I. M. De Rosa, F. Sarasini, and J. M. Kenny, "Morphological, thermal and mechanical characterization of okra (Abelmoschus esculentus) fibres as potential reinforcement in polymer composites," *Compos. Sci. Technol.*, vol. 70, no. 1, pp. 116–122, 2009.

[18] S. K. Ramamoorthy, M. Skrifvars, and A. Persson, "A review of natural fibers used in biocomposites: Plant, animal and regenerated cellulose fibers," *Polym. Rev.*, vol. 55, no. 1, pp. 107–162, 2015.

[19] N. Rajini, T. Sathishkumar, P. Navaneethakrishnan, S. Shankar, and R. Rajasekar, "Characterization of natural fiber and composites – A review," *J. Reinf. Plast. Compos.*, vol. 32, no. 19, pp. 1457–1476, 2013.

[20] R. M. Rowell, J. S. Han, and J. S. Rowell, “Characterization and factors effecting fibre properties,” *Nat. Polym. Agrofibers Compos.*, pp. 115–134, 2000.

[21] O. Faruk, A. K. Bledzki, H. P. Fink, and M. Sain, “Biocomposites reinforced with natural fibers: 2000-2010,” *Prog. Polym. Sci.*, vol. 37, no. 11, pp. 1552–1596, 2012.

[22] A. Bledzki and J. Gassan, “Composites reinforced with cellulose based fibres,” *Prog. Polym. Sci.*, vol. 24, no. 2, pp. 221–274, 1999.

[23] D. Jones, G. O. Ormondroyd, S. F. Curling, and C. M. Popescu, *Advanced High Strength Natural Fibre Composites in Construction*. Woodhead Publishing Series in Composites Science and Engineering: Number 74 Advanced, 2017.

[24] A. Célino, S. Fréour, F. Jacquemin, and P. Casari, “The hygroscopic behavior of plant fibers: a review,” *Front. Chem.*, vol. 1, no. January, pp. 1–12, 2014.

[25] A. K. Mohanty, M. Misra, and L. T. Drzal, “Surface modifications of natural fibers and performance of the resulting biocomposites: An overview,” *Compos. Interfaces*, vol. 8, no. 5, pp. 313–343, 2001.

[26] K. P. Dasan and A. Sonia, *Nanocellulose Polymer Nanocomposites*. Wiley, 2015.

[27] H. Kobayashi, H. Kaiki, A. Shrotri, K. Techikawara, and A. Fukuoka, “Hydrolysis of woody biomass by a biomass-derived reusable heterogeneous catalyst,” *Chem. Sci.*, vol. 7, no. 1, pp. 692–696, 2016.

[28] A. Bismarck, S. Mishra, and T. Lampke, “Plant Fibers as Reinforcement for Green Composites,” in *Natural Fibers, Biopolymers, and Biocomposites*, A. K. Mohanty, M. Misra, and L. T. Drzal, Eds. aylor & Francis, 2005.

[29] S. Taj, M. Munawar, and S. Ullah Khan, “Natural fiber-reinforced polymer composites,” *Proc. Pakistan Acad. Sci.*, vol. 44, no. 2, pp. 129–144, 2007.

[30] M. Zimniewska, M. Wladyka-Przybylak, and J. Mankowski, “Cellulosic Bast Fibers, Their Structure and Properties Suitable for Composite Applications,” in *Cellulose Fibers: Bio- and Nano-Polymer Composites*, Berlin, Heidelberg: Springer Berlin Heidelberg, 2011, pp. 97–119.

[31] A. Bourmaud, C. Morvan, A. Bouali, V. Placet, P. Perré, and C. Baley, “Relationships

between micro-fibrillar angle, mechanical properties and biochemical composition of flax fibers," *Ind. Crops Prod.*, vol. 44, pp. 343–351, 2013.

[32] M. R. Sanjay, P. Madhu, M. Jawaid, P. Senthamaraikannan, S. Senthil, and S. Pradeep, "Characterization and properties of natural fiber polymer composites: A comprehensive review," *J. Clean. Prod.*, vol. 172, pp. 566–581, 2018.

[33] K. L. Pickering, M. G. A. Efendy, and T. M. Le, "A review of recent developments in natural fibre composites and their mechanical performance," *Compos. Part A Appl. Sci. Manuf.*, vol. 83, pp. 98–112, 2016.

[34] M. P. Ho *et al.*, "Critical factors on manufacturing processes of natural fibre composites," *Compos. Part B Eng.*, vol. 43, no. 8, pp. 3549–3562, 2012.

[35] R. Latif, S. Wakeel, N. Zaman Khan, A. Noor Siddiquee, S. Lal Verma, and Z. Akhtar Khan, "Surface treatments of plant fibers and their effects on mechanical properties of fiber-reinforced composites: A review," *J. Reinf. Plast. Compos.*, vol. 38, no. 1, pp. 15–30, 2019.

[36] H. Y. Choi and J. S. Lee, "Effects of surface treatment of ramie fibers in a ramie/poly(lactic acid) composite," *Fibers Polym.*, vol. 13, no. 2, pp. 217–223, 2012.

[37] A. Celli, S. Kalia, C. L. Schauer, K. Thakur, and M. A. Kiechel, "Surface modification of plant fibers using environment friendly methods for their application in polymer composites, textile industry and antimicrobial activities: A review," *J. Environ. Chem. Eng.*, vol. 1, no. 3, pp. 97–112, 2013.

[38] A. K. Bledzki, A. A. Mamun, M. Lucka-Gabor, and V. S. Gutowski, "The effects of acetylation on properties of flax fibre and its polypropylene composites," *Express Polym. Lett.*, vol. 2, no. 6, pp. 413–422, 2008.

[39] S. Jose, S. Rajna, and P. Ghosh, "Ramie Fibre Processing and Value Addition," *Asian J. Text.*, vol. 7, no. 1, pp. 1–9, 2017.

[40] S. Mitra *et al.*, "Ramie : The Strongest Bast Fibre of Nature," *Tech. Bull. No. 8, Cent. Res. Inst. Jute Allied Fibres*, pp. 1–38, 2013.

[41] P. Banerjee *et al.*, "Evaluation of Ramie Fibre Quality : A Review," *Int. J. Bioresour. Sci.*, vol. 2, no. 1, pp. 65–69, 2015.

[42] M. Ahmed, S. K. Chattopadhyay, A. K. Chaphekar, R. S. Gaikwad, and S. K. Dey, "Characteristics of degummed ramie fibre and its cotton blended yarns," *Indian J. Fibre Text. Res.*, vol. 29, no. 3, pp. 362–365, 2004.

[43] S. N. Pandey, "Ramie fibre: Part II. Physical fibre properties. A critical appreciation of recent developments," *Text. Prog.*, vol. 39, no. 4, pp. 189–268, 2007.

[44] A. Kicińska-Jakubowska, E. Bogacz, and M. Zimniewska, "Review of Natural Fibers. Part I-Vegetable Fibers," *J. Nat. Fibers*, vol. 9, no. 3, pp. 150–167, 2012.

[45] Y. Cui, M. Jia, L. Liu, R. Zhang, L. Cheng, and J. Yu, "Research on the character and degumming process of different parts of ramie fiber," *Text. Res. J.*, vol. 88, no. 17, pp. 2013–2023, 2018.

[46] T. R. Teja, R. D. Venkata, A. L. Naidu, and M. V. A. Bahubalendruni, "Mechanical and chemical Properties of Ramie reinforced composites and manufacturing techniques...A Review Article," *Int. J. Res. Dev. Technol.*, vol. 8, no. 5, pp. 2349–3585, 2017.

[47] R. Kumar, S. Obrai, and A. Sharma, "Chemical modifications of natural fiber for composite material," *Pelagia Res. Libr.*, vol. 2, no. 4, pp. 219–228, 2011.

[48] M. Sood and G. Dwivedi, "Effect of fiber treatment on flexural properties of natural fiber reinforced composites: A review," *Egypt. J. Pet.*, vol. 27, no. 4, pp. 775–783, 2018.

[49] S. H. Aziz and M. P. Ansell, "The effect of alkalization and fibre alignment on the mechanical and thermal properties of kenaf and hemp bast fibre composites: Part 2 - cashew nut shell liquid matrix," *Compos. Sci. Technol.*, vol. 64, no. 9, pp. 1231–1238, 2004.

[50] Z. A. M. Ishak, D. Ariawan, M. S. Salim, R. M. Taib, and A. T. M. Z, "The effect of alkalization on the mechanical and water absorption properties of non-woven kenaf fiber / unsaturated-polyester composites produced by resin-transfer molding (RTM)," in *European Conference on Composite Materials, Seville, Spain, 22-26 June*, 2014.

[51] K. K. Samanta *et al.*, "Effect of Helium-Oxygen Plasma Treatment on Physical and

Chemical Properties of Cotton Textile," *Int. J. Bioresour. Sci.*, vol. 1, no. June, pp. 57–63, 2014.

[52] E. Bozaci *et al.*, "Effects of the atmospheric plasma treatments on surface and mechanical properties of flax fiber and adhesion between fiber-matrix for composite materials," *Compos. Part B Eng.*, vol. 45, no. 1, pp. 565–572, 2013.

[53] M. Radetic, P. Jovancic, N. Puac, and Z. L. Petrovic, "Environmental impact of plasma application to textiles," *J. Phys. Conf. Ser.*, vol. 71, no. 1, 2007.

[54] R. A. Jelil, *A review of low-temperature plasma treatment of textile materials*, vol. 50, no. 18. Springer US, 2015.

[55] T. Okumura, "Inductively coupled plasma sources and applications," *Phys. Res. Int.*, vol. 2010, no. 1, 2010.

[56] F. Fanelli and F. Fracassi, "Atmospheric pressure non-equilibrium plasma jet technology: general features, specificities and applications in surface processing of materials," *Surf. Coatings Technol.*, vol. 322, pp. 174–201, 2017.

[57] K.-Y. Lee, A. Delille, and A. Bismarck, "Greener Surface Treatments of Natural Fibres for the Production of Renewable Composite Materials," in *Cellulose Fibers: Bio- and Nano-Polymer Composites*, Berlin, Heidelberg: Springer Berlin Heidelberg, 2011, pp. 155–178.

[58] C. M. Chan, T. M. Ko, and H. Hiraoka, "Polymer Surface Modification By plasmas and photons," *Surf. Sci. Rep.*, vol. 24, pp. 1–54, 1996.

[59] G. S. choudhary U, Bhattacharyya R, "A Brief Review on Plasma Treatment of Textile Materials," *Adv. Res. Text. Eng.*, vol. 3, no. 1, pp. 1–4, 2018.

[60] D. Sun, "Surface modification of natural fibres using plasma treatment," in *Biodegradable Green Composites*, S. Kalia, Ed. John Wiley & Sons, Inc., 2016, pp. 18–39.

[61] Z. Zhou *et al.*, "Influence of absorbed moisture on surface hydrophobization of ethanol pretreated and plasma treated ramie fibers," *Appl. Surf. Sci.*, vol. 258, no. 10, pp. 4411–4416, 2012.

[62] M. B. Riekerink Olde, “Structural and Chemical Modification of Polymer Surfaces By Gas Plasma Etching,” University of Twente, 2001.

[63] S. Shahidi, M. Ghoranneviss, and B. Moazzenchi, “New advances in plasma technology for textile,” *J. Fusion Energy*, vol. 33, no. 2, pp. 97–102, 2014.

[64] U. Lommatzsch, D. Pasedag, A. Baalmann, G. Ellinghorst, and H. E. Wagner, “Atmospheric pressure plasma jet treatment of polyethylene surfaces for adhesion improvement,” *Plasma Process. Polym.*, vol. 4, no. SUPPL.1, pp. 1041–1045, 2007.

[65] X. Yuan, K. Jayaraman, and D. Bhattacharyya, “Mechanical properties of plasma-treated sisal fibre-reinforced polypropylene composites,” *J. Adhes. Sci. Technol.*, vol. 18, no. 9, pp. 1027–1045, 2004.

[66] X. Yuan, K. Jayaraman, and D. Bhattacharyya, “Effects of plasma treatment in enhancing the performance of woodfibre-polypropylene composites,” *Compos. Part A Appl. Sci. Manuf.*, vol. 35, no. 12, pp. 1363–1374, 2004.

[67] E. Sinha and S. Panigrahi, “Effect of plasma treatment on structure, wettability of jute fiber and flexural strength of its composite,” *J. Compos. Mater.*, vol. 43, no. 17, pp. 1791–1802, 2009.

[68] D. B. Miracle and S. L. Donaldson, “Introduction to Composites,” in *ASM Handbook Composites volume 21*, D. B. Miracle and S. L. Donaldson, Eds. ASM International, 2001, pp. 3–17.

[69] P. K. Mallick, *Fiber- Reinforced Composites, Materials, Manufacturing, and Design*, Third edit. Taylor & Francis Group, 2007.

[70] K. J. Anusavice, R. W. Phillips, C. Shen, and H. R. Rawls, *Phillips’ Science of Dental Materials*, 12th ed. Elsevier/Saunders, 2013.

[71] N. Saba, P. M. Tahir, and M. Jawaid, “A review on potentiality of nano filler/natural fiber filled polymer hybrid composites,” *Polymers (Basel).*, vol. 6, no. 8, pp. 2247–2273, 2014.

[72] M. Asim, N. Saba, M. Jawaid, M. Nasir, M. Pervaiz, and O. Y. Alothman, “A review on Phenolic resin and its Composites,” *Curr. Anal. Chem.*, vol. 14, pp. 1–13, 2018.

[73] T. B. Iyim, “Modification of High Ortho Novolac Resin with Diacids to Improve Its Mechanical Properties,” *J. Appl. Polym. Sci.*, vol. 106, pp. 46–52, 2007.

[74] E. C. Ramires and E. Frollini, “Tannin-phenolic resins: Synthesis, characterization, and application as matrix in biobased composites reinforced with sisal fibers,” *Compos. Part B*, vol. 43, no. 7, pp. 2851–2860, 2012.

[75] J. Zheng, “Studies of PF Resole/Isocyanate Hybrid Adhesives,” 2002.

[76] Y. Shudo, A. Izumi, K. Hagita, T. Nakao, and M. Shibayama, “Structure-mechanical property relationships in crosslinked phenolic resin investigated by molecular dynamics simulation,” *Polymer (Guildf).*, vol. 116, pp. 506–514, 2017.

[77] G. Astarloa Aierbe, J. M. Echeverría, M. D. Martin, A. M. Etxeberria, and I. Mondragon, “Influence of the initial formaldehyde to phenol molar ratio (F/P) on the formation of a phenolic resol resin catalyzed with amine,” *Polymer (Guildf).*, vol. 41, no. 18, pp. 6797–6802, 2000.

[78] C. Mougel, T. Garnier, P. Cassagnau, and N. Sintes-Zydowicz, “Phenolic foams: A review of mechanical properties, fire resistance and new trends in phenol substitution,” *Polymer (Guildf).*, vol. 164, no. November 2018, pp. 86–117, 2019.

[79] M. Niu and G. Wang, “The preparation and performance of phenolic foams modifed by active polypropylene glycol,” *Cell. Polym.*, vol. 32, no. 3, pp. 155–172, 2013.

[80] Y. Yu, Y. Wang, P. Xu, and J. Chang, “Preparation and Characterization of Phenolic Foam Modified with Bio-Oil,” *Materials (Basel).*, vol. 11, pp. 1–10, 2018.

[81] J. D. Megiatto, E. C. Ramires, and E. Frollini, “Phenolic matrices and sisal fibers modified with hydroxy terminated polybutadiene rubber: Impact strength, water absorption, and morphological aspects of thermosets and composites,” *Ind. Crops Prod.*, vol. 31, no. 1, pp. 178–184, 2010.

[82] J. Brown and Z. Mathys, “Plasma surface modification of advanced organic fibres: Part V Part V Effects on themechanical properties of aramid/phenolic composites,” *J. Mater. Sci.*, vol. 32, pp. 2599–2604, 1997.

[83] P. S. Parameswaran, M. G. Bhuvaneswary, and E. T. Thachil, “Control of Microvoids in Resol Phenolic Resin Using Unsaturated Polyester,” *J. Appl. Polym. Sci.*, vol. 113,

pp. 802–810, 2009.

[84] S. H. Goodman, *Handbook of thermoset plastics*, Second edi. Noyes Publications, 1998.

[85] A. Gardziella, L. A. Pilato, and A. Knop, "Economic Significance, Survey of Applications, and Six Bonding Functions," in *Phenolic Resins*, Berlin, Heidelberg: Springer Berlin Heidelberg, 2000, pp. 122–487.

[86] S. Sulaiman, R. Yunus, N. A. Ibrahim, and F. Rezaei, "Effect of Hardener on Mechanical Properties of Carbon Fibre Reinforced Phenolic Resin Composites," *J. Eng. Sci. Technol.*, vol. 3, no. 1, pp. 79–86, 2008.

[87] G. N. Manikandan and K. Bogeshwaran, "Effect of curing time on phenolic resins using latent acid catalyst," *ChemTech Res*, vol. 9, no. 01, pp. 30–37, 2016.

[88] E. S. De Medeiros, a M. Agnelli, K. Joseph, and L. H. De Carvalho, "Curing Behavior of a Novolac-Type Phenolic Resin Analyzed by Differential Scanning Calorimetry," *J. Appl. Polym. Sci.*, vol. 90, pp. 1678–1682, 2003.

[89] K. P. Singh and G. R. Palmese, "Enhancement of phenolic polymer properties by use of ethylene glycol as diluent," *J. Appl. Polym. Sci.*, vol. 91, no. 5, pp. 3096–3106, 2004.

[90] L. Pilato, "Phenolic resins: 100 Years and still going strong," *React. Funct. Polym.*, vol. 73, no. 2, pp. 270–277, 2013.

[91] H. S. L. Ku, F. Cardona, M. Trada, and G. Vigier, "Flexural properties of sawdust reinforced phenolic composites: Pilot study," *J. Appl. Polym. Sci.*, vol. 114, no. 3, pp. 1927–1934, 2009.

[92] J. Wolfrum and G. W. Ehrenstein, "Interdependence between the curing, structure, and the mechanical properties of phenolic resins," *J. Appl. Polym. Sci.*, vol. 74, no. 13, pp. 3173–3185, 1999.

[93] C. Kaynak and C. C. Tasan, "Effects of production parameters on the structure of resol type phenolic resin/layered silicate nanocomposites," *Eur. Polym. J.*, vol. 42, pp. 1908–1921, 2006.

[94] H. Alamri, I. M. Low, and Z. Alothman, “Mechanical, thermal and microstructural characteristics of cellulose fibre reinforced epoxy/organoclay nanocomposites,” *Compos. Part B Eng.*, vol. 43, no. 7, pp. 2762–2771, 2012.

[95] S. S. Nair, S. Wang, and D. C. Hurley, “Nanoscale characterization of natural fibers and their composites using contact-resonance force microscopy,” *Compos. Part A Appl. Sci. Manuf.*, vol. 41, no. 5, pp. 624–631, 2010.

[96] H. N. Dhakal, Z. Y. Zhang, and M. O. W. Richardson, “Effect of water absorption on the mechanical properties of hemp fibre reinforced unsaturated polyester composites,” *Compos. Sci. Technol.*, vol. 67, no. 7–8, pp. 1674–1683, 2007.

[97] I. M. Low *et al.*, “Mechanical and fracture properties of cellulose-fibre-reinforced epoxy laminates,” *Compos. Part A Appl. Sci. Manuf.*, vol. 38, no. 3, pp. 963–974, 2007.

[98] G. Marsh, “Next step for automotive materials,” *Mater. Today*, vol. 6, no. 4, pp. 36–43, 2003.

[99] J. Foulk, D. Akin, R. Dodd, and C. Ulven, “Production of Flax Fibers for Biocomposites,” in *Cellulose Fibers: Bio- and Nano-Polymer Composites*, Berlin, Heidelberg: Springer Berlin Heidelberg, 2011, pp. 61–95.

[100] S. Prabhakaran, V. Krishnaraj, M. Senthil Kumar, and R. Zitoune, “Sound and vibration damping properties of flax fiber reinforced composites,” in *Procedia Engineering*, 2014, vol. 97, pp. 573–581.

[101] Y. Na and G. Cho, “Sound absorption and viscoelastic property of acoustical automotive nonwovens and their plasma treatment,” *Fibers Polym.*, vol. 11, no. 5, pp. 782–789, 2010.

[102] G. Zak, M. Haberer, C. B. Park, and B. Benhabib, “Mechanical properties of short-fibre layered composites: Prediction and experiment,” *Rapid Prototyp. J.*, vol. 6, no. 2, pp. 107–118, 2000.

[103] C. L. Tucker and E. Liang, “Stiffness predictions for unidirectional short-fiber composites: Review and evaluation,” *Compos. Sci. Technol.*, vol. 59, no. 5, pp. 655–671, 1999.

[104] A. Kelly and W. R. Tyson, “Tensile properties of fibre-reinforced metals: Copper/tungsten and copper/molybdenum,” *J. Mech. Phys. Solids*, vol. 13, no. 6, pp. 329–350, 1965.

[105] E. A. O. Al-bahadly, “The Mechanical Properties of Natural Composites,” Swinburne University of Technology, 2013.

[106] H. L. Cox, “The elasticity and strength of paper and other fibrous materials,” *Br. J. Appl. Phys.*, vol. 3, no. 3, pp. 72–79, 1952.

[107] G. W. Beckermann and K. L. Pickering, “Engineering and evaluation of hemp fibre reinforced polypropylene composites: Micro-mechanics and strength prediction modelling,” *Compos. Part A Appl. Sci. Manuf.*, vol. 40, no. 2, pp. 210–217, 2009.

[108] E. Rojo, M. V. Alonso, M. Oliet, B. Del Saz-Orozco, and F. Rodriguez, “Effect of fiber loading on the properties of treated cellulose fiber-reinforced phenolic composites,” *Compos. Part B Eng.*, vol. 68, pp. 185–192, 2015.

[109] M. G. Maya, S. C. George, T. Jose, and M. S. Sreekala, “Mechanical Properties of Short Sisal Fibre Reinforced Phenol Formaldehyde Eco-Friendly Composites,” *Polym. from Renew. Resour.*, vol. 8, no. 1, pp. 27–43, 2017.

[110] M. Maleque, F. Y. Belal, and S. M. Sapuan, “Mechanical properties study of pseudo-stem banana fiber reinforced epoxy composite,” *Arab. J. Sci. Eng.*, vol. 32, no. 2B, pp. 359–364, 2007.

[111] S. Joseph, M. S. Sreekala, Z. Oommen, P. Koshy, and S. Thomas, “A comparison of the mechanical properties of phenol formaldehyde composites reinforced with banana fibres and glass fibre,” *Compos. Sci. Technol.*, vol. 62, pp. 1857–1868, 2002.

[112] Z. Zhou *et al.*, “Hydrophobic surface modification of ramie fibers with ethanol pretreatment and atmospheric pressure plasma treatment,” *Surf. Coatings Technol.*, vol. 205, no. 17–18, pp. 4205–4210, 2011.

[113] L. Y. Mwaikambo and M. P. Ansell, “Chemical modification of hemp, sisal, jute, and kapok fibers by alkalization,” *J. Appl. Polym. Sci.*, vol. 84, no. 12, pp. 2222–2234, 2002.

[114] T. P. Sathishkumar, P. Navaneethakrishnan, and S. Shankar, “Tensile and flexural

properties of snake grass natural fiber reinforced isophthallic polyester composites," *Compos. Sci. Technol.*, vol. 72, no. 10, pp. 1183–1190, 2012.

[115] M. kabir M., W. H., A. T., C. F., and L. K. T., "Effects of Natural Fibre Surface on Composite Properties : a Review," *Energy, Environ. Sustain.*, pp. 94–99, 2011.

[116] D. E. Alves *et al.*, "Ecodesign of automotive components making use of natural jute fiber composites," *J. Clean. Prod.*, vol. 18, pp. 313–327, 2010.

[117] D. Saravana Bavan and G. C. Mohan Kumar, "Potential use of natural fiber composite materials in India," *J. Reinf. Plast. Compos.*, vol. 29, no. 24, pp. 3600–3613, 2010.

Chapter 3: Materials and Methods

A complete and detailed overview of all the materials, techniques, and methods used in this research project is presented in this chapter. As this thesis contains published articles, most of the methods described in this chapter are also included in the articles, respective methods sections.

The experimental work of this project was divided into four parts. The first part investigated the microstructure of different plant fibres. The second part investigated the effects of low pressure plasma treatment on the surface characteristics and fibre strength of ramie fibres. The third part optimised the curing conditions and mechanical properties of the resole phenolic resin. The last part involved the fabrication of the composites and testing their respective properties.

Section 3.1: Materials

Section 3.1.1: Fibres

Different types of plant fibres, i.e., flax (Linum usitatissimum), jute (Corhorus capsularis), sisal (Agave sisalana), and ramie (Boehmeria nivea) fibres were supplied by Wild Fibres store, UK, and used as received for the experiments.

Section 3.1.2: Polymer matrix

In this project, a thermoset resole commercial phenolic resin called Cellobond J2027X was kindly provided by Caleb Technical Products Ltd., UK, and used as a matrix for the composites. In addition, slow action acid catalyst (Cellobond Phencat 382) and fast action acid catalyst (Cellobond Phencat 10) provided by the same company (Caleb Technical Products Ltd., UK) were also used in this study as a curing agents. The physical properties and the curing conditions of the resole phenolic resin as well as the chemical composition of both catalysts (phencat 382 and phencat 10) are presented in details in chapter 6 (respective method section).

Section 3.2: Low pressure plasma surface treatments

In this research project, a Diener electronic Zepto plasma surface cleaner with a borosilicate glass cylindrical chamber and power supply frequency of 40 kHz was used to modify the surface of ramie fibres. Each sample was prepared for the plasma treatment accordingly to the test to be performed (see section 5.2 in chapter 5). Thereafter, the prepared samples were placed inside the chamber and then the chamber was evacuated to 0.1 mbar in order to remove any contaminants from the chamber. After that the chamber was flooded by air and the flow rate was controlled by a flowmeter. The ramie fibres were plasma treated at four different times: 1, 2, 3, and 4 minutes with a plasma power of 100 W and chamber pressure of 0.3 mbar. Plasma treatments and sample preparation were carried out in an environment of 22 ± 3 °C and 40% relative humidity.

Section 3.3: Single fibre tensile testing

The tensile test of untreated and plasma treated single ramie fibres was carried out to evaluate the fibre mechanical properties before and after plasma treatments. For this purpose, a Zwick Roell tensile testing machine with a 500 N load cell was used. The sample preparation for the single fibre tensile testing is presented in details in chapter 5 (respective method section). The test was performed with a constant cross-head displacement rate of 40 %/min and according to the ASTM D 3822-01 standard. The force-strain values were recorded during the test and from these values the fibres ultimate tensile strength and Young's modulus were determined. The tensile properties of single plant fibres can be highly effected by the cross-sectional area measurements [1][2]. Therefore, in this study, two different methods were used to determine the cross-sectional area (for more details, see section 5.2.6 in chapter 5). The tests were carried out at room temperature (22 ± 3 °C).

Section 3.4: Fibre surface wettability measurements

A drop shape analyser instrument (DSA 100-Kruss) was used to evaluate the effect of plasma treatment on the surface wettability of single ramie fibre. Resole type phenolic resin and its slow action acid catalyst (phencat 382) were used as a test liquid in this experiment. This kind of thermoset resins is frequently used as a polymer matrix in natural fibre-composites [3]. The sample preparation and testing procedure for the surface wettability measurements are presented in details in chapter 5 (respective method section). A very basic and commonly used relation (Equation 3.1) describing wettability with respect to the contact angle of a drop in equilibrium with a solid surface was given by Young. It relates the interfacial free energies of the three interfaces the drop comes into contact with, when placed on a solid surface, namely the solid/liquid (γ_{SL}), solid/vapor (γ_{SV}) and liquid/vapor (γ_{LV}) interfaces using the equation below [4]. The line of contact with the three co-existing phases of the system makes an angle of contact (θ) with the surface, as shown in Figure 3-1.

$$\cos\theta = \frac{\gamma_{SV} - \gamma_{SL}}{\gamma_{LV}} \qquad (3.1)$$

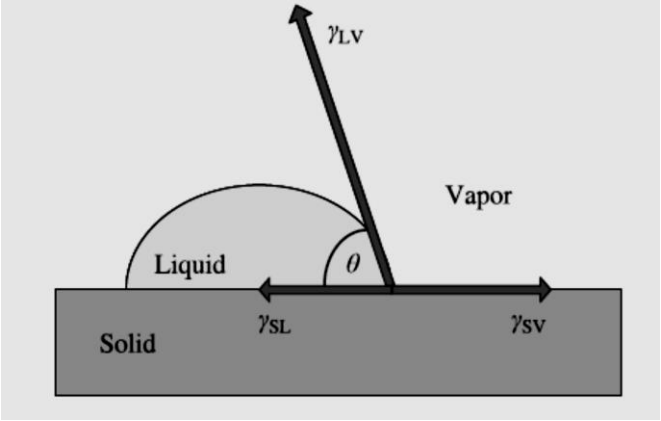

Figure 3-1: *A liquid drop in equilibrium state on a surface, as presented by Young. Adopted from [4].*

The fibre-liquid angle values were taken as the average of at least 3 measurements collected along the fibre surface. However, this is not a standard contact angle determination method as the angles measurements on single fibres are experimentally challenging, almost

impossible to measure due to the high curvature variation at the interface [5]. In order to fully assess the fibre surface wettability and surface adhesion properties in the context of fibre-composites, the experiment was developed by curing the samples using Thermo Scientific Heraeus oven. After that optical microscopy (Nikon Eclipse LV150) was used to observe the fibre-matrix wetting area of the cured samples. Furthermore, the fibre-matrix interface was also observed using Low Voltage Scanning Electron Microscopy (LV-SEM) for all different samples.

Section 3.5: Resole phenolic resin-curing process

Considering the ability of the phenolic resin to be cured either with the application of heat only (using long cure cycle) or with the addition of a curing agent (using short cure cycle), two different curing schedules were used to cure the phenolic resin:

1- Long cure cycle, the as received resole phenolic resin was poured into a PTFE mould and then placed in an autoclave to be cured using the cure cycle presented in chapter 6 (section 6.2.2).

2- Short cure cycle, the as received resole phenolic resin was first mixed with either slow action acid catalyst (phencat 382), or fast action acid catalyst (phencat 10), and then poured into the PTFE mould to be placed in an autoclave using the cure cycle presented chapter 6 (section 6.2.2). The catalyst ratio was maintained at 5 wt% of the resin for all samples.

Section 3.6: Fabrication of the composites

Untreated and plasma treated short-ramie-fibres reinforced phenolic resin composites were fabricated using a method which was based on making mats of randomly oriented short fibres. The procedure of making mats is presented in chapter 7 (respective method section). Two types of phenolic resins were prepared: (1) phenolic resin without the addition of curing agent and (2) phenolic resin with the addition of fast action acid catalyst (phencat 10). The

prepared resins were then poured on the already prepared mats and then placed in the autoclave to be cured using the two different curing cycles depending on the resin type. The content of ramie fibres for each fabricated composites was 10%, 15%, and 20 % by weight.

Section 3.7: Flexural properties

The flexural test (three point bending) was carried out to evaluate the mechanical properties of phenolic resins as well as the properties of short-ramie-fibre-phenolic composite samples. The test was performed using a Lloyd TA500 tensometer in accordance with ASTM D790 (standard test methods for flexural properties of unreinforced and reinforced plastics and electrical insulating materials). The tests were carried out at room temperature (22 ± 3 °C) with crosshead speed of 2.0 mm/min.

The ultimate bending results (strength and modulus) of all specimens were obtained as an average of seven specimens per test condition.

Section 3.8: Low Voltage Scanning Electron Microscopy (LV-SEM)

Polymers are generally susceptible to beam-induced radiation damage and, as non-conductors, they charge heavily under the scanning electron microscope (SEM) beam. An extremely efficient alternative for the analysis of polymers is the field emission gun (FEG) source, low-voltage scanning electron microscope (LVSEM). The high brightness produced by the FEG allows the electron probe to be focused down to nanometre dimensions yet still retain enough intensity to produce usable signal levels. Furthermore, the high probe intensity produces acceptable signal intensities at very low accelerating voltages (nominally l-2 kV). This affords major advantages such as negligible beam damage of samples and absence of the need for coating samples with conducting films to eliminate sample charging under the beam. The latter is a double advantage for a high-resolution instrument because at high magnifications one wants information about the ‘neat’ surface, not the detailed morphology of the coating [6]. Therefore, in this study, LV-SEM (FEI Nova Nano SEM 450) was used to observe the microstructure of different plant fibres (flax, jute, sisal, and ramie) as well as

the surface morphology of untreated and plasma treated single ramie fibres. Moreover, the tensile fractured surfaces of the single ramie fibres were observed using LV-SEM. In addition, the LV-SEM technique was also used for the morphology observation of the flexural fractured surfaces of phenolic resins and its composites. The observations were performed using a low accelerating voltage (1 kV) with a typical vacuum pressure of 10^{-5} mbar and a working distance of about 4-4.5 mm. Secondary electron images were collected using two different detectors: Everhart-Thornley Detector (ETD) for low magnification images and Through-Lens Detector (TLD) for high magnification images.

Section 3.9: Fourier Transform Infrared Spectroscopy (FTIR)

Infrared spectroscopy is the method which scientists use to determine the structures of molecules with the molecules' characteristic absorption of infrared radiation. Infrared spectrum is molecular vibrational spectrum. The IR spectrum is commonly presented as transmittance versus wave number. Functional groups have their characteristic fundamental vibrations which give rise to absorption at certain frequency range in the spectrum as shown in Figure 3-2a-b. However, several functional groups may absorb at the same frequency range, and a functional group may have multiple-characteristic absorption peaks, especially for 1500-650 cm^{-1}, which is called the fingerprint region (Figure 3-2b). The fingerprint region is often the most complex and confusing region to interpret, and is usually the last section of a spectrum to be interpreted. However, the utility of the fingerprint region is that the many bands there provide a fingerprint for a molecule. Each band in a spectrum can be attributed to stretching or bending mode of a bond. Almost all the fundamental vibrations appear in the mid-infrared region (4000 ~ 400 cm^{-1}) because the absorption radiation of most organic compounds and inorganic ions is within this region . Hence, characterisation of functional groups in substances according to the frequencies and intensities of absorption peaks is feasible, and also structures of molecules can be proposed [7].

In this study a PerkinElmer Frontier spectrometer was used to investigate the surface chemical compositions of untreated and plasma treated ramie fibres in ATR mode (detail of sample preparation and experimental procedure are presented in chapter 5, respective method section). In addition, the same spectrometer was also used to investigate the chemical composition of all cured phenolic resins using the KBr pellet method (detail of sample preparation and experimental procedure are presented in chapter 6, respective method section). In both cases, the tests were performed at room temperature (22 ± 3 °C) with a wavenumber range between 4000 cm^{-1} and 600 cm^{-1}.

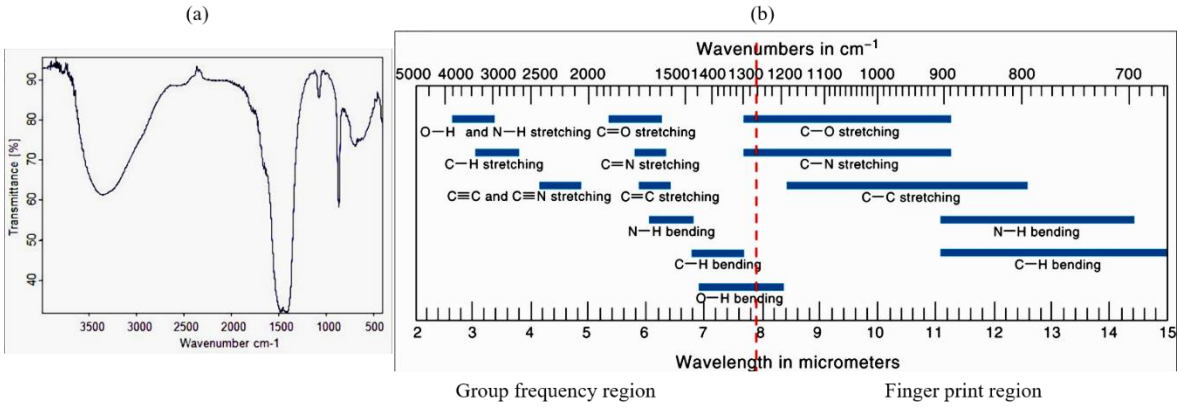

Figure 3-2: *(a) IR Spectrum and (b) Its correlation in characterisation of functional group in substance. Adapted from [7].*

Section 3.10: References

[1] N. M. Everitt, N. T. Aboulkhair, and M. J. Clifford, "Looking for Links between Natural Fibres' Structures and Their Physical Properties," in *Conference Papers in Materials Science*, 2013, pp. 1–10.

[2] J. L. Thomason, J. Carruthers, J. Kelly, and G. Johnson, "Fibre cross-section determination and variability in sisal and flax and its effects on fibre performance characterisation," *Compos. Sci. Technol.*, vol. 71, no. 7, pp. 1008–1015, 2011.

[3] M. Asim, N. Saba, M. Jawaid, M. Nasir, M. Pervaiz, and O. Y. Alothman, "A review on Phenolic resin and its Composites," *Curr. Anal. Chem.*, vol. 14, pp. 1–13, 2017.

[4] D. K. Sarkar and M. Farzaneh, "Superhydrophobic coatings with reduced ice

adhesion," *J. Adhes. Sci. Technol.*, vol. 23, no. 9, pp. 1215–1237, 2009.

[5] S. Rebouillat, B. Letellier, and B. Steffenino, "Wettability of single fibres - beyond the contact angle approach," *Int. J. Adhes. Adhes.*, vol. 19, no. 4, pp. 303–314, 1999.

[6] J. H. Butler, D. C. Joy, G. F. Bradley, and S. J. Krause, "Low voltage scanning electron microscopy of polymers," *Polymer (Guildf).*, vol. 36, no. 9, pp. 1781–1790, 1995.

[7] T. N. Shaikh and S. A. Agrawal, "Qualitative and Quantitative Characterization of Textile Material by Fourier Transform Infra-Red. A Brief Review," *Int. J. Innov. Res. Sci. Eng. Technol.*, vol. 3, no. 1, pp. 8496–8502, 2014.

Chapter 4: Low-Voltage SEM of Natural Plant Fibres: Microstructure Properties (Surface and Cross-Section) and their Link to the Tensile Properties

Procedia Engineering 200 (2016)

Sameer F. Hamad*, Nicola Stehling, C. Holland, J. P. Foreman, C. Rodenburg

Department of Materials Science and Engineering, The University of Sheffield, UK

This chapter has been published as a conference paper in Procedia Engineering, Elsevier. I performed all the experimental work contained within, including sample preparation, mechanical testing, SEM imaging, and wrote the initial draft.

Abstract: In this study, the microstructure of different natural plant fibres (flax, jute, ramie, and sisal fibres) were characterised by using low-voltage Scanning Electron Microscopy (LV-SEM). The LV-SEM observations indicated that jute and sisal fibres exhibit less variation in terms of the fibre cross-sectional area, internal lumen shape and size, and cell wall thickness in comparison to flax and ramie fibres. We find that this is also reflected in the tensile properties of the fibres. The tensile properties of single ramie fibres and their fracture behaviour was investigated in detail. The stress-strain behavior showed two distinctive regimes. For linear curves, the tensile strength varies from 648-1086 MPa whereas nonlinear curves result in much lower values (177-452) MPa. This variation was linked to differences in the microstructure of the fibers. The LV-SEM of the tensile fracture surfaces of ramie fibres revealed details on the cell wall structure and its fracture behaviour under tensile load. Moreover, the SEM images confirm that the collapse of the primary cell wall generally leads to a non-linear stress-strain curve for single ramie fibres.

Section 4.1: Introduction

Natural plant fibres such as jute, flax, hemp, sisal, and ramie fibres are increasingly being used as reinforcements in polymer matrix composites [1], due to their wide availability, low cost, eco-friendliness, low density, and high specific mechanical properties [2][3]. Moreover, the high density, non-recyclability, health hazards, high energy consumption and environmental issues of synthetic fibres [4][5] have motivated many researchers to investigate sustainable materials. Natural plant fibres represent a renewable resource and form an interesting class of reinforcing materials, which can be used as a replacement for synthetic fibres in polymer composites [5].

However, the mechanical properties of natural plant fibres typically vary over a large range [6]–[9], partly due to variability typical for biological samples, but also due to errors arising from testing techniques [3][6]. Natural plant fibres have a complex structure and organization, which can be considered as a natural composite material consisting of cellulose fibrils embedded in an amorphous matrix of hemicellulose and lignin [2][3][6][10]. The single plant fibres have a typical structure that consists of a central lumen surrounded by a thick cell wall [2]. The fiber cell wall is formed from two main layers: a very thin primary cell wall (70-110 nm) [11], and a secondary cell wall, which is made up of three sub-layers (S1, S2, and S3) [7]. S2 is the thickest layer (3-13 μm thick) [11] in the cell wall and represents the most important layer which determines the mechanical properties of the fibres [12][13]. Each layer of the fibre cell wall is composed mainly of cellulose, hemicellulose and lignin [7][14]. The long chain cellulose molecules, often referred to as microfibrils, are organized in a crystalline network [7]. The typical diameter of these microfibrils are in the range of 10-30 nm and they are made up of 30-100 of cellulose molecules in the form of an extended chain. The microfibrils greatly contribute to the mechanical strength of the fibres

[15][16], and thus the complex structure of natural plant fibres can highly influence the fibre properties.

Fibre singular testing techniques also can influence the apparent fibre properties. The reported tensile properties of single fibres are highly effected by the cross-sectional area [6][8][9]. Some of the variation in tensile properties commonly reported in the literature are likely due to inaccurate cross-sectional area measurements of single fibres. The assumption that natural plant fibres have a uniform and circular cross sectional area is the most common method employed in the literature to calculate the cross-sectional area of single fibres [6][7][17]–[19]. Most natural plant fibres exhibit considerable deviation from circularity in their cross-sectional area [7], therefore, the conventional method which is based on the fibre diameter measurement may not be a suitable method to calculate the cross-sectional area. For example, Thomason and Carruthers [8], found that the average values of the cross-sectional area obtained from the fibre diameter measurements of flax and sisal fibres are almost double that of the actual cross-sectional area, leading to the underestimation of tensile properties by up to 60% . Hu et al. [20] also reported that the conventional method of cross-sectional area measurements leads to inaccurate results with high standard deviations.

The review of the literature shows that fibre microstructure and also the fibre testing techniques can highly influence the fibre properties. Therefore, this study aims to investigate the microstructure of different natural plant fibres (flax, jute, ramie, and sisal fibres) by using low voltage scanning electron microscopy (LV-SEM). The link between fibre microstructure and property variations of these fibres was also studied. The tensile testing of single ramie fibres followed by SEM observations of the fractured fibres indicated details on the fibre microstructure and mechanical properties of the cell wall. The true cross-sectional area of single ramie fibres was measured by analysis of LV-SEM images using image J software.

The obtained tensile strength results were compared to other reported results assuming circularity, in terms of standard deviations.

Section 4.2: Materials and experimental procedure

Flax, Jute, ramie, and sisal fibres were used in this study. The as received fibres were cryo-fractured in order to investigate the fibre cross-section structure. A LV-SEM (Nova Nano SEM 450) was used to observe the fibre microstructure. Natural plant fibres are not conductive materials, therefore, the observations were performed using a low accelerating voltage (1 kV) to avoid fibre charging. The images were collected using a through lens detector (TLD) at 4.5 mm working distance with a beam deceleration of 2000 V.

A Zwick Roll tensile testing machine with a 500 N load cell was used to test the tensile strength of single ramie fibres. The test was carried out at a constant crosshead displacement rate of 40 %/min. In accordance with the ASTM D 3822-01 standard the single ramie fibre was mounted on the paper card with a 5 mm gauge length by using cyanoacrylate glue. The fibres were carefully glued in the exact centre of the card as shown in Figure 4-1. Thereafter, samples were loaded into the testing machine and just before starting the test, the supporting side of the card was carefully cut. The tests were carried out at room temperature (22 ± 3 °C). During the test the force-strain values were recorded and these values were used to measure the fibre tensile strength properties. Only samples which broke in the middle of their gauge length were used to calculate the tensile strength, whereas the fibres which broke near to the glue clamp or card frame were not used in the calculations.

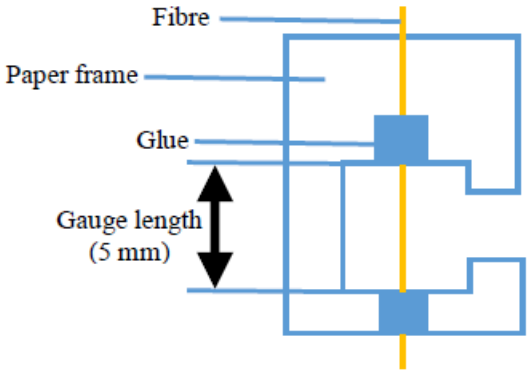

Figure 4-1: *Schematic representation of the paper frame for the single fibre tensile testing.*

After testing, the cross-sectional area can be estimated from the fractured sample due to the elastic behaviour of the plant fibres. LV-SEM was used to observe the cross-section of the fractured fibres, as shown in Figure 4-2. Fractured fibres with a flat and clear cross-section were selected for the cross-section area calculations. The SEM images were used to calculate the actual cross-sectional area of the fractured fibres by using image J software. The hollow structure (lumen) can be clearly seen as demonstrated in the example in Figure 4-2. This area was found to be about 10% of the total cross-sectional area and was excluded from the total area.

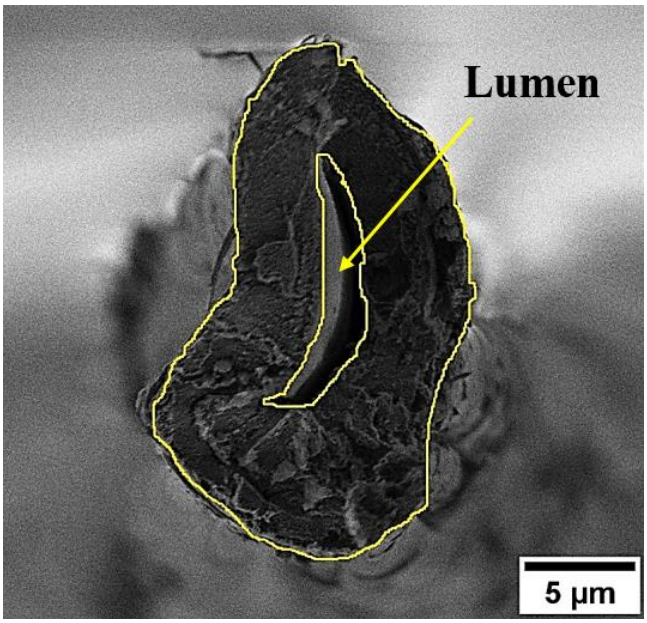

Figure 4-2: *Cross-sectional area determination of single ramie fibre using image J software.*

Section 4.3: Results and Discussion

Section 4.3.1: Microstructure comparison of different fibres

The SEM images of the cross-sections of flax, jute, ramie, and sisal fibres are shown in Figure 4-3. It can be seen that jute and sisal fibres are in the form of a bundle, that the single fibres are combined by means of middle lamella (ML). The flax fibres are in a partly separated bundle exposing the single fibres, and the ramie is in the form of a single fibre. All fibres show similar structures, comprising a lumen in the centre which is surrounded by several cell walls. We observe that the cross-section shape, cell wall thickness, internal lumen size and shape vary substantially for the different materials. For instance, our flax and ramie fibres show irregular internal lumen shape and more polygonal fibre cross-section. In contrast, jute and sisal fibres show similar structure in terms of cross-section shape and the internal lumen shape and size are almost circular. Analysis of the tensile strength data in the literature [21] shows that jute and sisal fibres have smaller variations in reported tensile strength values than flax and ramie fibres (Figure 4-4), which we believe could be due to the greater variation in fibre microstructure of the flax and ramie fibres, as indicated by SEM observations. In addition, the higher density and strength of flax fibres reported in the literature [21], could partly be explained due to the smaller lumen and dense cell wall structure compared to other fibres.

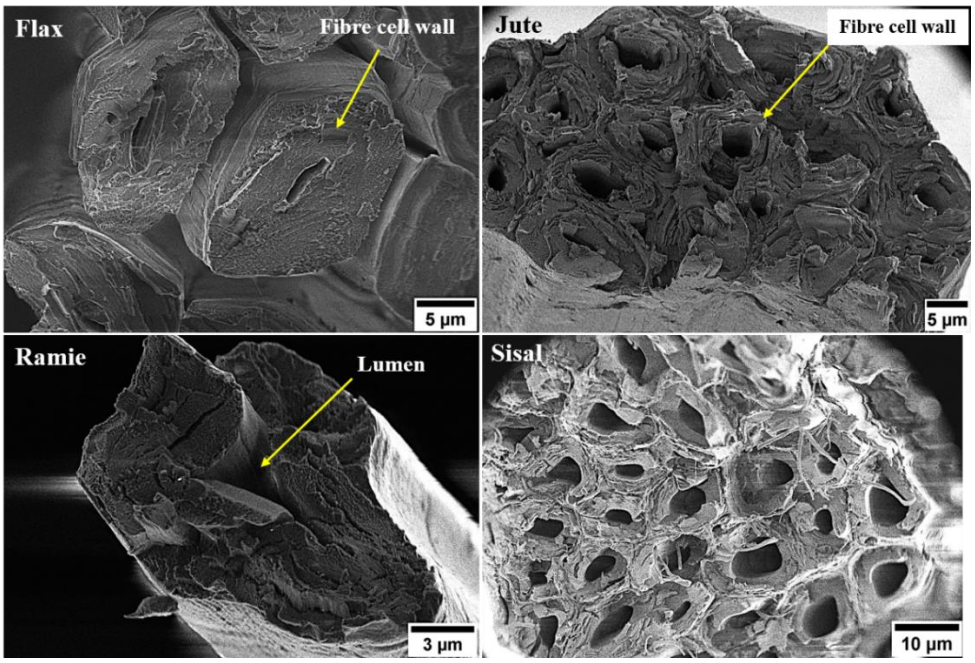

Figure 4-3: *SEM images of the cross-section of flax, ramie, jute, and sisal fibres.*

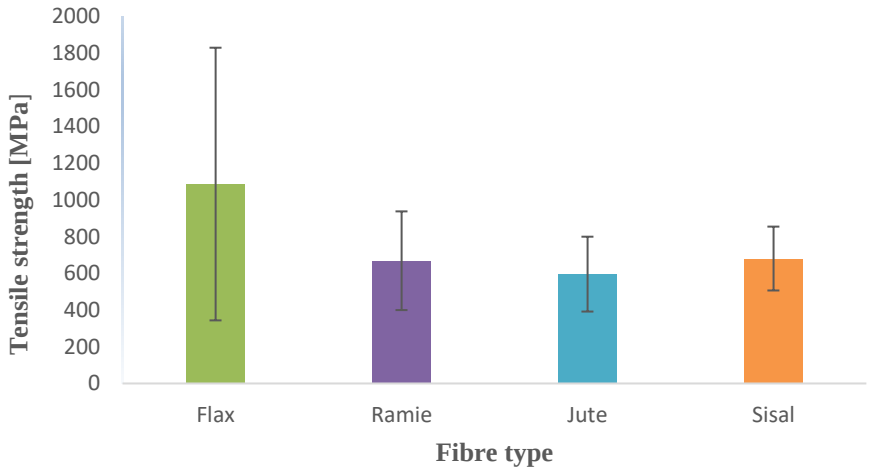

Figure 4-4: *Bars represent the relative variation, and error bars represent the range of the tensile strength values of flax, ramie, jute, and sisal fibres based on data reported in [21].*

Section 4.3.2: ***Microstructure of ramie fibres visible on tensile fracture surfaces***

30 single ramie fibres were investigated after tensile fracture. The LV-SEM observations of the cell wall structure of ramie fibres followed by image J analysis showed that the thickness of the primary wall was approximately 100 nm, as shown in Figure 4-5a,b. This is in the range of primary wall thickness reported for hemp fibres [11]. It can also be seen from Figure 4-5a, that the secondary cell wall main consists of two phases: (1) bright nanoscale features (~ 30-70 nm), and (2) the dark phase in between. Based on literature reports that fibre cell

wall can be considered as a natural composite [22], the bright nanostructures features would be expected to be crystalline cellulose microfibrils embedded in non-crystalline regions of hemicellulose and lignin (Figure 4-5a). The observed cracks between the layers of the cell wall (Figure 4-5a), are possibly due to the interlaminar stress which formed during the fracture process.

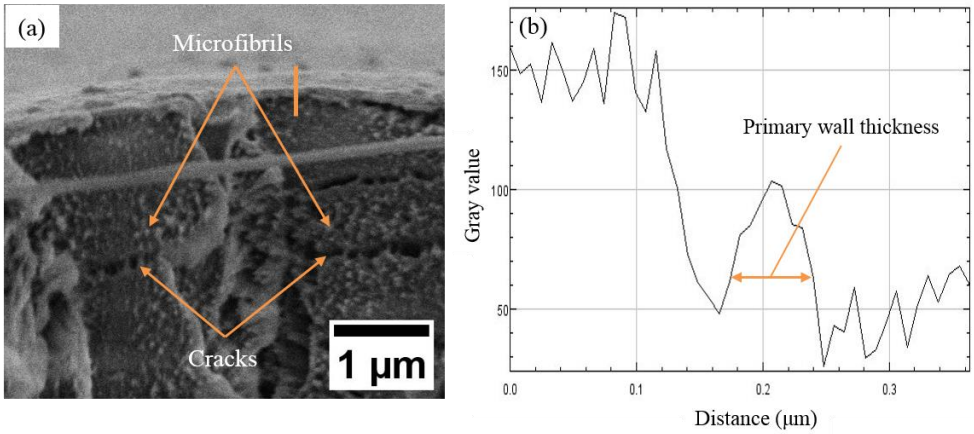

Figure 4-5: *(a) SEM image of the cell wall of ramie fibre, (b) the line profile of the orange vertical line in* ***Figure 4-5****a.*

Section 4.3.3: ***Fracture behaviour of single ramie fibres under tensile load***

The typical stress-strain behaviour of a single ramie fibre in the tensile test is demonstrated in Figure 4-6a. It can be seen that the curve is almost linearly elastic without any signs of plastic deformation. Similar behaviour and shape of plots were found for plant fibres reported in other works [6][23][24]. The LV-SEM observations of the fractured fibres showed a very flat and clear fracture end (Figure 4-7a). However, some of the tested fibres showed two regions (non-linear) of the stress-strain curve (Figure 4-6b). Mukherje [25] reported that the initial region of the stress-strain curve of sisal fibres is mostly due to the collapses of the weak primary cell wall and decohesion between fibre cells. The SEM observations in this work clearly show the collapse of the primary cell wall, as illustrated in Figure 4-7b. Such fibres were found to have lower strength values than those with a linear stress-strain curve, which is possibly due to the defects and cracks that already present in the cell wall as well as the weak bond between the primary and secondary wall. On the other

hand, some other tested fibres showed that different fibre cells have fractured in different planes (Figure 4-8). According to Silva [26], this behaviour of fibre cells is probably due to the variability in the fibre cell strength and also due to cell wall flaws. Such fibres showed a linear stress-strain curve. These variations in the fibre cell wall fracture can strongly influence the fibre properties and therefore large scatter was found in the values of the tensile strength of ramie fibres in this study. However, the standard deviation of the tensile strength values obtained from linear curves only in this study was (872 ± 190) MPa considerably lower than that reported elsewhere [27] as (936 ± 320) MPa. We believe this is due to the more accurate method used to calculate the cross-sectional area of single fibres.

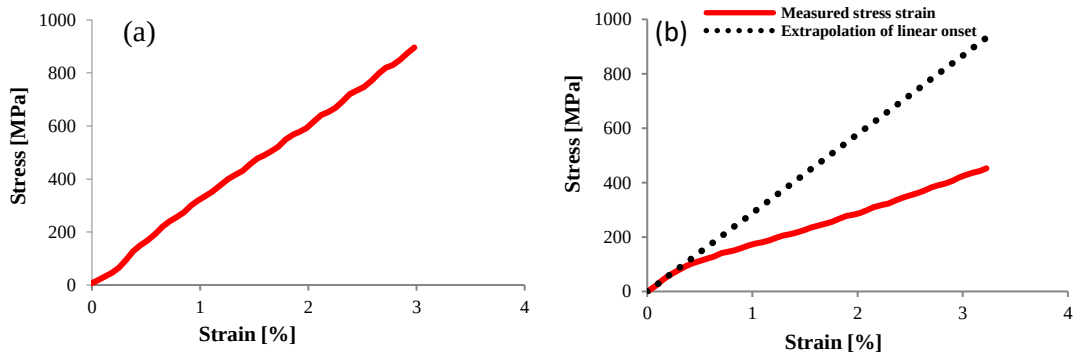

Figure 4-6: *The stress-strain curve of the single ramie fibre (a) example of linear curve, (b) example of non-linear curve, the extrapolation of the linear onset results in curve very similar to (a), the beginning of the deviation from this curve might indicate primary wall failure.*

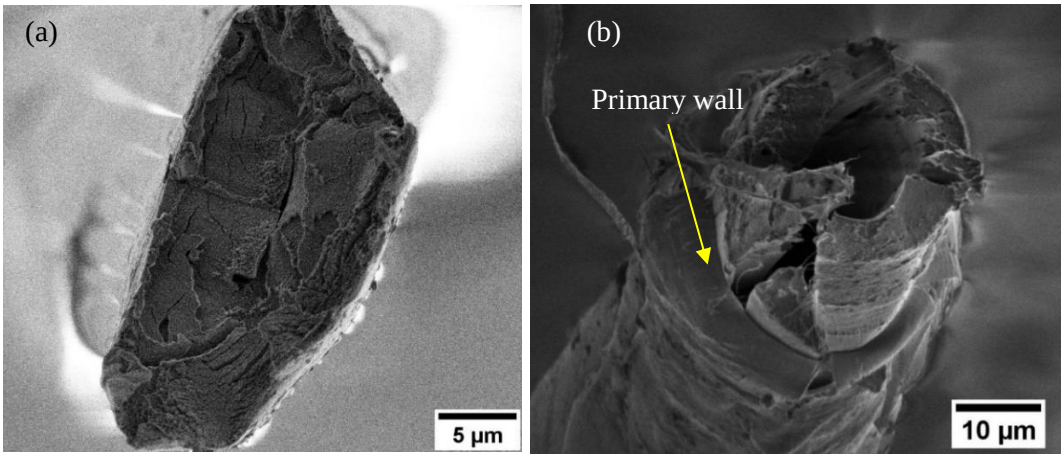

Figure 4-7: *SEM images of the fractured surface of single ramie fibres under tensile load (a) fractured in a flat surface, (b) showing the collapse and retraction of the weak primary wall and subsequent protrusion of the secondary wall.*

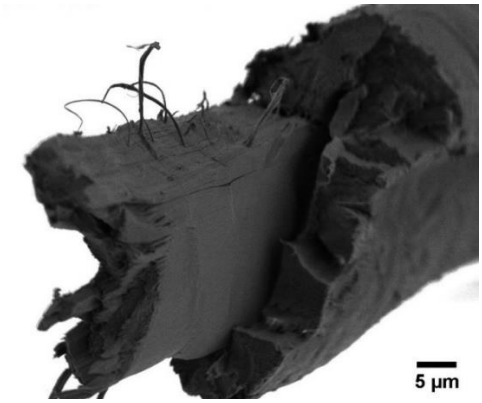

Figure 4-8: *SEM image of the fractured surface of single ramie fibre under tensile load showing different fibre cells have fractured in different planes.*

Section 4.4: Conclusions

LV-SEM observations in this work showed that the jute and sisal fibres exhibit less variation in their microstructure than those of flax and ramie fibres. This can be reflected on their mechanical properties. Detailed investigation for example of ramie fibre shows that some variation is due to differences in fracture behaviour (e.g. collapse of primary wall and variability in cell wall strength), but further variation might be due to the methods of cross-sectional area measurement. The latter can be minimized through the use of our LV-SEM technique. Hence, LV-SEM is powerful tool for the understanding of the fracture behavior of plant fibres.

Acknowledgements

S. Hamad thanks the Iraqi Ministry of Higher Education and Scientific Research, University of Misan. C. Rodenburg and C. Holland thank EPSRC (EP/N008065/1), (EP/K005693/1) respectively.

Section 4.5: References

[1] E. Poriķe and J. Andersons, “Strength-length scaling of elementary hemp fibers,” *Mech. Compos. Mater.*, vol. 49, no. 1, pp. 69–76, 2013.

[2] A. Célino, S. Fréour, F. Jacquemin, and P. Casari, “The hygroscopic behavior of plant fibers: a review,” *Front. Chem.*, vol. 1, no. January, pp. 1–12, 2014.

[3] K. Oksman, A. P. Mathew, R. Långström, B. Nyström, and K. Joseph, “The influence

of fibre microstructure on fibre breakage and mechanical properties of natural fibre reinforced polypropylene," *Compos. Sci. Technol.*, vol. 69, no. 11–12, pp. 1847–1853, 2009.

[4] D. M. Matoke, G. M.; Owido, S.F.; Nyaanga, "Effect of Production Methods and Material Ratios on Physical Properties of the Composites," *Am. Int. J. Contemp. Res.*, vol. 2, no. 2, pp. 208–213, 2012.

[5] M. Thiruchitrambalam, A. Athijayamani, S. Sathiyamurthy, and A. Syed Abu Thaheer, "A review on the natural fiber-reinforced polymer composites for the development of roselle fiber-reinforced polyester composite," *J. Nat. Fibers*, vol. 7, no. 4, pp. 307–323, 2010.

[6] N. M. Everitt, N. T. Aboulkhair, and M. J. Clifford, "Looking for Links between Natural Fibres' Structures and Their Physical Properties," in *Conference Papers in Materials Science*, 2013, vol. 2013, pp. 1–10.

[7] V. Placet, F. Trivaudey, O. Cisse, V. Gucheret-Retel, and M. L. Boubakar, "Diameter dependence of the apparent tensile modulus of hemp fibres: A morphological, structural or ultrastructural effect?," *Compos. Part A Appl. Sci. Manuf.*, vol. 43, no. 2, pp. 275–287, 2012.

[8] J. L. Thomason, J. Carruthers, J. Kelly, and G. Johnson, "Fibre cross-section determination and variability in sisal and flax and its effects on fibre performance characterisation," *Compos. Sci. Technol.*, vol. 71, no. 7, pp. 1008–1015, 2011.

[9] J. R. M. D'Almeida, M. H. P. Mauricio, and S. Paciornik, "Evaluation of the cross-section of lignocellulosic fibers using digital microscopy and image analysis," *J. Compos. Mater.*, vol. 46, no. 24, pp. 3057–3065, 2012.

[10] W. Gindl, H. S. Gupta, T. Schöberl, H. C. Lichtenegger, and P. Fratzl, "Mechanical properties of spruce wood cell walls by nanoindentation," *Appl. Phys. A Mater. Sci. Process.*, vol. 79, no. 8, pp. 2069–2073, 2004.

[11] A. Thygesen, G. Daniel, H. Lilholt, and A. B. Thomsen, "Hemp Fiber Microstructure and Use of Fungal Defibration to Obtain Fibers for Composite Materials," *J. Nat. Fibers*, vol. 2, no. 4, pp. 19–37, 2006.

[12] M. J. John and R. D. Anandjiwala, “Recent Developments in Chemical Modification and Characterization of Natural Fiber-Reinforced Composites,” *Polym. Compos.*, vol. 116, no. 1, pp. 187–207, 2008.

[13] S. Kalia *et al.*, “Cellulose-based bio- and nanocomposites: A review,” *Int. J. Polym. Sci.*, vol. 2011, 2011.

[14] S. Andersson, R. Serimaa, T. Paakkari, P. SaranpÄÄ, and E. Pesonen, “Crystallinity of wood and the size of cellulose crystallites in Norway spruce (Picea abies),” *J. Wood Sci.*, vol. 49, no. 6, pp. 531–537, 2003.

[15] S. Thomas, S. A. Paul, L. A. Pothan, and B. Deepa, “Natural Fibres: Structure, Properties and Applications,” in *Cellulose Fibers: Bio- and Nano-Polymer Composites*, I. Kalia, S., Kaith, B. S., Kaur, Ed. Springer-Verlag Berlin Heidelberg, 2011, pp. 3–42.

[16] S. Kalia, B. S. Kaith, and I. Kaur, “Pretreatments of natural fibers and their application as reinforcing material in polymer composites-a review,” *Polym. Eng. Sci.*, vol. 49, no. 7, pp. 1253–1272, 2009.

[17] F. Tomczak, T. H. D. Sydenstricker, and K. G. Satyanarayana, “Studies on lignocellulosic fibers of Brazil. Part II: Morphology and properties of Brazilian coconut fibers,” *Compos. Part A Appl. Sci. Manuf.*, vol. 38, no. 7, pp. 1710–1721, 2007.

[18] I. M. De Rosa, J. M. Kenny, D. Puglia, C. Santulli, and F. Sarasini, “Morphological, thermal and mechanical characterization of okra (Abelmoschus esculentus) fibres as potential reinforcement in polymer composites,” *Compos. Sci. Technol.*, vol. 70, no. 1, pp. 116–122, 2009.

[19] K. L. Pickering, G. W. Beckermann, S. N. Alam, and N. J. Foreman, “Optimising industrial hemp fibre for composites,” *Compos. Part A Appl. Sci. Manuf.*, vol. 38, no. 2, pp. 461–468, 2007.

[20] W. Hu, M.-T. Ton-That, F. Perrin-Sarazin, and J. Denault, “An Improved Method for Single Fiber Tensile Test of Natural Fibers,” *Polym. Eng. Sci.*, pp. 819–825, 2010.

[21] K. L. Pickering, M. G. A. Efendy, and T. M. Le, “A review of recent developments

in natural fibre composites and their mechanical performance," *Compos. Part A Appl. Sci. Manuf.*, vol. 83, pp. 98–112, 2016.

[22] R. K and D. S, "A review - future aspect of natural fiber reinforced composite," *Polym. from Renew. Resour.*, vol. 7, no. 2, pp. 43–60, 2016.

[23] L. Osorio, E. Trujillo, A. W. Van Vuure, and I. Verpoest, "Morphological aspects and mechanical properties of single bamboo fibers and flexural characterization of bamboo/ epoxy composites," *J. Reinf. Plast. Compos.*, vol. 30, no. 5, pp. 396–408, 2011.

[24] A. Shahzad, "A study in physical and mechanical properties of hemp fibres," *Adv. Mater. Sci. Eng.*, vol. 2013, pp. 1–9, 2013.

[25] P. S. Mukherjee and K. G. Satyanarayana, "Structure and properties of some vegetable fibres. Part 1: Sisal fibre," *J. Mater. Sci.*, vol. 19, pp. 3925–3934, 1984.

[26] F. de A. Silva, N. Chawla, and R. D. de T. Filho, "Tensile behavior of high performance natural (sisal) fibers," *Compos. Sci. Technol.*, vol. 68, no. 15–16, pp. 3438–3443, 2008.

[27] Z. Zhou *et al.*, "Hydrophobic surface modification of ramie fibers with ethanol pretreatment and atmospheric pressure plasma treatment," *Surf. Coatings Technol.*, vol. 205, no. 17–18, pp. 4205–4210, 2011.

Chapter 5: Exploiting Plasma Exposed, Natural Surface Nanostructures in Ramie Fibres for Polymer Composite Applications

Materials, MDPI 1631 (2019)

Sameer F. Hamad[1,2,*], Nicola Stehling[1], Simon A. Hayes[3], Joel P. Foreman[1] and C. Rodenburg[1]

[1] Department of Materials Science and Engineering, The University of Sheffield, Sheffield S1 3JD, UK; nastehling1@sheffield.ac.uk (N.S.); j.foreman@sheffield.ac.uk (J.P.F.); c.rodenburg@sheffield.ac.uk (C.R.)
[2] College of Engineering, University of Misan, Maysan 62001, Iraq
[3] Department of Multidisciplinary Engineering Education, The University of Sheffield, Sheffield S3 7RD, UK; s.a.hayes@sheffield.ac.uk
* Correspondence: sfhamad1@sheffield.ac.uk or Sfhamad3@gmail.com; Tel.: +44-74-7855-7071

This chapter has been published as an article paper in Materials, MDPI. I performed all the experimental work contained within, including sample preparation, mechanical testing, FTIR and SEM characterisations, and wrote the initial draft.

Abstract: Nanoscale surface morphology of plant fibres has important implications for the interfacial bonding in fibre-polymer composites. In this study, we investigated and quantified the effect of plasma surface modification on ramie plant fibres as a potential tool for simple and efficient surface modification. The extensive investigation of the effects of plasma treatment of the fibre surface nano-morphology and its effect on the fibre-polymer interface was performed by Low Voltages Scanning Electron Microscopy (LV-SEM), infrared spectroscopy (FT-IR) analysis, fibre-resin angle measurements and mechanical (tensile) testing. The LV-SEM imaging of uncoated plasma treated fibres reveals nanostructures such as microfibrils and elementary fibrils and their importance for fibre mechanical properties, fibre wettability, and fibre-polymer matrix interlocking which all peak at short plasma treatment times. Thus, such treatment can be an effective in modifying the fibre surface characteristics and fibre-polymer matrix interlocking favourably for composite applications.

Section 5.1: Introduction

Natural plant fibres are increasingly being used as a reinforcement in polymer matrix composites especially in applications where lighter and stronger materials are required, for instance in automotive and aerospace applications [1][2]. The unique characteristics of natural plant fibres like high specific strength and stiffness with low density have motivated many researchers to use them as a replacement for synthetic fibres in polymer composites. For example, the specific modulus of ramie fibres (29-85 GPa/g cm^{-3}) can be higher than thus of E-glass fibres (29 GPa/g cm^{-3}) [3][4] and they boast wide availability, eco-friendliness, non-toxic nature, and less abrasiveness to plastic processing equipment [5][6].

Among lignocellulosic fibres, ramie fibre is one of the most widely used fibres in the field of polymer composites due to its high crystallinity and commercial availability [7]–[9] as well as being the longest and one of the strongest fine textile fibres [10][11]. Ramie fibres are single cell structures with length and diameter varying from 60-250 mm and 11-80 μm respectively [11]. The cell wall consists of oriented semi-crystalline cellulose microfibrils, a few nanometres in diameter, embedded in an amorphous matrix of lignin and noncellulosic compounds like hemicellulose and pectins [12]. The high tensile strength microfibrils form the fundamental structural unit of the cell wall and provide mechanical strength to the fibre [13]. Although the semi-crystalline cellulose microfibrils represent the main structural components of the fibre cell wall, the amorphous matrix of hemicellulose, lignin, and pectin also highly influence the fibre surface properties [14]. Based on previous studies, the presence of these noncellulosic compounds on the surface of ramie fibres have resulted in relatively poor surface adhesion properties in different polymer matrices such as epoxy resin [7], polylactic acid (PLA) [15], and polypropylene [16]. Therefore, the challenge is to remove the amorphous constituents from the fibre surface and expose the crystalline

cellulose microfibrils, thus roughening the surface and also increasing the surface area available for mechanical and chemical bonding to polymer matrices [17].

Plasma treatment presents an attractive method for the surface modification of various materials. It offers many advantages compared with chemical treatments such as simplicity, low energy consumption, short treatment times, low cost, and it does not require water or any potentially hazardous chemicals [18]–[20]. Depending on the experimental conditions, plasma surface modification of natural plant fibres can induce different effects such as surface cleaning, surface etching, crosslinking, and functionalization [21]–[25]. Most of the previous studies have used plasma treatment for surface cleaning, increasing the surfaces microroughness, and to create hydrophilic/hydrophobic surfaces [26]–[28]. However, very few studies [29][30] have used plasma treatment as a method to produce nanoscale structures for plant fibres which can roughen the fibre surface without affecting or changing the bulk properties. Moreover, and according to our knowledge, the relationship between those nanoscale surface structures and fibre mechanical properties has not been studied for the case of single (elementary) fibres.

Therefore, in the present study we use plasma surface treatment with the goal of maximising the exposure of crystalline cellulose microfibrils by removing the amorphous constituents like hemicellulose and lignin from the fibre surface, without adversely affecting the fibre mechanical properties. To identify and image the crystalline cellulose microfibrils within elementary fibre we present a detailed investigation of the surface topography and single fibre mechanical testing of ramie fibres under different durations of plasma treatment. We use Low Voltage Scanning Electron Microscopy (LV-SEM) to observe the presence and orientation of nanoscale structures (cellulose microfibrils) on the fibre surface after plasma treatment without any sample coating and subsequently investigate the relationship between exposed nanostructures, surface wettability, fibre-phenolic matrix interlocking, and single

fibre mechanical properties, to define what constitutes optimal plasma treatment conditions for ramie fibre – phenolic polymer composites.

Section 5.2: Experimental work

Section 5.2.1: Materials

Ramie fibres (Boehmeria nivea) were purchased from Wild Fibres store, Birmingham, UK and used as received for the experiments (Figure 5-1a). The most frequent single fibre diameter (Figure 5-1b) of the supplied fibres were in the range of 30-40 μm (Figure 5-1c). The fibres' origin and extraction method is not disclosed by the supplier. For the polymer matrix, a resole commercial phenolic resin (Cellobond J2027X) and a slow acting acid catalyst (phencat 382) were supplied by Caleb Technical Products Ltd., Usk, UK, and used as a test liquid for the contact angle measurements.

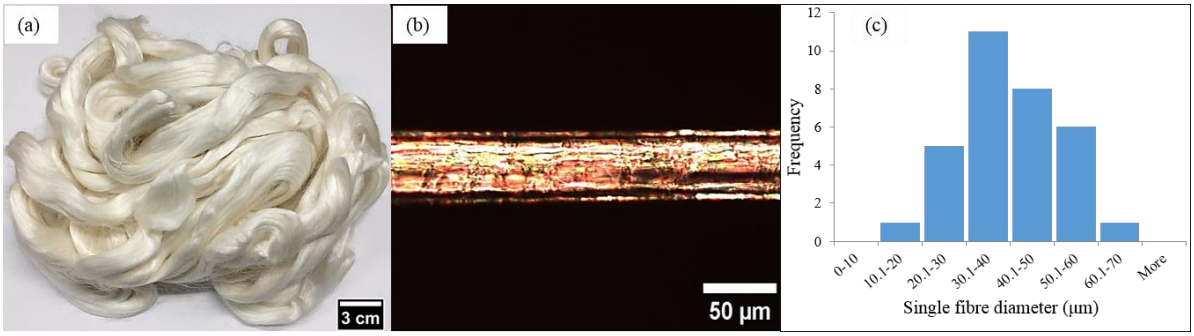

Figure 5-1: *Ramie fibres (a) supplied bundle of ramie fibres, (b) optical microscopy image of single ramie fibre, and (c) histogram shows the most frequented diameter for single fibres, measured using optical microscopy images such as in (b).*

Section 5.2.2: Low pressure plasma surface treatment

In this investigation, a Zepto plasma-surface cleaner (Diener electronic GmbH, Ebhausen, Germany) with a borosilicate glass cylindrical chamber (2.6 Litre) and power supply frequency of 40 kHz (Figure S1 in Supplementary Materials) was used to treat ramie fibres. The samples were prepared for the plasma treatment accordingly to the analysis to be performed: for the LV-SEM observations, single fibres were randomly selected and straightened to be held vertically on the SEM stub with a length of about 10 mm. The ends of each fibre were mounted on the stub with silver conductive paint and then inserted into

the plasma chamber (Figure S2a in Supplementary Materials). For the Attenuated Total Reflectance-Fourier Transform Infrared spectroscopy (ATR-FTIR) characterisation, a bundle of ramie fibres (30-50 mm long) were well distributed onto the sample holder (SEM stub), fixed on one side by carbon adhesive tape and then inserted into the plasma chamber (Figure S2b in Supplementary Materials). For the contact angle measurements, a single fibre with a length of about 40 mm was straightened and held vertically on a clean glass slide. A small piece of a card (0.4 mm thick) was placed in between the ends of each single fibre and the slide in order to prevent the fibre/slide contact and also to make sure the plasma uniformly treated all sides of the fibre (Figure S2c in Supplementary Materials). For the single fibre tensile testing, single fibres were randomly selected and mounted on a cardboard frame by using cyanoacrylate glue and then inserted into the plasma chamber (Figure S2d in Supplementary Materials). After that the plasma chamber was evacuated to 0.1 mbar of pressure to remove any contaminants from the chamber. Thereafter, the chamber was flooded with air and the gas flow rate was controlled by a flowmeter. Plasma was generated at 100 W and the chamber pressure was adjusted to 0.3 mbar. Ramie fibres were treated at four different durations: 1, 2, 3, and 4 minutes. All sample preparation and plasma treatments were performed in an environment of 22 ± 3 °C and 40% RH.

Section 5.2.3: Surface and cross section observations of ramie fibres

A Nova Nano SEM 450 Scanning Electron Microscopy (FEI, Brnp-Cernovice, Czechia) was used to observe the fibre surface topography of untreated and plasma treated fibres. Moreover, single ramie fibres were cryo-fractured in the liquid nitrogen in order to observe the fibre cell wall structure by LV-SEM. The fracture surfaces of tensile test samples were also observed by LV-SEM. Natural plant fibres are not conductive materials, therefore, the observations were performed using a low accelerating voltage (1 kV) to avoid fibre charging. The images were collected using a through lens detector (TLD) at around 4.5 mm working

distance with a beam deceleration of 2000 V. Fast Fourier Transform (FFT) image analysis method in ImageJ was used to observe the nanoscale structure orientation on the fibre surface.

Section 5.2.4: Attenuated total reflectance-Fourier Transform Infrared Spectroscopy (ATR-FTIR)

A PerkinElmer FTIR spectrometer (PerkinElmer, Waltham, MA, USA) was used to investigate the surface chemical compositions of untreated and plasma treated ramie fibres in single reflection diamond ATR accessory with an angle of incidence of 16° from the perpendicular. Typically, the depth of light penetration in this technique is a few microns, depending on the wavelength, the angle of incidence, the refractive indices, and the sample [31]. In this study, the test was conducted at room temperature (22 ± 3 °C) with a wavenumber range between 4000 cm^{-1} to 600 cm^{-1} and the average of scan repetitions was 8 scans for each sample (untreated and plasma treated fibres) at 2 cm^{-1} of resolution.

Section 5.2.5: Wettability measurements

To evaluate the effect of plasma treatment on the fibre surface wettability, the single-fibre drop technique was used using drop-shape analyser instrument (DSA 100-Kruss, Hamburg, Germany). Phenolic resin and its catalyst (phencat 382) were mixed in the ratio of 100:5 w/w and then used as a test liquid. This kind of resin is usually used as a matrix in polymer-fibre composites [32]. A 5 μL droplet was placed on the fibre surface using a microliter syringe. The drop shape was fitted with the Young-Laplace method and the angles were measured after 30 s of placing a drop onto the fibre surface. The angle values were taken as the average of at least 3 measurements obtained along the fibre surface. However, this is not a standard contact angle measurement as contact angle on single fibres is experimentally difficult, almost impossible to measure. This is due to the high curvature variation at the interface [33]. Therefore, to fully assess the surface wettability and surface adhesion properties in the context of composites, we have developed the experiment by curing the

samples at 80 C for 3 h using oven (Thermo Scientific Heraeus, Waltham, MA, USA). Thereafter, the fibre wetting area of the cured samples was observed using optical microscopy (Nikon Eclipse LV150, Tokyo, Japan). In addition, the fibre/matrix interface was also observed using LV-SEM for all different cured samples.

Section 5.2.6: Tensile Test of Single ramie fibres

A tensile testing machine (Zwick Roell, Ulm, Germany) with a 500 N load cell was used to test the mechanical tensile properties of single ramie fibres. Thirty isolated single fibres were prepared for untreated and plasma treated fibres at different times (1, 2, 3, and 4 min). Each single fibre with a gauge length of 5 mm was mounted on a cardboard frame by using cyanoacrylate glue. The fibres were carefully glued in the exact centre of the cardboard. Thereafter, the sample was clamped onto the testing machine and just before the beginning of each test, the supporting side of the card was carefully cut off. The samples were tested at a constant crosshead displacement rate of 40 %/min and according to the ASTM D 3822-01 standard. The tests were carried out at room temperature (22 ± 3 °C). During the test, the force-strain values were recorded, and these values were used to measure the fibre tensile properties (ultimate strength and Young's modulus). Only samples that broke in the middle of their gauge length were used to calculate the tensile strength and Young's modulus, whereas the fibres that broke near to the glue clamp or card frame were not used in the calculations.

The cross-sectional area measurements highly affect the final tensile properties of single fibres [34]. Therefore, in this study, two different methods were used to determine the cross sectional area:

1. Before testing the fibre, images at different locations along the fibre gauge length were taken using an optical microscope (Nikon Eclipse LV150, Tokyo, Japan). The cross-section of each single fibre was assumed to be circular. The fibre diameter was

directly measured from the images and hence the cross-sectional area of each single fibre was calculated from the average of three apparent fibre diameter measurements (30 samples for each treatment time).

2. As the single fibre failure is elastic without any signs of plastic deformation, it can be assumed that the cross-sectional area of the fractured fibres has not changed significantly after the test. Therefore, after testing, LV-SEM was used to observe the cross-section area of the fractured fibres. Fractured fibres with a flat and clear cross-section end (Figure 5-2a) were selected for the cross-section area calculations whereas fractured fibres that split into fibrils (Figure 5-2b) were not included in the results as accurate area measurements were not possible for these samples. Thereafter, the collected LV-SEM images were used to calculate the actual cross-sectional area of the fractured fibres by using image J software. The hollow structure (lumen) can be clearly seen in Figure 2a, excluded from the total area. The sample size for each treatment time varied depending on fracture surface end (Table S1 in the Supplementary Materials).

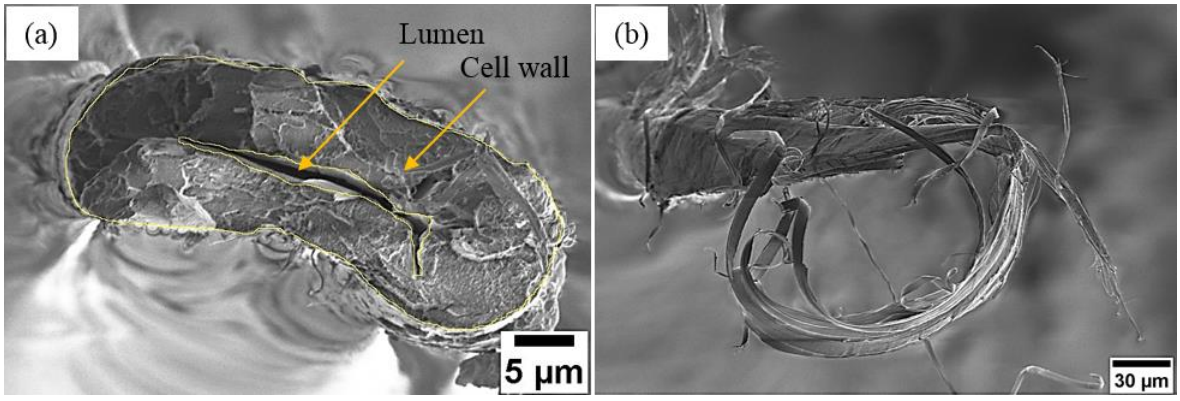

Figure 5-2: *LV-SEM images of the fractured surface of single ramie fibres under tensile load (a) example of flat cross-section end and (b) example of single fibre split into fibrils. More SEM images are shown in the Supplementary Materials (Figures S3 and S4).*

Section 5.3: Results and discussion

Section 5.3.1: Microstructure of single ramie fibre

The as received fibres were cryo-fractured in order to investigate the fibre cross section structure by LV-SEM (Figure 5-3a). The LV-SEM observations highlight that the cross-section of single ramie fibre is irregular in shape with a central lumen surrounded by a thick cell wall. The cross-section view also shows that the cell wall structure of ramie fibre is composed of multiple layers. However, the structure of ramie fibre shown in Figure 5-3a is the typical structure of ramie fibres and most of natural plant fibres such as flax, hemp, kenaf and nettle fibres [35]. It can also be seen from the detailed investigation of the cell wall in Figure 5-3b that it mainly consists of bright nanoscale structures, which are expected to be crystalline cellulose microfibrils embedded in non-crystalline regions of hemicellulose and lignin. In addition, the cell wall structure of the tensile fractured sample (Figure 5-3c) shows the same features as in Figure 5-3b, indicating these bright nanoscale features are not cryogenic surface artefacts. These nano-scale features (Figure 5-3b) appear to be in the range of 10-40 nm in diameter, and are thus consistent with crystalline cellulose microfibrils [36].

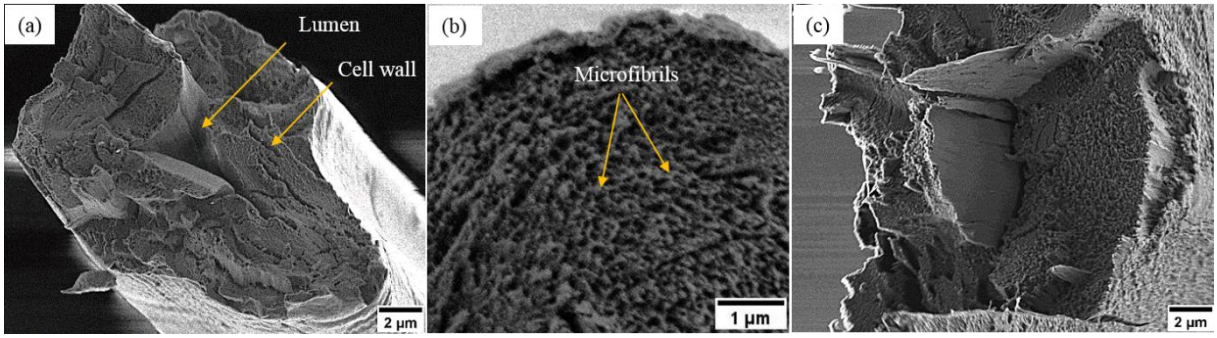

Figure 5-3: *LV-SEM images of the cross section of ramie fibre (a) overview of the cryo-fractured single ramie fibre, (b) the cryo-fractured cell wall, (c) the tensile fractured cell wall, more SEM images are shown in the Supplementary Materials (Figure S5).*

Section 5.3.2: Surface morphology analysis

The surface morphology of untreated and plasma treated ramie fibres are shown in Figure 5-4. It can be visually verified that the surface roughness of the untreated fibre (Figure 5-4a) varies locally, with roughness at different scales. For instance it is rough on the microscale

as shown in Figure 5-4a (right edge) and even more pronounced in Figure 5-5a whereas it is smooth and almost homogenous on the nanoscale (Figure 5-4a centre) which is due to the primary amorphous layer that consists of waxes, pectins, and proteinaceous material [15][37][38]. However, 1 min of plasma treatment (Figure 5-4b) reveals nanoscale bright structures on the fibre surface, which lead to a rougher surface. These nanoscale structures are randomly oriented on the fibre surface as indicated by FFT image in Figure 5-4b (bottom left). It can also be seen from Figure 5-4b that most of the impurities have been removed from the fibre surface when compared to the untreated surface (arrows in Figure 5-4a). It has been reported that polymer chains in the amorphous state can be etched by plasma more easily than in the crystalline state [29][39]. Therefore, we attribute these nanoscale features to the crystalline cellulose microfibrils which remain after selective etching of the amorphous portions by plasma treatment. Moreover, these nanoscale structures have a similar diameter (10-40 nm) to those appear on the cross-section. Besides, it has been reported in the literature that the nanoscale surface features of plasma treated ramie fibres show secondary electron emission characteristics distinct from the matrix, further supporting the hypothesis that they are crystalline features in a more amorphous matrix [40].

When increasing the plasma treatment time to 2 min, those bright nanostructures (microfibrils) are seen more clearly on the fibre surface with their increased height indicating a large amount of amorphous material has been removed, leading to an increased surface roughness as presented in Figure 5-4c. Such effects contribute effectively to the improvements of the fibre surface wettability and also the fibre mechanical properties (discussed in Sections 5.3.4 and 5.3.5).

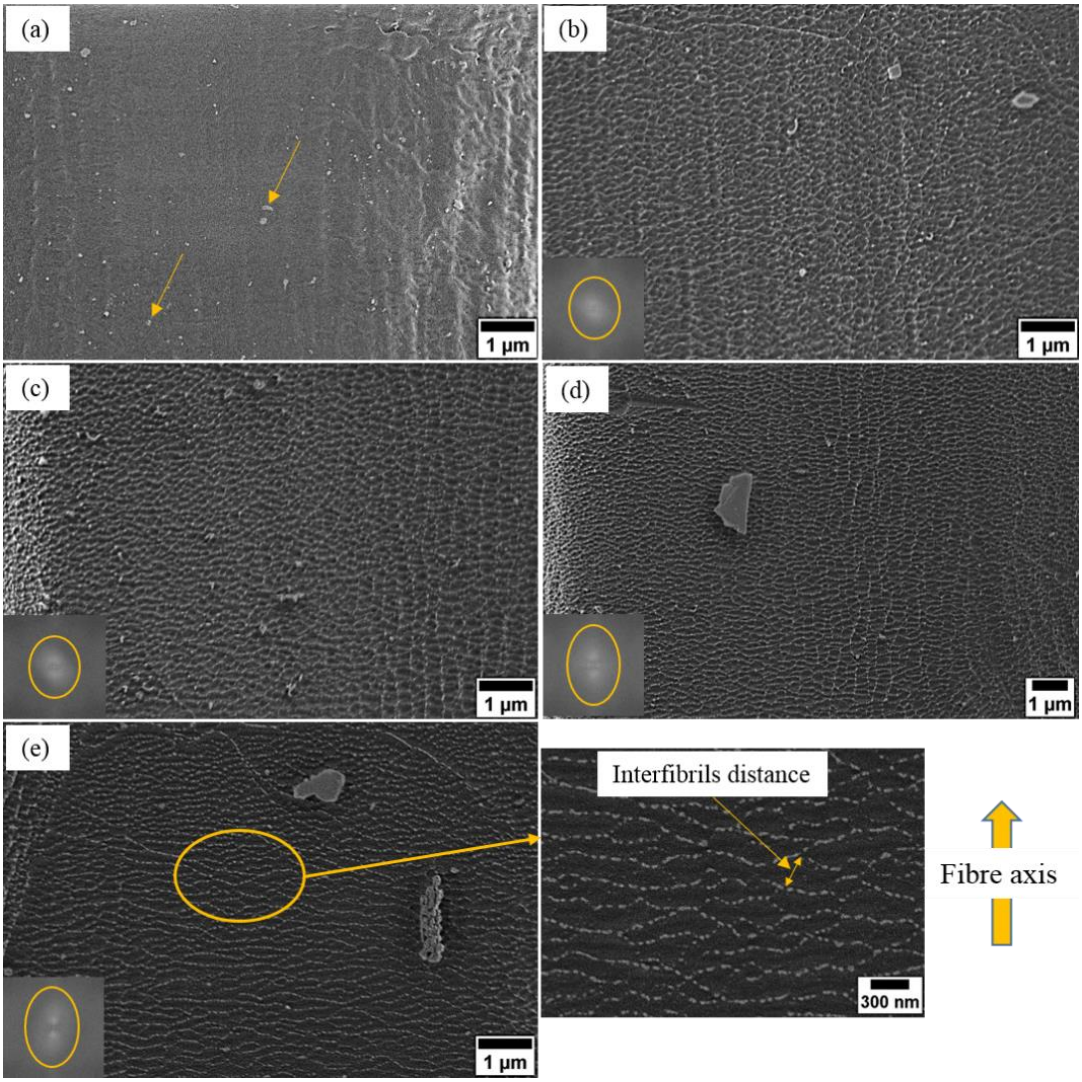

Figure 5-4: *LV-SEM images of ramie fibres with their FFT images (bottom left) (a) untreated (yellow arrows point to impurities), and plasma treated for (b) 1, (c) 2, (d) 3, and (e) 4 min treatment duration with surface details marked by the yellow circle.*

However, longer plasma treatment durations (3 and 4 min) leads to fewer, more isolated microfibrils as well as increases in the interfibrillar distance, especially after 4 min of plasma treatment as shown in Figure 5-4d,e. Besides, the FFT images (bottom left) in Figure 5-4d,e show that the microfibrils were aligned differently from those in Figure 5-4b,c. Therefore, we assume that most of the outer layer of the primary cell wall having been etched by plasma from the fibre surface, such that the inner face of the primary wall is exposed. According to our previous study [41] the thickness of the primary cell wall of ramie fibre is approximately 100 nm. Moreover, it has been reported that microfibrils are agglomerates of elementary

fibrils with diameter of 3.5 nm [42]. Based on the sizes of nanofeatures (~4.5 nm) being very close in to the reported diameter of elementary fibrils [42] in Figure 5-4e (surface details), we assume that after 4 min of plasma treatment the microfibrils have been broken up into their elementary fibrils. This can also explain the observed isolated appearance of fibrils and the increase in the interfibrillar distance after 4 min of plasma treatment. Such effects were found to have a major role in determining the fibres mechanical properties (see Section 5.3.5).

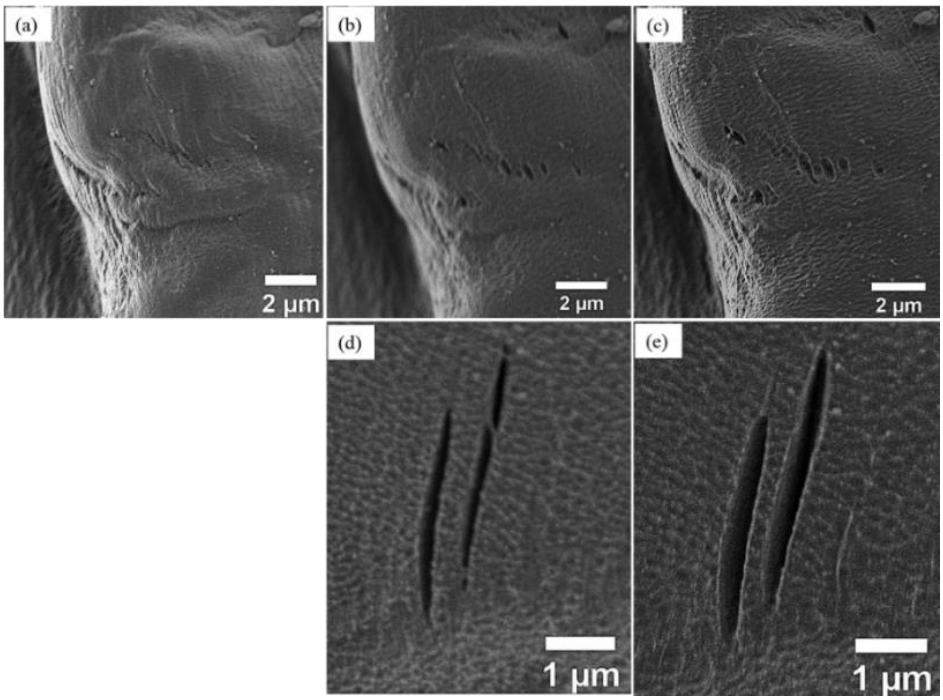

Figure 5-5: *LV-SEM images of ramie fibres show the influence of plasma treatment on the pre-existing holes and cracks on the fibre surface, (a) untreated, (b) and (d) 2 min, (c) and (e) 3 min.*

According to our LV-SEM observations, the plasma treatment is not creating holes or cracks on the fibre surface even after 4 min treatment duration. However, it is also important to mention that the LV-SEM observations in this work indicated that any pre-existing holes or cracks became wider and deeper as the treatment duration increases as shown in Figure 5-5.

Section 5.3.3: Surface chemical structure analysis

The ATR-FTIR absorption spectra of untreated and plasma treated ramie fibres are shown in Figure 5-6. All spectra show many absorption bands that are mostly related to specific characteristic groups of the fibre components such as cellulose, hemicellulose, lignin, and waxes. Table 5-1 shows the standard [43]–[46] and the observed peak positions of ramie fibres, as well as the changes in the peak intensities after plasma treatment. However, very limited changes have been observed in the ATR-FTIR spectra of the plasma treated fibres, in comparison to the untreated fibres. The explanation for this is that the surface chemical changes after plasma treatment are expected to be limited to the topmost layer of the fibre surface while the depth of chemical information obtained by ATR-FTIR reported to be well below 1 μm the surface of the material being analysed [47]. This is further proves that short time of plasma treatment did not alter the fibre bulk properties.

The changes for the plasma treated fibres were observed in two main absorption cellulose bands (3220 cm^{-1} and 1024 cm^{-1}), particularly after 4 min of plasma treatment. They are characteristic bands of the hydroxyl groups (O-H) present in the cellulose structures [44]. The reduction in the intensity of these two bands could be due to the partial removal of the cellulose microfibrils from the fibre surface after 4 min of plasma treatment, which is also in line with our LV-SEM observations. Also, changes were observed in the intensity of band at 1738 cm^{-1} after 2 min of plasma treatment (Figure 5-6(i)). This characteristic band corresponding to the carbonyl (C=O) stretching of acetyl groups in cellulose and hemicellulose [43][44]. The reduction in the intensity of this band after plasma treatment may be due to the removal of the amorphous cellulose and hemicellulose from the fibre surface [48]. In addition to the reduction of the intensity band of 1738 cm^{-1} after plasma treatment, it can also be seen there is a much narrower peak for the plasma treated fibres (2, 3, and 4 min) which might be due to the remaining of the crystalline cellulose [44].

Moreover, the peak near 1640 cm^{-1} is assigned to the absorbed water in crystalline cellulose [44]. This peak is found to decrease gradually with plasma treatment (Figure 5-6(ii)). Morshed et al. [44] and Sinha [45] suggested that the decreasing in the intensity of the band at 1650 cm^{-1} for the plasma treated fibre is probably due to the temperature effect and bond cleavage with plasma to form free radicals. The band near 1235 cm^{-1} is possibly due to the (C-O) vibration of esters, ethers, and phenolic groups related to the presence of waxes on the fibre surface and the decreasing of this band after plasma treatment (Figure 5-6(iii)) is probably due to the removal of waxes from fibre surface [46].

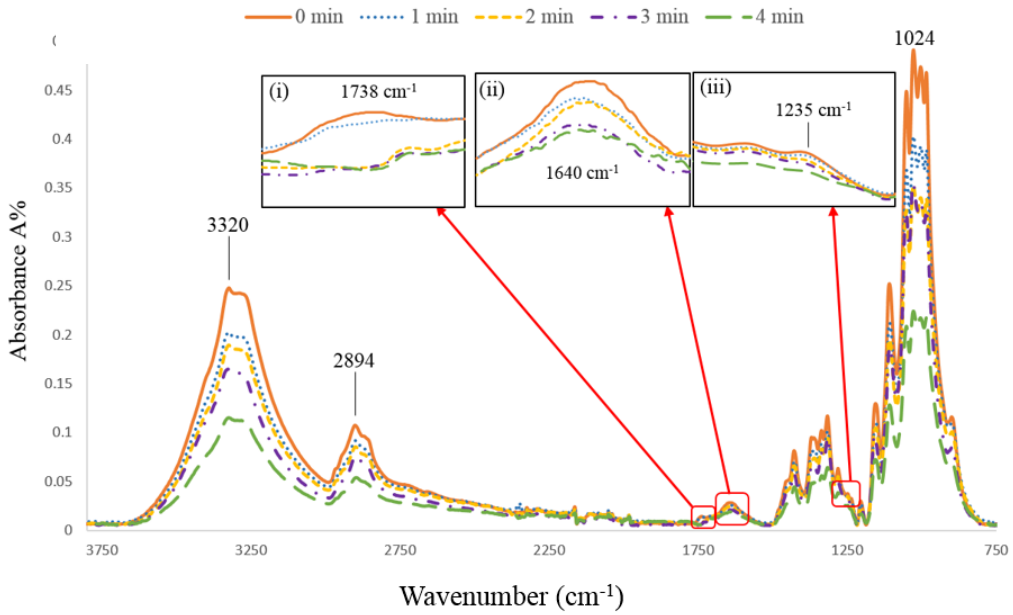

Figure 5-6: *ATR-FTIR spectra of untreated and plasma treated ramie fibres at with enlarge sections of (i) carbonyl (C=O) stretching in cellulose and hemicellulose, (ii) water in crystalline cellulose, and (iii) the C-O vibration of esters, ethers and phenolic groups.*

Table 5-1: *Standard [43]–[46] and observed FTIR absorption peak position for ramie fibres.*

Structural bond	Associated components	Standard peak position (cm^{-1})	Measured peak position (cm^{-1})	Effect of plasma treatment
OH stretching	Cellulose	3200~3600	~3320	Started to decrease after 3 min
CH_2 stretching	Cellulose & hemicellulose	~2925	2894	None
C=O stretching	Cellulose & hemicellulose	1725~1750	1738	Decreased after 2 min
H-O-H bending	Absorbed water	~1650	1640	Decreased gradually with treatment time
CH_2 deformation	Lignin	1435~1480	1423	None
CH_3 bending	Lignin	1340~1390	1354	None
CH_2 wagging	Lignin	~1320	1316	None
C-O stretching	Waxes	1275~1185	1235	Decreased gradually with treatment
C-O stretching	Cellulose	1160~1000	1094	None
O-H deformation	Cellulose	1080~1030	1024	Started to decrease after 3 min
β-Glucosidic linkage	Hemicellulose	~885	898	None

Section 5.3.4: Surface wettability of fibres

The fibre surface changes that occur due to the plasma treatment lead to changes in the surface wetting characteristics, which were quantified by single-fibre angle measurements. Generally, surfaces with smaller contact angle (less than 65°) are considered as wettable surfaces and hydrophilic properties (high surface energy) [49], and a liquid drop tends to spread across the surface. Figure 5-7 shows the angle values between a single ramie fibre (untreated and plasma treated at various times) and phenolic resin. It can be seen that the angle of untreated fibres was 49.0° ± 1.9, while that of 1 min plasma treated fibres shows a smaller angle, 38.0° ± 2.2. However, no further clear decrease is observed with increasing treatment time (Figure 5-7). Modifications in the surface characteristics such as surface

roughness and surface chemistry cause changes in the surface wettability. It has been reported that hydrophilic materials will appear more weattible as the surface roughness increases, while more hydrophobic in hydrophobic materials [50]. Therefore, the observed enhancement of the fibre surface wettability after plasma treatment can be attributed to increased surface roughness and greater exposure of crystalline cellulose microfibrils as well as the removal of the amorphous materials such as lignin and waxes from the fibres outermost layer (observed by LV-SEM and ATR-FTIR and discussed in Sections 5.3.2 and 5.3.3). In addition, plasma treatment often introduces more polar groups such as hydroxyl groups on the fibre surface by oxidation of cellulose, which could also improve the fibre surface wettability.

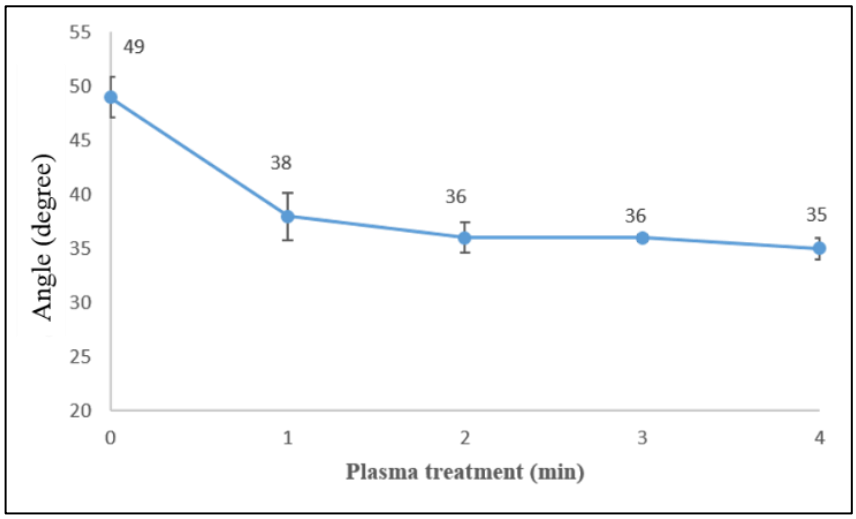

Figure 5-7: *Angle values of single ramie fibres (plasma treated at various times) and phenolic resin.*

The surface tension forces between fibre and phenolic resin enable the resin to spread across the fibre surface, as shown in Figure 5-8a(ii). These forces are highly dependent on surface roughness, crystallographic orientation, and chemical composition [50]. Therefore, for the plasma treated fibres (Figure 5-8b(ii)), there was a significant increase in the wetting area compared to the untreated fibre, which also correlates with the angle values. Moreover, the interfacial bond strength between fibres and matrix is an important factor in controlling the final mechanical properties for composites. Therefore, here we investigated the fibre-matrix

interface using LV-SEM for all different samples. Figure 5-8a(iii) shows the untreated fibre-matrix interface. The defibrillation of the fibre surface and the long fibre pull out as well as a noticeable gab between fibre and matrix can be clearly seen, which indicates the poor surface adhesion between fibres and matrix. This could be due to the surface smoothness and the non-uniform fibre surface which results in fibre surface defibrillation and poor mechanical interlocking between fibre and matrix. However, the 1 min of plasma treated fibre (Figure 5-8b(iii)) shows shorter fibre pull out than the untreated fibre and more uniform fibre surface without defibrillation. This could be due to the improved surface roughness that is caused by plasma treatment, as well as the removal of the non-cellulosic compounds like hemicellulose and waxes from the fibre surface. After 2 min of plasma treatment (Figure 5-8c(iii)), the interface between the phenolic matrix and the ramie fibre is almost continuous. The rough surface with greater exposure of crystalline cellulose microfibrils after 2 min of plasma treatment (observed by LV-SEM (Section 5.3.2)) enlarge the interfacial area, which may improve the fibre-matrix interaction. After 3 min of plasma treatment (Figure 5-8d(iii)), there was a fibre-matrix debonding and fibre pull out, which indicates the poor fibre-matrix interlocking. Besides, 4 min of plasma treatment also showed a fibre pull out and a gap between fibre and matrix (Figure 5-8e(iii)). These results were in a good agreement with the LV-SEM and ATR-FTIR analysis, which revealed that after a long time of plasma treatment (3 & 4 min) there was a partial removal of the cellulose microfibrils from the fibre surface resulting in fewer nanostructures and hence smaller interface area.

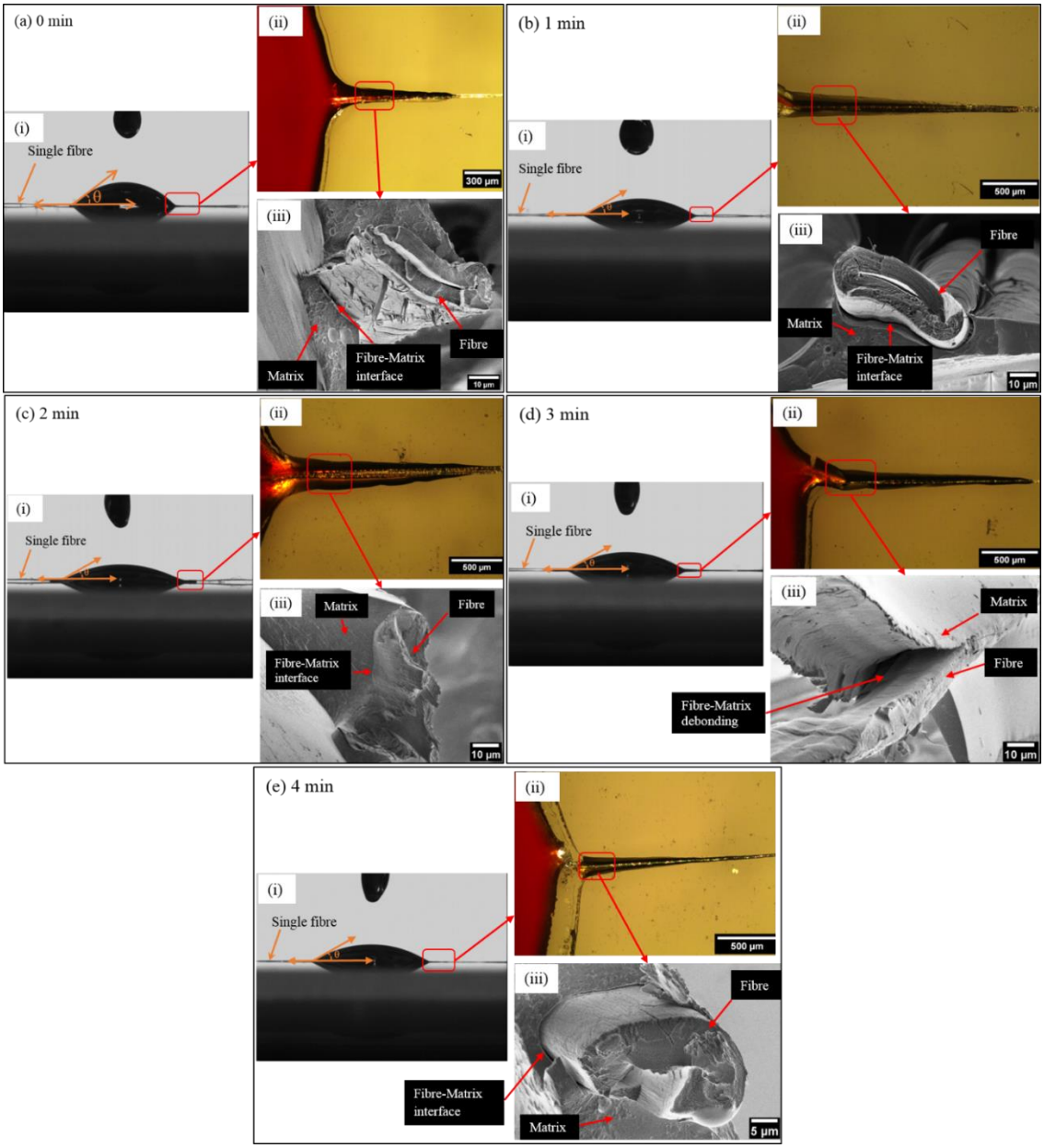

Figure 5-8: *Phenolic resin drops on single ramie fibres plasma treated at various times: (a) 0 min, (b) 1 min, (c) 2 min, (d) 3 min, and (e) 4 min. Subfigures display: (i) contact angle image of single ramie fibre with phenolic resin, (ii) optical microscopy image of single ramie fibre wetted by phenolic resin after curing, and (iii) LV-SEM image of single ramie fibre/phenolic resin interface.*

Section 5.3.5: Single fibre mechanical properties

The fractured surface morphology of the tensile test of single ramie fibres is shown in Figure 5-9. It can be seen that some of the fractured fibres showed a very flat end surface (Figure 5-9a) whereas some other fractured fibres showed different fibre cells have fractured in different planes (Figure 5-9b). This behaviour of fibre cells is probably due to the variability

in the fibre cell strength and also due to cell wall flaws [51]. It has been found that the variations in the fibre cell wall fracture can strongly influence the final fibre properties [41]. In addition, multiple cracks were observed (arrows in Figure 5-9) on the fractured surfaces, which is probably due to the stress during testing passing through weak regions which are composed of amorphous hemicellulose and lignin.

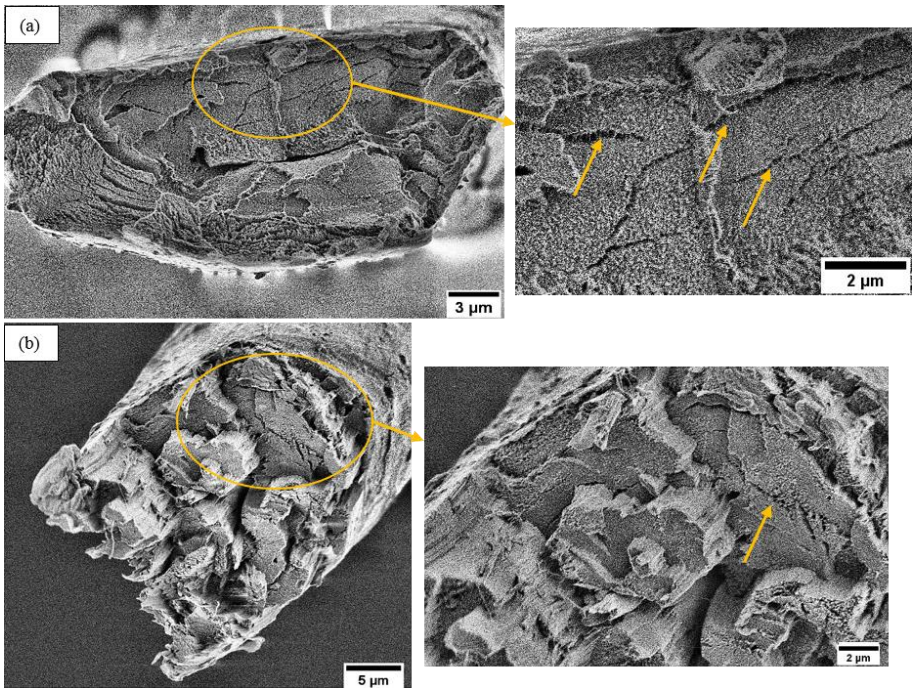

Figure 5-9: *LV-SEM images of the fractured surface of single ramie fibres under tensile load (a) overview of a flat fractured surface with a detail cell wall structure inside yellow circle (b) overview of an irregular fractured surface with a detail cell wall structure inside yellow circle. Yellow arrows highlight cracks.*

To determine to what extent plasma treatment durations affect the mechanical properties of ramie fibres, tensile properties (strength and Young's modulus) were measured. Using the two different methods to measure the cross-sectional area of single fibres described in the experimental section, the strength and Young's modulus with plasma treatment time were evaluated. The non-circular cross-section of single ramie fibre is clearly illustrated in Figure 5-9a, hence, assuming a circular cross-section in measuring the cross-sectional area may not be sufficient to accurately assessing the single fibre properties (Figure S6 in Supplementary Materials). Even though it means a reduction in sample size, we present the tensile results

calculated using the second method using LV-SEM images to yield more accurate results. The results using fibre diameter measurements follow broadly the same trend, albeit with erroneous absolute values for the strength and Young's modulus, and are shown in the Supplementary Materials. Based on the LV-SEM measurements, the average tensile strength and Young's modulus of untreated fibres were 872 MPa and 31 GPa respectively (Figure 5-10). However, it can be seen that there are no significant changes in between the average values of tensile strength and Young's modulus for 0, 1 and 2 min of plasma treatment which confirms that the short time of plasma treatment did not change the fibre bulk properties. With longer plasma treatment durations (3 and 4 min), the tensile strength and Young's modulus values were found to decrease gradually. This could be due to the widening of the initial cracks and holes on the fibre surface, and also it might be due to the removal of most of the non-cellulosic binding materials as well as the partial removal of the cellulose microfibrils from the fibre surface, as indicated by LV-SEM results in Section 5.3.2. Moreover, the LV-SEM results presented above show that after 4 min of plasma treatment the microfibrils were broken up into their individual elementary fibrils with a clear increase in the interfibrillar distance. This could also provide an explanation for the low tensile properties after 4 min of plasma treatment.

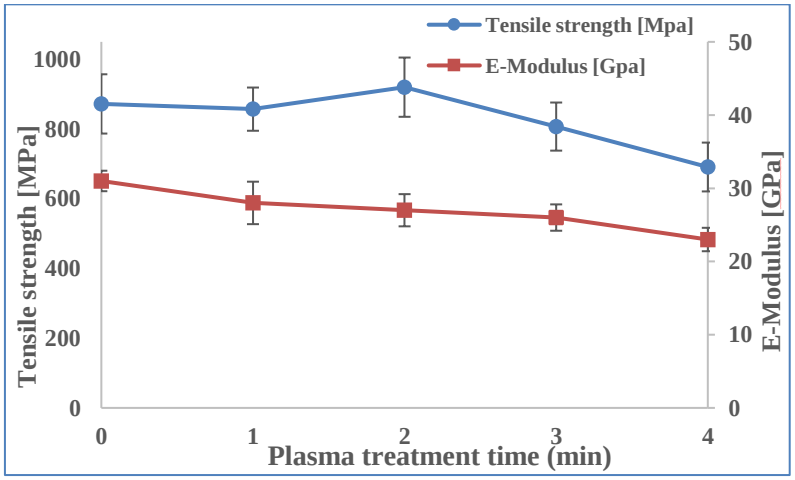

Figure 5-10: *The tensile strength and Young's modulus of untreated and plasma treated fibres, values based on actual cross sectional area measurements from SEM images.*

Section 5.4: Conclusions

Plasma-surface treatment of ramie fibres has created surface nanoscale structures after only 1 min of treatment. We identified these nanostructures to be crystalline cellulose microfibrils and report for the first time direct observation of the elementary fibrils. Exposing cellulose microfibrils resulted in a nanoscale surface roughness which increases the surface area and led to better wettability and fibre-matrix interaction. The use of plasma-surface modification could have immense benefits in the production of fibre-polymer composites with good interface integrity and could pose a big step forward in replacing fossil-fuel-based fibres.

Acknowledgments

S.F.H. gratefully acknowledge the Iraqi Ministry of Higher Education and Scientific Research and its representative in the UK, the Iraqi Attaché in London for financial support. N.S. thanks EPSRC for funding of her doctoral training studentship (1816190). J.P.F. thanks Peter Willson at Caleb Technical Products for providing the phenolic resin. We also gratefully acknowledge Chris Holland for his help and support in performing the single fibre tensile test.

Section 5.5: References

[1] E. Poriķe and J. Andersons, "Strength-length scaling of elementary hemp fibers," *Mech. Compos. Mater.*, vol. 49, no. 1, pp. 69–76, 2013.

[2] S. Thomas, S. A. Paul, L. A. Pothan, and B. Deepa, "Natural Fibres: Structure, Properties and Applications," in *Cellulose Fibers: Bio- and Nano-Polymer Composites*, I. Kalia, S., Kaith, B. S., Kaur, Ed. Springer-Verlag Berlin Heidelberg, 2011, pp. 3–42.

[3] K. L. Pickering, M. G. A. Efendy, and T. M. Le, "A review of recent developments in natural fibre composites and their mechanical performance," *Compos. Part A Appl. Sci. Manuf.*, vol. 83, pp. 98–112, 2016.

[4] C. Elanchezhian, B. V. Ramnath, G. Ramakrishnan, M. Rajendrakumar, V. Naveenkumar, and M. K. Saravanakumar, "Review on mechanical properties of

natural fiber composites.," *Mater. Today Proc.*, vol. 5, no. 1, pp. 1785–1790, 2018.

[5] K. Oksman, A. P. Mathew, R. Långström, B. Nyström, and K. Joseph, "The influence of fibre microstructure on fibre breakage and mechanical properties of natural fibre reinforced polypropylene," *Compos. Sci. Technol.*, vol. 69, no. 11–12, pp. 1847–1853, 2009.

[6] D. M. Matoke, G. M.; Owido, S.F.; Nyaanga, "Effect of Production Methods and Material Ratios on Physical Properties of the Composites," *Am. Int. J. Contemp. Res.*, vol. 2, no. 2, pp. 208–213, 2012.

[7] X. Liu and L. Cheng, "Influence of plasma treatment on properties of ramie fiber and the reinforced composites," *J. Text. Inst.*, vol. 31, no. 15, pp. 1723–1734, 2017.

[8] Q. Zhang, Y. Jiang, L. Yao, Q. Jiang, and Y. Qiu, "Hydrophobic surface modification of ramie fibers by plasma-induced addition polymerization of propylene," *J. Adhes. Sci. Technol.*, vol. 29, no. 8, pp. 691–704, 2015.

[9] C. Xu, Y. Gu, Z. Yang, M. Li, Y. Li, and Z. Zhang, "Mechanical properties of surface-treated ramie fiber fabric/epoxy resin composite fabricated by vacuum-assisted resin infusion molding with hot compaction," *J. Compos. Mater.*, vol. 50, no. 9, pp. 1189–1198, 2016.

[10] G. Koronis, A. Silva, and A. P. Soares Dias, "Development of green composites reinforced with ramie fabrics: Effect of aging on mechanical properties of coated and uncoated specimens," *Fibers Polym.*, vol. 15, no. 12, pp. 2618–2624, 2014.

[11] S. N. Pandey, "Ramie fibre: Part II. Physical fibre properties. A critical appreciation of recent developments," *Text. Prog.*, vol. 39, no. 4, pp. 189–268, 2007.

[12] L. H. Thomas *et al.*, "Structure of Cellulose Microfibrils in Primary Cell Walls from Collenchyma," *Plant Physiol.*, vol. 161, no. 1, pp. 465–476, 2013.

[13] Y. Nishiyama, U. J. Kim, D. Y. Kim, K. S. Katsumata, R. P. May, and P. Langan, "Periodic disorder along ramie cellulose microfibrils," *Biomacromolecules*, vol. 4, no. 4, pp. 1013–1017, 2003.

[14] E. Sinha and S. K. Rout, "Influence of fibre-surface treatment on structural, thermal and mechanical properties of jute fibre and its composite," *Bull. Mater. Sci.*, vol. 32, no. 1, pp. 65–76, 2009.

[15] H. Y. Choi and J. S. Lee, "Effects of surface treatment of ramie fibers in a ramie/poly(lactic acid) composite," *Fibers Polym.*, vol. 13, no. 2, pp. 217–223, 2012.

[16] Z. Zhou *et al.*, "Hydrophobic surface modification of ramie fibers with ethanol pretreatment and atmospheric pressure plasma treatment," *Surf. Coatings Technol.*,

vol. 205, no. 17–18, pp. 4205–4210, 2011.

[17] A. Pietak, S. Korte, E. Tan, A. Downard, and M. P. Staiger, "Atomic force microscopy characterization of the surface wettability of natural fibres," *Appl. Surf. Sci.*, vol. 253, no. 7, pp. 3627–3635, 2007.

[18] R. A. Jelil, *A review of low-temperature plasma treatment of textile materials*, vol. 50, no. 18. Springer US, 2015.

[19] N. Yaman, E. Özdoğan, N. Seventekin, and H. Ayhan, "Plasma treatment of polypropylene fabric for improved dyeability with soluble textile dyestuff," *Appl. Surf. Sci.*, vol. 255, no. 1, pp. 6764–6770, 2009.

[20] C. W. Kan, K. Chan, C. W. M. Yuen, and M. H. Miao, "Surface properties of low-temperature plasma treated wool fabrics," *J. Mater. Process. Technol.*, vol. 83, no. 1–3, pp. 180–184, 1998.

[21] E. Bozaci *et al.*, "Effects of the atmospheric plasma treatments on surface and mechanical properties of flax fiber and adhesion between fiber-matrix for composite materials," *Compos. Part B Eng.*, vol. 45, no. 1, pp. 565–572, 2013.

[22] N. H. Prakash, B. Sarma, S. Gopi, and A. Sarma, "Surface and moisture characteristics of jute using a D.C. glow discharge argon plasma," *Instrum. Sci. Technol.*, vol. 44, no. 1, pp. 73–84, 2016.

[23] E. Sinha and S. Panigrahi, "Effect of plasma treatment on structure, wettability of jute fiber and flexural strength of its composite," *J. Compos. Mater.*, vol. 43, no. 17, pp. 1791–1802, 2009.

[24] H. Barani and A. Calvimontes, "Effects of oxygen plasma treatment on the physical and chemical properties of wool fiber surface," *Plasma Chem. Plasma Process.*, vol. 34, no. 6, pp. 1291–1302, 2014.

[25] D. Parida, M. Jassal, and A. K. Agarwal, "Functionalization of cotton by in-situ reaction of styrene in atmospheric pressure plasma zone," *Plasma Chem. Plasma Process.*, vol. 32, no. 6, pp. 1259–1274, 2012.

[26] A. Vesel, M. Mozetic, S. Strnad, Z. Peršin, K. Stana-Kleinschek, and N. Hauptman, "Plasma modification of viscose textile," *Vacuum*, vol. 84, no. 1, pp. 79–82, 2009.

[27] K. K. Samanta *et al.*, "Effect of Helium-Oxygen Plasma Treatment on Physical and Chemical Properties of Cotton Textile," *Int. J. Bioresour. Sci.*, vol. 1, no. June, pp. 57–63, 2014.

[28] K. K. Samanta, A. G. Joshi, M. Jassal, and A. K. Agrawal, "Study of hydrophobic finishing of cellulosic substrate using He/1,3-butadiene plasma at atmospheric

pressure," *Surf. Coatings Technol.*, vol. 213, pp. 65–76, 2012.

[29] B. Balu, V. Breedveld, and D. W. Hess, "Fabrication of 'roll-off' and 'sticky' superhydrophobic cellulose surfaces-via plasma processing," *Langmuir*, vol. 24, no. 9, pp. 4785–4790, 2008.

[30] L. Jiang, K. J. Park-Lee, R. M. Clinton, Z. Tang, V. Breedveld, and D. W. Hess, "Mechanical durability of liquid repellent coatings," *Surf. Coatings Technol.*, vol. 328, no. August, pp. 182–191, 2017.

[31] J. Oelichmann, "Surface and depth-profile analysis using FTIR spectroscopy," *Fresenius' Zeitschrift f??r Anal. Chemie*, vol. 333, no. 4–5, pp. 353–359, 1989.

[32] M. Asim, N. Saba, M. Jawaid, M. Nasir, M. Pervaiz, and O. Y. Alothman, "A review on Phenolic resin and its Composites," *Curr. Anal. Chem.*, vol. 14, pp. 1–13, 2018.

[33] S. Rebouillat, B. Letellier, and B. Steffenino, "Wettability of single fibres - beyond the contact angle approach," *Int. J. Adhes. Adhes.*, vol. 19, no. 4, pp. 303–314, 1999.

[34] N. M. Everitt, N. T. Aboulkhair, and M. J. Clifford, "Looking for Links between Natural Fibres' Structures and Their Physical Properties," *Conf. Pap. Med.*, vol. 2013, pp. 1–10, 2013.

[35] A. Kicińska-Jakubowska, E. Bogacz, and M. Zimniewska, "Review of Natural Fibers. Part I-Vegetable Fibers," *J. Nat. Fibers*, vol. 9, no. 3, pp. 150–167, 2012.

[36] H. Meier, "Chemical and morphological aspects of the fine structure of wood," *Pure Appl. Chem.*, vol. 5, no. 1–2, 1962.

[37] D. B. Szymanski and D. J. Cosgrove, "Dynamic Coordination of Cytoskeletal and Cell Wall Systems during Plant Cell Morphogenesis," *Curr. Biol.*, vol. 19, no. 17, pp. R800–R811, 2009.

[38] S. O. Han and H. Y. Choi, "Morphology and surface properties of natural fiber treated with electron beam," *Microsc. Sci. Technol. Appl. Educ.*, no. 1880, pp. 1880–1887, 2010.

[39] E. Wohlfart *et al.*, "Nanofibrillar patterns by plasma etching: The influence of polymer crystallinity and orientation in surface morphology," *Macromolecules*, vol. 43, no. 23, pp. 9908–9917, 2010.

[40] N. Stehling *et al.*, "New perspectives on nano-engineering by secondary electron spectroscopy in the helium ion and scanning electron microscope," *MRS Commun.*, vol. 8, no. 2, pp. 226–240, 2018.

[41] S. F. Hamad, N. Stehling, C. Holland, J. P. Foreman, and C. Rodenburg, "Low-Voltage SEM of Natural Plant Fibers: Microstructure Properties (Surface and Cross-

Section) and their Link to the Tensile Properties," *Procedia Eng.*, vol. 200, pp. 295–302, 2017.

[42] G. Chinga-Carrasco, "Cellulose fibres, nanofibrils and microfibrils: The morphological sequence of MFC components from a plant physiology and fibre technology point of view," *Nanoscale Res. Lett.*, vol. 6, no. 1, pp. 1–7, 2011.

[43] D. Romanzini, H. L. Ornaghi Junior, S. C. Amico, and A. J. Zattera, "Preparation and characterization of ramie-glass fiber reinforced polymer matrix hybrid composites," *Mater. Res.*, vol. 15, no. 3, pp. 415–420, 2012.

[44] M. M. Morshed, M. M. Alam, and S. M. Daniels, "Plasma treatment of natural jute fibre by RIE 80 plus plasma tool," *Plasma Sci. Technol.*, vol. 12, no. 3, pp. 325–329, 2010.

[45] E. Sinha, "Effect of cold plasma treatment on macromolecular structure, thermal and mechanical behavior of jute fiber," *J. Ind. Text.*, vol. 38, no. 4, pp. 317–339, 2009.

[46] A. I. S. Brígida, V. M. A. Calado, L. R. B. Gonçalves, and M. A. Z. Coelho, "Effect of chemical treatments on properties of green coconut fiber," *Carbohydr. Polym.*, vol. 79, no. 4, pp. 832–838, 2010.

[47] J. Hnilica, L. Potočňáková, M. Stupavská, and V. Kudrle, "Rapid surface treatment of polyamide 12 by microwave plasma jet," *Appl. Surf. Sci.*, vol. 288, pp. 251–257, 2014.

[48] P. J. Herrera-Franco and A. Valadez-González, "A study of the mechanical properties of short natural-fiber reinforced composites," *Compos. Part B Eng.*, vol. 36, no. 8, pp. 597–608, 2005.

[49] E. A. Vogler, "Structure and reactivity of water at biomaterial surfaces," *Adv. Colloid Interface Sci.*, vol. 74, no. 1–3, pp. 69–117, 1998.

[50] J. Levón, "Microbial adhesion on biomaterials and the sources of human beta-defensin-3 in septic joint implant loosening," University of Helsinki, 2017.

[51] F. de A. Silva, N. Chawla, and R. D. de T. Filho, "Tensile behavior of high performance natural (sisal) fibers," *Compos. Sci. Technol.*, vol. 68, no. 15–16, pp. 3438–3443, 2008.

Section 5.6: Supplementary Materials

Figure S1. *Low pressure plasma - Diener electronic Zepto.*

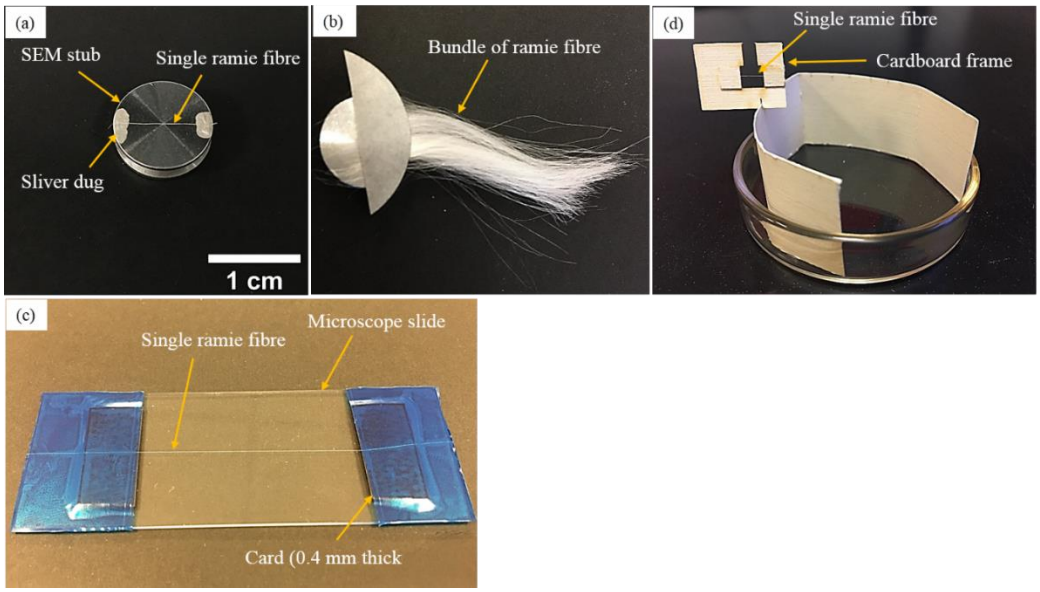

Figure S2. *Sample preparation (a) SEM sample, (b) FTIR sample, (c) contact angle sample, and (d) single fibre tensile testing sample.*

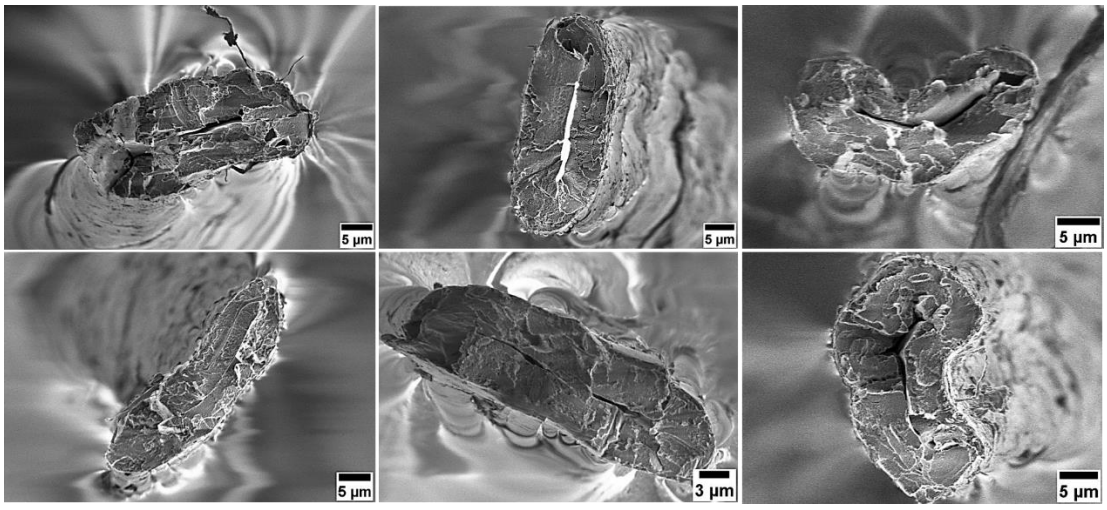

Figure S3. *Examples of SEM images of the fractured surface of single ramie fibres show the flat and clear fracture end after tensile testing.*

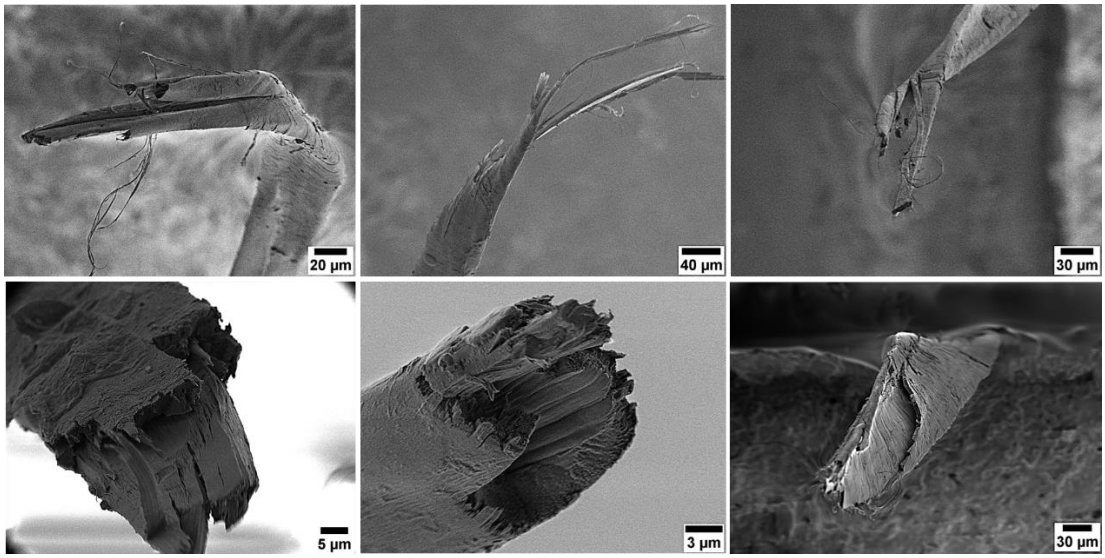

Figure S4. *Examples of SEM images of the fractured surface of single ramie fibres show the irregular fracture end after tensile testing.*

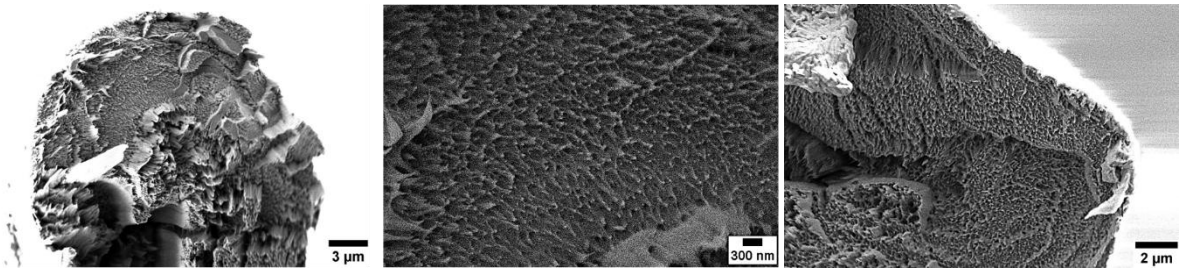

Figure S5. *SEM images of the cell wall of ramie fibres after tensile testing show the microfibrils.*

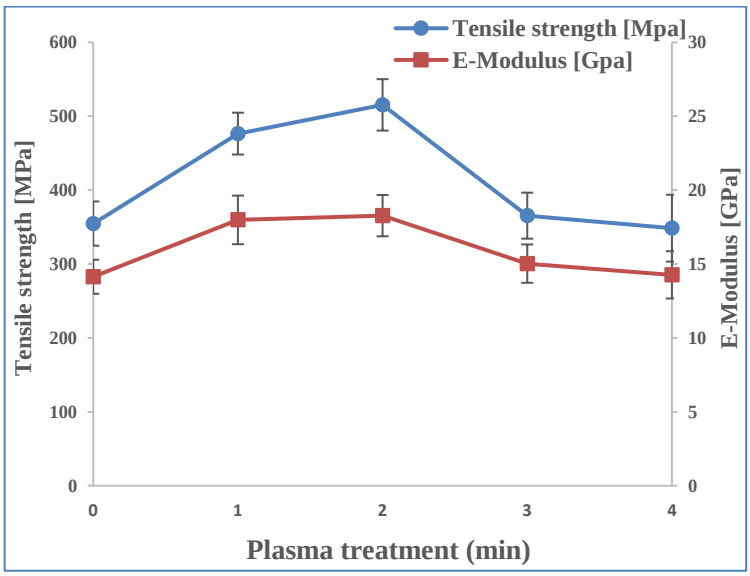

Figure S6. *The tensile strength and Young's modulus of untreated and plasma treated fibres, values based on fibre diameter measurements (assuming circular cross section).*

Table S1. *The sample size for each fibre (untreated and plasma treated) that used to determine the tensile strength and Young's modulus using the actual cross sectional area.*

Fibre	Sample size
0 min	5
1 min	10
2 min	9
3 min	10
4 min	11

Chapter 6: Optimizing size and distribution of voids in phenolic resins through the choice of catalyst types

Journal of Applied Polymer Science 48249 (2019)

Sameer F. Hamad[1,2]*, Nicholas Farr[1], Teng Fei[1], Nur F. Shukor[1], Julian S. Dean[1], Simon A. Hayes[3], Joel P. Foreman[1], C. Rodenburg[1]

[1]*Department of Materials Science and Engineering, the University of Sheffield, UK*

[2]*College of Engineering, University of Misan, Iraq*

[3]*Department of Multidisciplinary Engineering Education, the University of Sheffield, UK*

Correspondence to: Sameer F. Hamad (E-mail: sfhamad1@sheffield.ac.uk or sfhamad3@gmail.com)

This chapter has been published as an article paper in Journal of Applied Polymer Science, Wiley. I performed all the experimental work contained within, including sample preparation, mechanical testing, FTIR and SEM characterisation, and wrote the initial draft. The finite element modelling in Section 6.3.4 was performed by Julian Dean.

Original article is accessible at https://onlinelibrary.wiley.com/doi/full/10.1002/app.48249

Abstract: Phenolics are widely used for over a century in different industries due to their chemical resistance and thermo-mechanical properties. However, the presence of voids in phenolic resins has negative effects on the mechanical properties and a conventional approach is to avoid these by utilising very long cure cycles. Our alternative approach investigates the tailoring of void size and distribution to achieve a better balance between processing time and mechanical properties. Therefore, we produced phenolic resin with a void free microstructure by a long cure cycle as a reference. To alter the void size and distributions, we utilised different catalysts and a short cure cycle to obtain phenolic resins and test their flexural properties with respect to the reference. We investigated the fracture surfaces of all materials by SEM, FTIR and compared results to finite element modelling that confirmed the effects of different void size and distributions on the mechanical properties.

Section 6.1: Introduction

Phenolics or phenol-formaldehyde resins are amongst the oldest thermosetting polymers, with excellent ablative properties, low smoke density, high chemical resistance and thermal stability [1]–[5]. Such resins have been used in a broad range of applications such as moulding compounds, thermal insulation materials, coatings, laminates, wood products industry, and structural adhesives [6][7], and most of all as light weight foams in aerospace applications [8][9]. Furthermore, phenolics are also utilised as a matrix material for composite applications in the sport and construction industries due to their capability of withstanding highly corrosive environments [10]. However, it might be seen surprising even nowadays phenolic resins still suffer from the slow crosslinking rate and the high curing temperature [11]. Moreover, the mechanical properties of phenolic resins can be compromised by porosity and how to control it to a desired level still poses a scientific and industrial challenge [12]. The reason for this is the long and complex polymerisation process together with the generation of water and formaldehyde as by products. Void free phenolic parts usually require long heating cycles [13], thus not only taking a long time to produce but their production is also energy intensive. Here we investigate how to minimize any loss in mechanical properties as a consequence of implementing a short curing cycle.

Phenolic resins are produced from the polycondensation reaction of the phenol and formaldehyde. Based on the formaldehyde/phenol molar ratios and curing properties, phenolic resin is characterised into two main categories: novolac and resole resins [14][15][16]. Generally, both cured phenolic resin types (novolac and resole) are almost identical in terms of mechanical properties and chemical resistance [17]. Novolacs are synthesised in the presence of an acid catalyst with an excess of phenol, and do not react further without a curing agent. Hence, to produce a crosslinked structure of novolac resin, curing agents such as hexamethylenetramine (HMTA) must be added [17]. However, the

resin of interest for liquid moulding is resole resin [16]. Resoles are prepared in the presence of an alkaline catalyst with an excess of formaldehyde, producing a soluble and fusible prepolymer. Resole structures contain reactive hydroxymethyl groups and by heating, a crosslinked structure can be produced [17].

During the crosslinking of the phenol-formaldehyde resin, the release of the by-products becomes very difficult as the resin viscosity rises [18]. Consequently, the presence of these by-products in the cured resin can lead to porosity in the form of macro [13] or microvoids (8-10 μm in size) [16], which adversely affects the mechanical properties of the final cured resin [16]. However, it has been reported that phenolic resin with void free microstructures could be produced if the gelation time is kept long enough for the water vapour to be released [13][19]. This approach requires a very long heat cure cycle which is not favourable for most industries due to time and energy consumption issues. Therefore, there have been many attempts to accelerate the crosslinking rate of the phenolic resins with the use of different curing agents [20]–[23] but in each case, the formation of voids cannot be avoided.

No existing approaches allow void free microstructures to be achieved with a short cure cycle, therefore, a novel approach to optimise the microvoids size and distribution in a fast curing process for better mechanical properties at minimum processing time is proposed as an alternative. This investigation is inspired by the observation that in phenolic foams with deliberately high void volumes, the void diameter and distribution do affect the mechanical properties in a way that is not predicted by any current models [24]. Not only the void volume fraction but void diameter and void distribution were empirically found to be of importance in determining the final mechanical properties. However, the void size distributions (100-450 μm) obtained in phenolic foams [25] are significantly larger than those in phenolics intended as bulk materials or as matrix for composite materials. For the latter group of materials few studies have considered the effects of the void size and distribution on the final

mechanical properties of the cured phenolic resins [26]. Most studies have focused on the investigation of the effects of formaldehyde/phenol (F/P) molar ratios [27]–[29], reaction conditions (temperature, time) [26], degree of condensation [30], catalyst concentrations [26], and catalyst type [31] on the final properties of the cured resins. Here we investigate the possibility of changing the catalyst type to tailor void size and distributions in order to enable fast resin curing while minimising the effect of voids on the mechanical properties in comparison to the reference sample.

The objective of this study is to investigate the optimum void size and diameter distribution as well as the spatial distribution of the voids in the phenolic produced in a fast curing process and compare their mechanical properties to a void free reference phenolic. To this end a cross-linked resole phenolic resin material was produced using a long cure cycle (4 days) without the use of a catalyst. A slow action acid catalyst (Phencat 382) and a fast action acid catalyst (Phencat 10) were then utilised to produce two phenolic resin samples types with varying void sizes and distributions and mechanical properties (strength and modulus obtained from bending tests). To visualise and quantify detailed void structures, diameters and distributions, low voltage scanning electron microscopy (LV-SEM) was used to image the fractured surface of the above three types of cured phenolic resin. The latter enables the observation of highly localised variation in chemistry and crack behaviour. To account for effects introduced by the variation of average chemical composition all of the cured phenolic resins where subject to analysis by Fourier Transform Infrared (FTIR).

Section 6.2: Experimental

Section 6.2.1: Materials

In this study, a resole commercial phenolic resin called Cellobond J2027X was used (kindly supplied by Caleb Technical Products Ltd., UK). This kind of resin is usually available as a water-based controlled-viscosity resin which can be cured either with the application of heat only (long cure cycle) or at lower temperature (60 °C), short cure cycle (3 hours), with the

use of a strong acid catalyst [16]. It is suitable for fabrication of fibre composites by hand layup and resin transfer moulding [32]. Two types of catalyst (Cellobond Phencat 382 and Cellobond Phencat 10) supplied by the same company (Caleb Technical Products Ltd., UK) were used in this study. Phencat 382 is a relatively slow action acid catalyst (working life 4 hours) which is activated at low temperature, typically 60-80 °C [16]. It is an acid based catalyst consisting of phosphoric acid, C3-9-alkyl esters (75-90 %) and phosphoric acid (10-25 %) by weight. Phencat 10 is a general purpose catalyst for processes such as contact moulding giving working life of about 20 min. It is composition consists of p-toluenesulphonic acid (35-50 %) and phosphoric acid (10-25 %) by weight.

Section 6.2.2: Curing process of commercial resole phenolic resin

Two different curing schedules were used to cure the resole phenolic resin:

1- Long cure cycle, the as received resole phenolic resin was poured into a PTFE mould and then placed in an autoclave to be cured using the cure cycle presented in Figure 6-1.

2- Short cure cycle, the resole phenolic resin was first mixed with either slow action acid catalyst (phencat 382), or fast action acid catalyst (phencat 10), and then poured into the PTFE mould to be placed in an autoclave using a short cure cycle presented in Table 6-1. The catalyst ratio was maintained at 5 wt% of the resin for all samples.

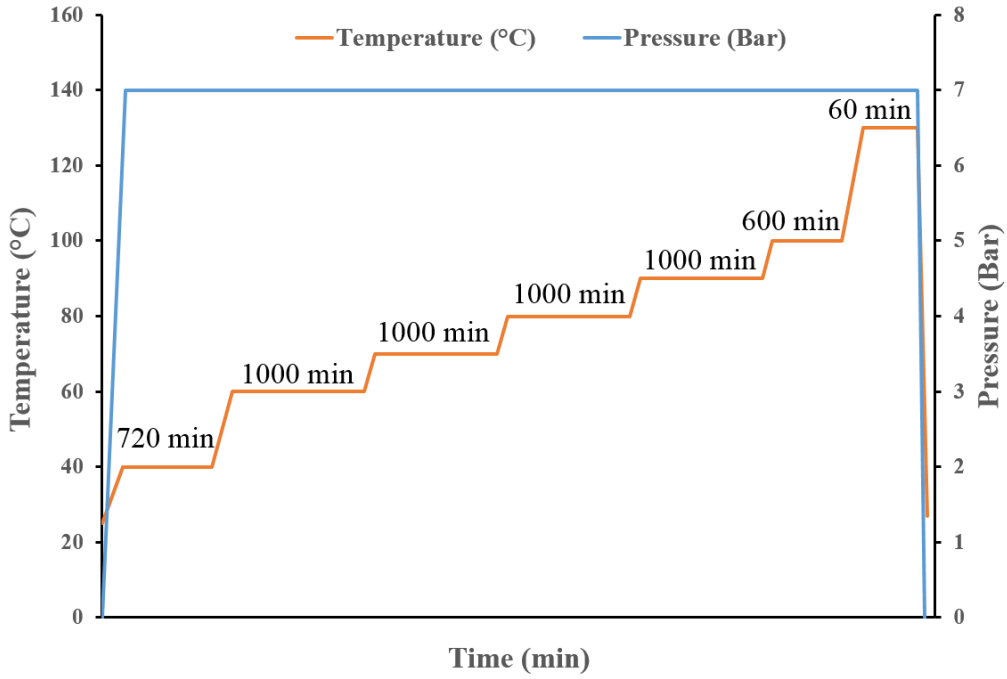

Figure 6-1: *Long cure cycle used to cure phenolic resin without any catalyst. The heating ramp rate and pressure ramp rate were 2 °C/min and 0.3 Bar/min respectively.*

Table 6-1: *Short cure cycle used to cure phenolic resin with the addition of catalyst.*

Temperature (°C)	Temperature ramp rate (°C/min)	Pressure (Bar)	Pressure ramp rate (Bar/min)	Dwell time (min)
80	2.00	7.00	0.30	180
130	2.00	7.00	0.00	60
27	2.00	0.00	0.20	0.00

Section 6.2.3: Characterisation

Section 6.2.3.1: Scanning Electron Microscopy SEM

Scanning Electron Microscopy (FEI Nova Nano SEM 450) was used for the morphology observation of the fracture surface of the flexural strength samples. Unlike standard SEM analysis, no conductive coating was deposited onto the samples. Therefore, a low accelerating voltage (1 kV) was used to avoid sample surface charging and damage with typical vacuum pressure of 10^{-5} mbar, and a working distance of about 4mm. Secondary electron images were collected using either an Everhart-Thornley Detector (ETD) for low

magnification images or a Through Lens Detector (TLD) to obtain high magnification images.

Section 6.2.3.2: Fourier Transform Infrared Spectroscopy (FTIR)

The chemical composition of all cured phenolic resins was investigated using a PerkinElmer Frontier spectrophotometer. To prepare the FTIR sample pellet, 2 mg of sample powder (ground from the bulk sample) was diluted with 300 mg of spectroscopic grade KBr. The test was performed at room temperature (22 ± 3 °C) with a wavenumber range between 4000 cm^{-1} to 600 cm^{-1} and the average of scan repetitions was 32 scans for each sample at 2 cm^{-1} of resolution. Before loading the sample, a background spectrum was taken as a control.

Section 6.2.3.3: Flexural Test

The flexural properties (strength and modulus) of all specimens were determined using a Lloyd TA500 tensometer. The test was performed according to the ASTM D790 (standard test methods for flexural properties of unreinforced and reinforced plastics and electrical insulating materials) with a span to sample thickness ratio of 16. Crosshead speeds of all tests was 2.0 mm/min. The tests were performed at room temperature (22 ± 3 °C).

The ultimate bending results of each type of phenolic resin were calculated as an average of seven specimens per test condition. The flexural modulus was determined from the following formula:

$$\mathrm{E} = \frac{L^3 F}{4 w h^3 d} \qquad (6.1)$$

Where *E* is modulus of elasticity in bending (MPa), *L* is the support span (mm), *F* is the peak load (N), *w* is the width of the sample (mm), *h* is the thickness (mm), and *d* is the sample deflection (mm).

Section 6.3: Results and discussion

Section 6.3.1: Fracture surface characterisation

The fracture surfaces obtained by the bending test of the three types of cured phenolic resin were observed by LV-SEM and their micrographs are shown in Figure 6-2. A homogenous fracture surface without any micron sized voids was observed for the reference sample cured without catalyst, using the long cure cycle (Figure 6-1), as shown in Figure 6-2a. A higher magnification image (Figure 6-2b) reveals the presence of a large number of bright nanostructures with diameters well below 100 nm. Their dimensions are consistent with previous electron microscopy studies of replicas of fractured phenolic resin surfaces [33]. These structures were interpreted as localised areas of increased crosslinking density [33] but the observed contrast would have been consistent with voids too. A few such bright nanostructures can be seen also in at the fracture surface of the specimens prepared with the slow action catalyst shown in Figure 6-2c and d. However, the latter fracture surfaces also show clear evidence of voids with diameters that reach from hundreds of nanometres to several micrometres. This is more easily seen in the diameter distribution histograms in Figure 6-3a which was derived from the binary images (Figure 6-4a). Likewise, we present SEM images of the fracture surfaces obtained from materials produced with a fast action catalyst in Figure 6-2e and f and the respective diameter distribution histogram in Figure 6-3b. The histogram was derived from the binary images presented in in Figure 6-4b. The histogram (Figure 6-3b) shows clearly that the overwhelming majority of structures is of submicron size, with an average diameter of 0.52±0.15 μm, while the SEM images demonstrates the dense and homogenous coverage (Figure 6-2f) of the fracture surface with spherical features.

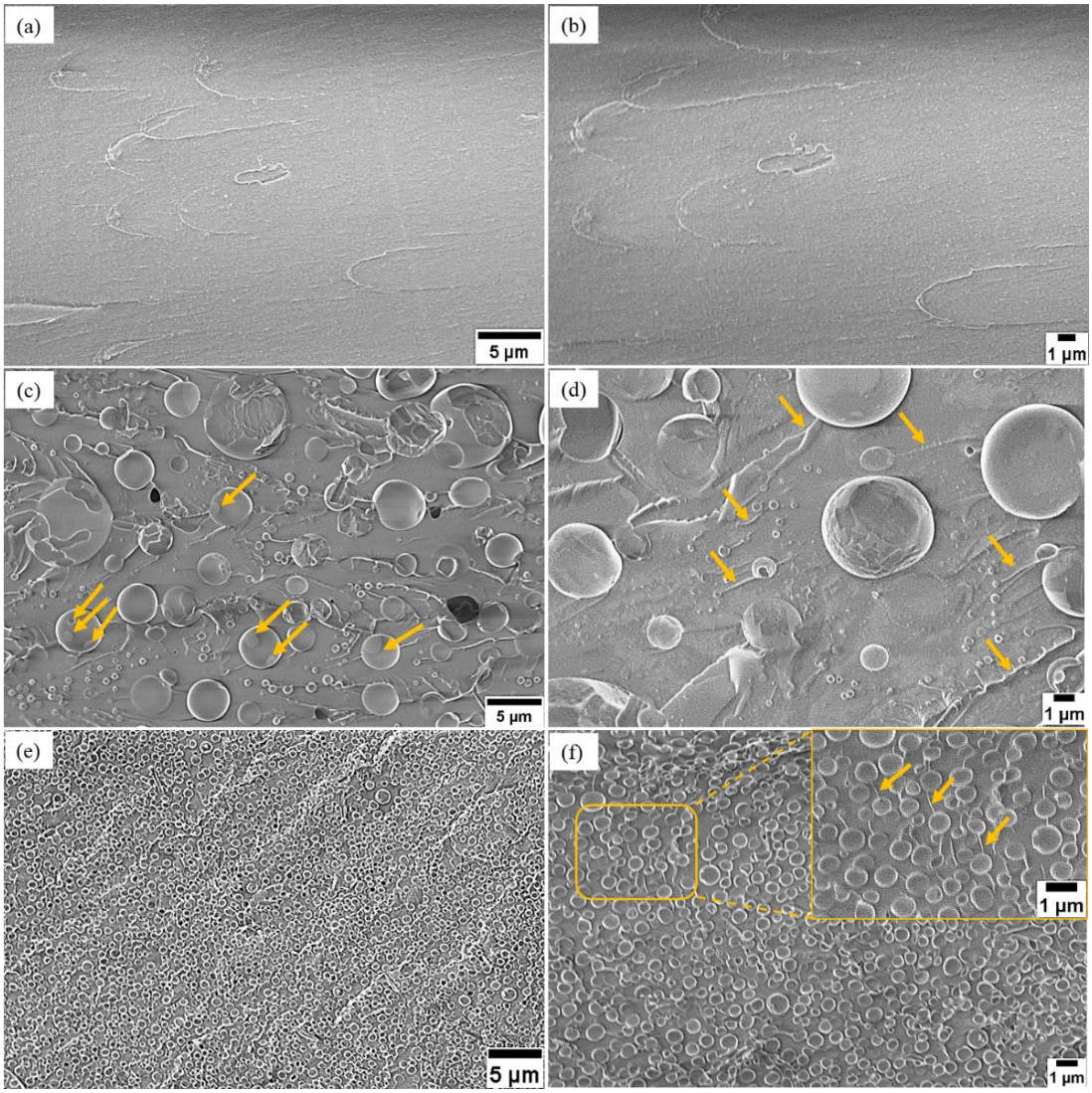

Figure 6-2: *LV-SEM micrographs of the fracture surface of the three types of cured phenolic resins, (a) low and (b) high magnification images of phenolic resin cured using long cure cycle without added catalyst, (c) low and (d) high magnification images of phenolic resin cured with the addition of slow action catalyst (phencat 382), and (e) low and (f) high magnification images of phenolic resin cured with the addition of fast action catalyst (phencat 10). Arrows in (c) indicate the bubbles coalescence. Arrows in (d) and (f) (insert micrograph) indicate the cracks.*

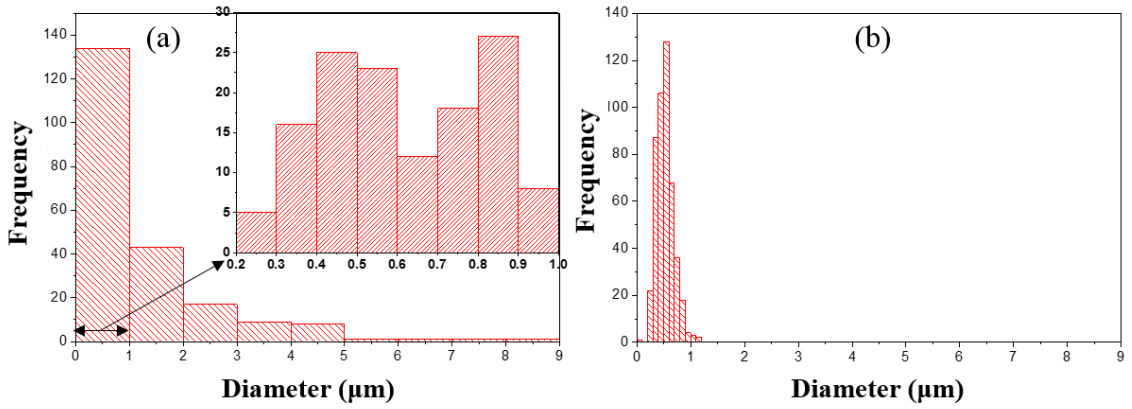

Figure 6-3: *Histogram of voids diameter distribution: (a) phenolic resin cured with a slow action catalyst (phencat 382), and (b) phenolic resin cured with a fast action catalyst (phencat 10).*

To understand the origin of the patterns is worth noting that a combination of small-angle neutron scattering (SANS) and small-angle X-ray scattering (SAXS) experiment on phenolic resins revealed that rough interfaces between voids and phenolic matrix with a fractal dimensions ~2.46 to 2.6 exist [34]. This fractal dimension is consistent with the existence of Apollonian arrangement for which a fractal dimensions of 2.4739465 was established [35]. Apollonian packing is found and used in the controlled preparation of ordered porous films exploiting Breath Figures, to produce so called Breath Figure arrays (BFA) [36]. In BFA fabrication the irregular pore arrays are observed if water droplet can coalesce while homogenous pore arrays when the coalesce of water droplets can be prevented.

Therefore, all of the observations in Figure 6-2 can be understood in terms of time available before the gel point is reached. If this is long enough for the release of the water vapour before the start of crosslinking in the resin structure [19], the formation of voids can be prevented as is the case in the reference material (Figure 6-2a). In contrast, with the use of catalysts, the crosslinking rate of the phenol-formaldehyde resins is relatively fast. As the amount of water in the resin increased during the reaction, molecular clusters can form that then nucleate when the saturation level at a given temperature and pressure is locally

exceeded [12]. This leads to phase-separation and produces water domains [32]. With the fast action catalyst (Figure 6-2e and f), the crosslinking rate is very fast (only 20 minutes working life according to the technical data sheet) and the gelation time is very short. Therefore, the trapped water, present as result of the complex polymerization process including the release of formaldehyde and water as by-products [37], will not be able to be released or diffuse, resulting in a homogenous distribution of voids with the very narrow size distribution as seen in Figure 6-3b. In contrast, with the use of a slow action catalyst (material in Figure 6-2c and d), the cross linking rate is slower (4 hours working life according to the technical data sheet) and the gelation time is longer. Therefore, the generated water can move and coalesce leading to the very broad size distribution of voids, as well as a wide variation in distances between voids. Larger voids tend to be surrounded by void free zones as can be seen in the binary image and distance map in Figure 6-4a. The distance between small voids in Figure 6-4a is similar to that found in the distance map obtained from the material made by the fast action catalyst (Figure 6-4b). However, the distance to larger voids in Figure 6-4a is substantially larger than the distance in Figure 6-4b. The above is also reflected in Figure 6-4c, which compares the distances between voids in the materials made using slow and fast action catalysts, respectively. While for the slow action catalysts distances between voids can exceed 4 μm, the use of fast action catalyst results in distances between voids < 1.5 μm. This difference is likely to play a critical role with regards to the mechanical properties, as the voids do seem to effect crack initiation and growth as evidenced by Fig 1d and f (indicated by arrows). Both Figures contain evidence of cracks (wide due to the edge effect). In the material produced from the slow action catalyst (Figure 6-2d) fewer but longer cracks are observed than in the material made with the fast action catalyst (Figure 6-2f (insert micrograph)). The longest cracks in Figure 6-2d are found

to propagate in the void free zones with no clear termination point, while all of the cracks visible in Figure 6-2f (insert micrograph) are terminated at both ends by voids.

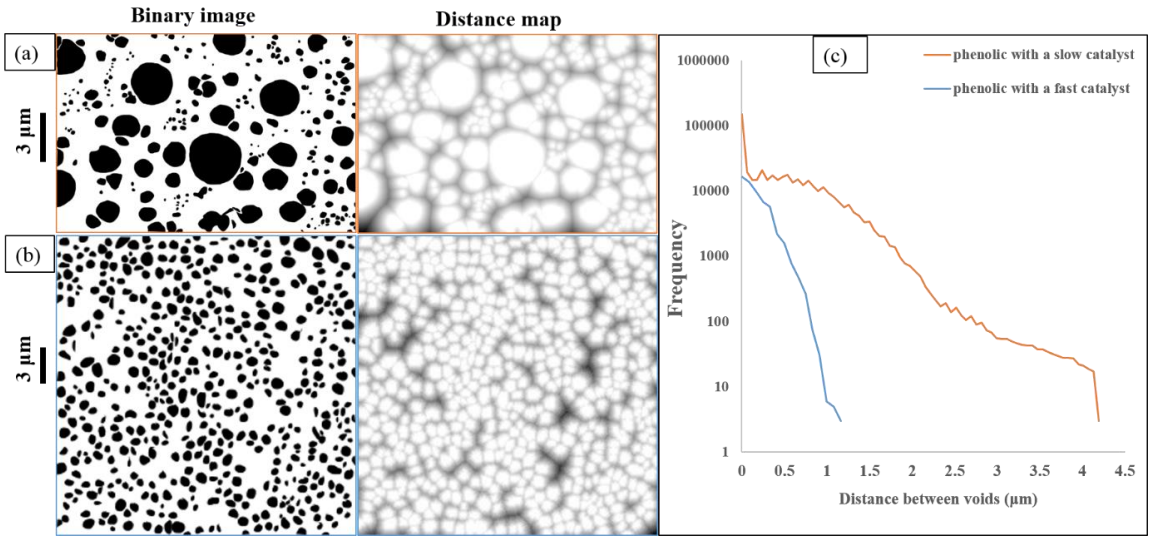

Figure 6-4: *Voids analysis in phenolic resins cured with (a) a slow action catalyst, and (b) a fast action acid catalyst. (c) Histogram of inter-voids distance for the images presented in (a) and (b). Image processing was performed using Fiji software [38].*

Further differences between the materials made using slow and fast action catalysts respectively is in the volume fraction taken up by the voids structures. We can only measure area fractions from the 2D SEM images (28% in materials from fast action catalyst & 33% in materials using slow action catalyst). However, the volume fraction is only directly proportional to the area fraction if the sectioning plane intersects the structural features at random. As are sections are produced by fracture the later condition is not necessarily fulfilled here, because as seen in Figure 1d (indicated by arrows) wide cracks are seen to run along the larger voids. While all of the above will affect the mechanical properties (see Sections 6.3.3 and 6.3.4 for full details), differences in chemistry as a result of using the different catalysts could also be responsible for the differences in mechanical properties.

Section 6.3.2: The chemical composition analysis

Results of FT-IR measurements are presented in Figure 6-5 in order to enable component identification of the products produced by the condensation reaction of phenol and

formaldehyde. The standard peak positions [39] and the observed peaks of the resole phenol/formaldehyde resins are assigned in SI (Table S1).

It was expected that both catalysts used would be observable through two clear absorption bands; one band at 1650 cm^{-1}, noted for hydrated phosphates P–OH and corresponding to O–H stretching and O–H deformation vibrations and second band between 1300 to 900cm^{-1} that is characteristic of P–O and C–O vibrations [40]. In this reaction these absorption bands cannot be independently isolated as both bands coincide with the phenolic resin bands at 1594 cm^{-1}, corresponding to the absorption of C=C of phenyl rings, and bands 1100 cm^{-1} which are characteristic of the C-H flexural of phenyl rings.

Two bands observed at 1630 cm^{-1} and 1612 cm^{-1} are of particular interest. The first band was noted as the C = O stretch (overlapped with OH scissors of water) which is characteristic of unreacted formaldehyde. This first band has higher intensity when the materials is made using a catalyst with a short cure cycle when compared to phenolic cured without a catalyst using long cure cycle. This absorption band can be interpreted in either of two ways: firstly the resins formed using a catalyst might have a slightly reduced cross linking density or secondly, and more likely, the acid catalyst pushes the equilibrium of the two step reaction towards the second step of the polymerisation of phenolic resin. Either interpretation results in less formaldehyde being used in the initial reaction and thus leads to the presence of unreacted formaldehyde. The latter is more likely because it is observable that the phenolic resin cured with a fast action acid catalyst showed a stronger 1630 cm^{-1} band when compared to that of phenolic resin cured with a slow action acid catalyst. This result would be expected as the fast catalyst is the more acidic.

An interesting feature is the absorption band present at 1612 cm^{-1}. This absorption band displays a greater intensity in the case of phenolic resin cured without catalyst than that of either catalyst. The band is caused by the C = C aromatic ring within a functional group of

phenol-formaldehyde resin. This is the product of the first step reaction of phenol and formaldehyde and therefore is consistent with the premise that the acid catalyst is slowing down the formation of this product.

Two interesting bands were also noted at 2912 cm^{-1} and 1100 cm^{-1}, these bands are attributed to methylene and ether bridges respectively [39]. Changes in the two bands values were observed between the two catalysts. These changes are expected to originate from the differences of the phenol bonding mechanism. It was noted that there was a reduction of ether bridges within phenolic resin cured with a fast action catalyst when compared to that of phenolic resin cured with a slow action catalyst and a consequential increase in methylene bridges in phenolic cured with fast catalyst when compared to that of phenolic cured with slow catalyst. The more acidic the catalyst, the more that the phenol is protonated and therefore the less nucleophilic it is. As a result it is less likely that it will follow a second mechanism and form ether bridges (see Figure 6-6). The results observed point to an increased likelihood that the first mechanism is the correct one. If so, the more acidic catalyst (fast action catalyst) will promote the formation of methylene bridges within the phenolic. Methylene bridges have a greater bond strength than that of ether bridges [41]. This can result in different mechanical properties of the phenolic due to more methylene bridges (see Section 6.3.3).

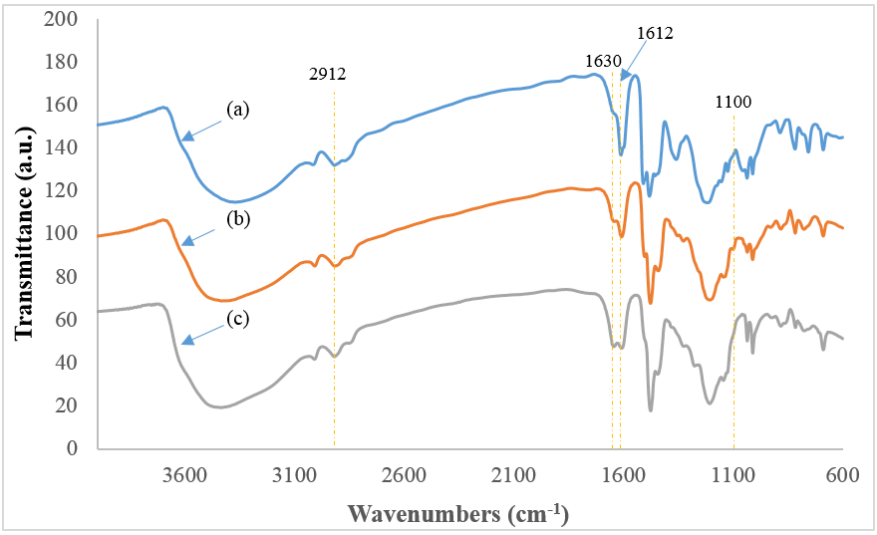

Figure 6-5: *The IR spectrum of phenol/formaldehyde resin cured: (a) without catalyst, (b) with a slow action catalyst (Phencat 382), and (c) with a fast action catalyst (Phencat 10).*

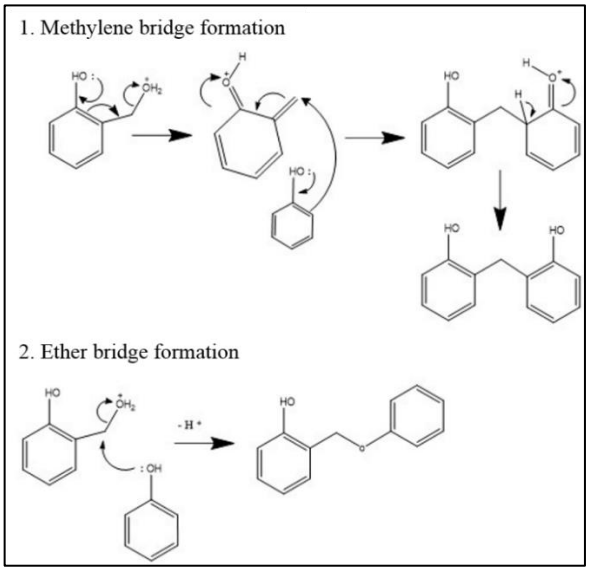

Figure 6-6: *Two possible reactions of phenol/formaldehyde resin with acid catalyst.*

Section 6.3.3: Flexural strength and modulus

The flexural properties of the three types of cured phenolic resins were determined and are presented in Table 6-2. It can be seen that the phenolic resin cured without a catalyst, using a long cure cycle (almost 4 days), has the highest average values of flexural strength (88 ± 18 MPa) and modulus (3.2 ± 0.28 GPa) in comparison to those of phenolic resins cured with catalysts. This is expected and can be explained in part by the reduced area of phenolic resin due to the presence of voids when prepared with catalysts. With the use of a slow action

catalyst, the flexural strength and modulus of the cured phenolic resin were decreased to 47.0 ± 8.0 MPa and 2.0 ± 0.25 GPa respectively. The presence of the voids in the cured resin increase the pressure on the surrounding resin and also they act as stress concentrators rendering the material more fragile [42][43]. When the sample is subjected to a load, stress and strain concentrations will be generated around the voids causing a local plastic deformation. Then with increasing load, cracks will be initiated and grow in the voids free resin zones, with the resultant reduction in the resin strength [44][45]. Such cracks were clearly observed by SEM image shown in Figure 6-2d.

Table 6-2: *Flexural properties of the three types of cured phenolic resins.*

Sample	Flexural strength (MPa)	STDEV	Flexural Modulus (GPa)	STDEV	Deflection (mm)	STDEV
Phenolic without catalyst	88	18	3.20	0.28	1.20	0.25
Phenolic with slow action catalyst (382)	47	8	2.0	0.25	0.99	0.11
Phenolic with fast action catalyst (10)	68	12	2.30	0.43	1.20	0.25

However, it is important to point out that the average values of the flexural strength (68 ± 12 MPa) and the flexural modulus (2.3±0.43 GPa) of the phenolic resin cured with a fast action catalyst were higher than those of phenolic resin cured with a slow action catalyst. Moreover, some of the tested samples from the phenolic resin cured with a fast action catalyst showed very close or even the same flexural strength values as some of phenolic resin cured without a catalyst (see Table S3 and Figure S1). By taking into account the void volume fraction, it has been noted that the flexural strength of the phenolic resin cured with a fast action catalyst was similar to the flexural strength of the reference sample (cured without catalyst). Whereas in the case of using a slow action catalyst, the flexural strength remains lower than that of reference and fast action cured samples.

Therefore, the differences in the flexural properties between the two phenolic resins (cured with either slow or fast action catalyst) can be attributed to both the structural and chemical changes presented in this paper. In terms of the chemical changes, it is possible that the presence of high prevalence methylene bridges in the case of using a fast action catalyst (as discussed within FTIR analysis in Section 6.3.2) could potentially improve the flexural properties of the cured resin. But more significantly it can be confirmed that the increase in the flexural properties in the case of using fast action catalyst were due to the void size and distribution in the cured resin. For instance, in phenolic foams, it has been found that the cell size and cell distribution have significant effects on the final mechanical properties of the foam. Smaller and more uniform cell size in the final cured foam will potentially improve the mechanical properties [24]. Similarly, in this study, the LV-SEM micrograph and image analysis of the fracture surface of the phenolic resin cured with a fast action catalyst shows small and uniform void diameter distribution, whereas a non-uniform void diameter distribution was observed in the case of using slow action catalyst (see Section 6.3.1).

To understand this further, it was thus confirmed that the void diameter distribution plays a major role in the crack initiation and propagation. Small cracks terminated at both ends by voids were observed in the fracture surface of phenolic resin cured with a fast action catalyst. It was assumed that the small and uniform distances between the small voids can help to prevent the crack propagation in the void free resin. This is in contrast, to the cracks in the case of using a slow action catalyst, were fewer and longer cracks exist, which are seen by SEM in Figure 6-2d to propagate in the void free area and also along the large voids. Moreover, the long boundary between the void free area and the large voids is also expected to accelerate the crack growth and hence the early sample failure. All the above were further confirmed by the model in Section 6.3.4.

Section 6.3.4: Finite element modelling

To study the effect of the void size and distribution of phenolic resin cured with slow and fast action catalyst has upon the stress concentration and ultimately the failure strength of the resins, we employ a simplistic finite element model. Experimental void sizes calculated in Figure 6-3 are directly implemented into a finite element model using an approach previously used to study the effect of electric field enhancement in electro-ceramic materials [46]. Treating the voids as hard spheres, the lists of diameters are randomised and then sequentially positioned randomly into a cube. This process continues until the effective density of the solid is reduced to 70% (assuming both materials have the same voids area fraction (30 %) for simplification). These spheres are then subtracted from the solid cube to form the semi-dense structure replicated the two materials. Due to the differences in size and number of voids for each system (as already seen in SEM images (Section 6.3.1)), the size of the cube is modified to save computation time. Hence, to create models for phenolic resin cured with a fast action catalyst requires approximately 300 voids in a cube of 5μm^3, whilst for phenolic resin cured with a slow action catalyst, approximately 150 voids in a cube of 15μm^3 are need to generate a 70% dense solid. An example for each model can be seen in Figure 6-7.

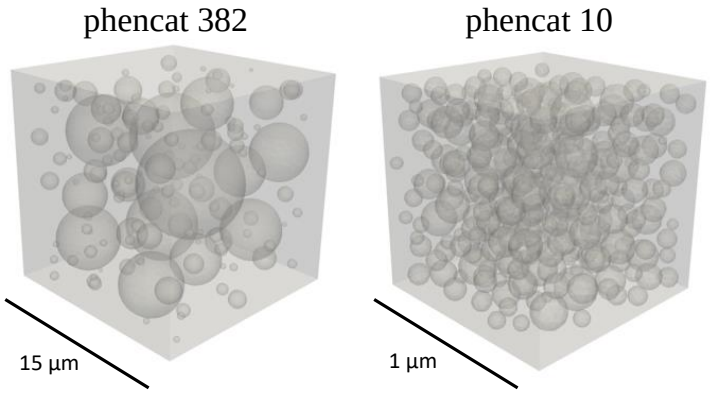

Figure 6-7: *The microstructural representations of phenolic resin cured with a slow action catalyst (Phencat 382) (~150 individual microvoids) and a fast action catalyst (Phencat 10) (~300 individual microvoids). Each model has an overall solid density of 70%.*

The models are then imported into COMSOL [47] and solved using the structural module. We assume the resin Young's modulus is 3.2 GPa with a Poisson's ratio of 0.3 [48]. The model assumes the resin is entirely elastic and isotropic. Due to the simplicity in performing the model with the tensile load instead of the bending load, we apply a tensile load of 21 MPa on the top surface as a reference. This value is chosen as it generates a maximum stress in both samples of approximately 88 MPa, the failure point of the microvoid free sample. The bottom surface was restricted in movement within plane and a single node in the centre of the surface fixed rigidly in all dimensions to not overly constrain the system. Symmetry was employed on the other four surfaces to replicate a central region of 'bulk' like material. The model was then discretised with over two-million tetrahedron elements, ensuring convergence of the results. Figure 6-8 shows von-Mises stress, highlight in red, the points at which failure may begin. In Figure 6-8a, it can be seen that the representation of phenolic resin cured with a slow action catalyst (phencat 382) generates significant stresses between the large voids (over 70 MPa), which extends over a few μm in length. This is in comparison to phenolic resin cured with a fast action catalyst (phencat 10) where stresses are as great but highly localised between the small particles and typically restricted to less than 1μm in length due to the proximity of the voids (Figure 6-8b). To highlight this further, we plot only the stresses greater than 70 MPa in Figure 6-8c and d as a top down view. It is clearly visible that for phenolic resin cured with a slow action catalyst high stresses are located around the circumference of larger voids in relation to the applied stress (Figure 6-8c) and extend through the system to other large voids. The same high stresses in phenolic resin cured with a fast action catalyst are only found between two closely placed voids (Figure 6-8d). If the yield strength of the material is considered to be the point at which a crack would form and spread, it is clear that for phenolic resin cured with a fast action catalyst, these cracks would be between neighbouring voids, travelling less than 1μm. Conversely, for phenolic resin

cured with a slow action catalyst, due to the increased distance between voids, the crack could propagate much further, and as such reach a critical point for fracture earlier. This is clearly consistence with the SEM micrographs shown in Figure 6-8e and f and also in good agreement with the flexural property results in Section 6.3.3 (Table 6-2).

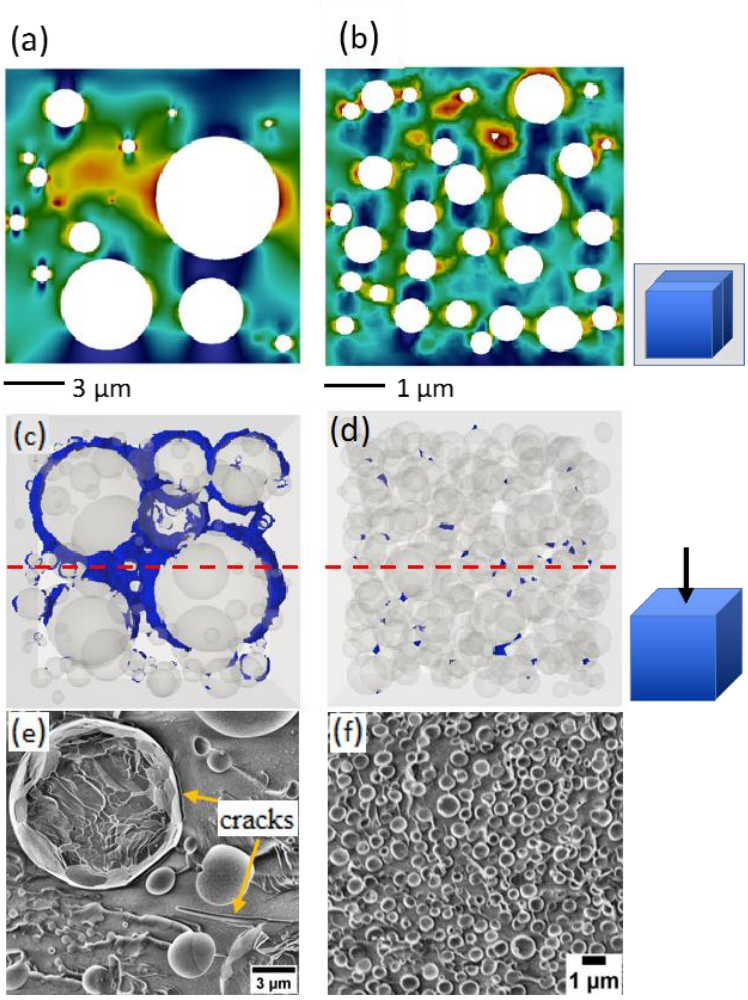

Figure 6-8: *The comparison of the stress distribution in models that represent phenolic resin cured with a slow action catalyst (phencat 382) (a,c) and phenolic resin cured with a fast action catalyst (phencat 10) (b,d). The resulting von-Mises stress is plotted (a,b) as a cross section of the cube. Red indicates a stress of 88MPa, while blue indicates a minimum stress of 0. Parts (c) and (d) are top down views of the model highlight only the top 20% of stresses (70-88MPa) within the system. The red-dashed line indicates the cross section seen in parts (a) and (b). Parts (e) and (f) are the SEM micrographs of the fracture surface of the phenolic cured with slow action catalyst and fast action catalyst respectively. The small images to the right of the figure highlight the direction of the image seen.*

Section 6.4: Conclusions

LV-SEM combined with the finite element modelling suggest that the size and spatial distribution of the voids in the cured phenolic resin are of great importance in determining the final mechanical properties of the resin. While the conventional approach in phenolic resins is to minimize or to avoid the void content in the cured resin, here we show that for the similar void content, achieving a homogenous void distribution is critical. More attention should be paid to the engineering of voids size and distribution. With the use of fast action catalyst in curing the resole phenolic resins, a better balance between the properties and cure cycle could be achieved.

Acknowledgements

Sameer F. Hamad gratefully acknowledge the Iraqi Ministry of Higher Education and Scientific Research and its representative in the UK, the Iraqi Cultural Attaché for the financial support. C. Rodenburg thanks the Engineering and Physical Sciences Research Council (EPSRC) for funding under EP/N008065/1. Nicholas Farr thanks EPSRC for funding of his doctoral training studentship. Joel P. Foreman thanks Peter Willson at Caleb Technical Products for providing the resin.

Section 6.5: References

[1] J. Wang and Y. F. Zhang, "Chemical Structure and Curing Characteristics of Phenol Formaldehyde Resins Catalyzed with Calcium Oxide," *Polym. - Plast. Technol. Eng.*, vol. 51, no. 12, pp. 1213–1217, 2012.

[2] D. Ratna and J. Karger Kocsis, "Thermomechanical properties and morphology of polyethylene oxide and phenolic resole blends," *J. Appl. Polym. Sci.*, vol. 127, no. 5, pp. 4039–4043, 2013.

[3] J. Wang, H. Jiang, and N. Jiang, "Study on the pyrolysis of phenol-formaldehyde (PF) resin and modified PF resin," *Thermochim. Acta*, vol. 496, no. 1–2, pp. 136–142, 2009.

[4] H. S. Budiono, E. Surojo, N. Muhayat, and W. W. Raharjo, "Effect of post curing method on flexural strength of composite friction brake," *MATEC Web Conf.*, vol.

159, pp. 1–6, 2018.

[5] H. Der Wu, M. S. Lee, Y. D. Wu, Y. F. Su, and C. C. M. Ma, “Pultruded Fiber-Reinforced Polyurethane-Toughened Phenolic Resin. 11. Mechanical Properties, Thermal Properties, and Flame Resistance,” *J. Appl. Polym. Sci.*, vol. 62, pp. 227–234, 1996.

[6] Ü. B. Alkan and N. Kızılcan, “In Situ Preparation of Resol/Sepiolite Nanocomposites,” *Procedia - Soc. Behav. Sci.*, vol. 195, pp. 2067–2075, 2015.

[7] Y. Zhang, S. Shen, and Y. Liu, “The effect of titanium incorporation on the thermal stability of phenol-formaldehyde resin and its carbonization microstructure,” *Polym. Degrad. Stab.*, vol. 98, no. 2, pp. 514–518, 2013.

[8] M. Niu and G. Wang, “The preparation and performance of phenolic foams modifed by active polypropylene glycol,” *Cell. Polym.*, vol. 32, no. 3, pp. 155–172, 2013.

[9] Y. Yu, Y. Wang, P. Xu, and J. Chang, “Preparation and Characterization of Phenolic Foam Modified with Bio-Oil,” *Materials (Basel).*, vol. 11, no. 11, p. 2228, 2018.

[10] M. Asim, N. Saba, M. Jawaid, M. Nasir, M. Pervaiz, and O. Y. Alothman, “A review on Phenolic resin and its Composites,” *Curr. Anal. Chem.*, vol. 14, pp. 1–13, 2018.

[11] J. Li *et al.*, “Curing properties of high-Ortho phenol-formaldehyde resins with co-catalysis,” *J. Appl. Polym. Sci.*, vol. 136, no. 12, pp. 1–9, 2019.

[12] C. Pupin, A. Ross, C. Dubois, J. Rietsch, and E. Ruiz, “Predicting porosity formation in phenolic resins for RTM manufacturing : The porosity map,” *Compos. Part A*, vol. 100, pp. 294–304, 2017.

[13] M. Natali, J. Kenny, and L. Torre, “Phenolic matrix nanocomposites based on commercial grade resols: Synthesis and characterization,” *Compos. Sci. Technol.*, vol. 70, no. 4, pp. 571–577, 2010.

[14] S. Sulaiman, R. Yunus, N. A. Ibrahim, and F. Rezaei, “Effect of Hardener on Mechanical Properties of Carbon Fibre Reinforced Phenolic Resin Composites,” *J. Eng. Sci. Technol.*, vol. 3, no. 1, pp. 79–86, 2008.

[15] G. N. Manikandan and K. Bogeshwaran, “Effect of curing time on phenolic resins

using latent acid catalyst," *ChemTech Res*, vol. 9, no. 01, pp. 30–37, 2016.

[16] K. P. Singh and G. R. Palmese, "Enhancement of phenolic polymer properties by use of ethylene glycol as diluent," *J. Appl. Polym. Sci.*, vol. 91, no. 5, pp. 3096–3106, 2004.

[17] E. S. De Medeiros, a M. Agnelli, K. Joseph, and L. H. De Carvalho, "Curing Behavior of a Novolac-Type Phenolic Resin Analyzed by Differential Scanning Calorimetry," *J. Appl. Polym. Sci.*, vol. 90, pp. 1678–1682, 2003.

[18] P. S. Parameswaran, M. G. Bhuvaneswary, and E. T. Thachil, "Control of microvoids in resol phenolic resin using unsaturated polyester," *J. Appl. Polym. Sci.*, vol. 113, no. 2, pp. 802–810, 2009.

[19] C. Kaynak and C. C. Tasan, "Effects of production parameters on the structure of resol type phenolic resin/layered silicate nanocomposites," *Eur. Polym. J.*, vol. 42, no. 8, pp. 1908–1921, 2006.

[20] L. He, R. Han, and Y. Zhang, "Cure characteristics of phenol-formaldehyde resin catalyzed with Ba(OH)2," *J. Adhes. Sci. Technol.*, vol. 23, no. 12, pp. 1639–1645, 2009.

[21] B. D. Park, B. Riedl, E. W. Hsu, and J. Shields, "Differential scanning calorimetry of phenol-formaldehyde resins cure- accelerated by carbonates," *Polymer (Guildf).*, vol. 40, no. 7, pp. 1689–1699, 1999.

[22] A. Singh, S. Aggrawal, and D. Lal, "Effect of Formaldehyde to Phenol Ratio in Phenolic Beads on Pore Structure , Adsorption and Mechanical Properties of Activated Carbon Spheres," *Def. Sci. J.*, vol. 69, no. 1, pp. 46–52, 2019.

[23] G. A. Aierbe, J. M. Echeverria, M. D. Martin, and I. Mondragon, "Kinetics of phenolic resol resin formation by HPLC. 2. Barium hydroxide," *Polymer (Guildf).*, vol. 39, no. 15, pp. 3467–3472, 1998.

[24] C. Mougel, T. Garnier, P. Cassagnau, and N. Sintes-Zydowicz, "Phenolic foams: A review of mechanical properties, fire resistance and new trends in phenol substitution," *Polymer (Guildf).*, vol. 164, no. November 2018, pp. 86–117, 2019.

[25] Q. Li *et al.*, "Effect of nano-titanium nitride on thermal insulating and flame-retardant

performances of phenolic foam," *J. Appl. Polym. Sci.*, vol. 133, no. 32, pp. 1–13, 2016.

[26] J. Wolfrum and G. W. Ehrenstein, "Interdependence Between the Curing , Structure , and the Mechanical Properties of Phenolic Resins," *J. Appl. Polym. Sci.*, vol. 74, pp. 3173–3185, 1999.

[27] G. Astarloa Aierbe, J. M. Echeverría, M. D. Martin, A. M. Etxeberria, and I. Mondragon, "Influence of the initial formaldehyde to phenol molar ratio (F/P) on the formation of a phenolic resol resin catalyzed with amine," *Polymer (Guildf).*, vol. 41, no. 18, pp. 6797–6802, 2000.

[28] C. C. Lin and H. Teng, "Influence of the formaldehyde-to-phenol ratio in resin synthesis on the production of activated carbons from phenol-formaldehyde resins," *Ind. Eng. Chem. Res.*, vol. 41, no. 8, pp. 1986–1992, 2002.

[29] X.-M. Hu, Y.-Y. Zhao, and W.-M. Cheng, "Effect of formaldehyde/phenol ratio (F/P) on the properties of phenolic resins and foams synthesized at room temperature," *Polym. Compos.*, vol. 36, no. 8, pp. 1531–1540, 2015.

[30] J. Monni, L. Alvila, and T. T. Pakkanen, "Structural and physical changes in phenol-formaldehyde resol resin, as a function of the degree of condensation of the resol solution," *Ind. Eng. Chem. Res.*, vol. 46, no. 21, pp. 6916–6924, 2007.

[31] M. F. G. Loustalot, S. Larroque, D. Grande, and P. Grenier, "Phenolic resins : 2 . Influence of catalyst type on reaction mechanisms and kinetics," *Polymer (Guildf).*, vol. 37, no. 8, pp. 1363–1369, 1996.

[32] N. A. St. John and J. R. Brown, "Flexural and interlaminar shear properties of glass-reinforced phenolic composites," *Compos. Part A Appl. Sci. Manuf.*, vol. 29, no. 8, pp. 939–946, 1998.

[33] R. A. Spurr, E. H. Erath, H. Myers, and D. C. Pease, "Curing Process in Phenolic Resin Electron-Microscopic Analysis," *Ind. Eng. Chem.*, vol. 49, no. 11, pp. 1839–1842, 1957.

[34] A. Izumi, T. Nakao, H. Iwase, and M. Shibayama, "Structural analysis of cured phenolic resins using complementary small-angle neutron and X-ray scattering and

scanning electron microscopy," *Soft Matter*, vol. 8, pp. 8438–8445, 2012.

[35] M. Borkovec and W. D. E. Paris, "The Fractal Dimension of The Apollonian Sphere Packing," *Appear. Fractals*, vol. 2, no. 4, pp. 521–526, 1994.

[36] A. Zhang, H. Bai, and L. Li, "Breath Figure : A Nature-Inspired Preparation Method for Ordered Porous Films," *Chem. Rev.*, vol. 115, p. 9801−9868, 2015.

[37] H. S. L. Ku, F. Cardona, M. Trada, and G. Vigier, "Flexural properties of sawdust reinforced phenolic composites: Pilot study," *J. Appl. Polym. Sci.*, vol. 114, no. 3, pp. 1927–1934, 2009.

[38] J. Schindelin *et al.*, "Fiji - an Open Source platform for biological image analysis," *Nat Methods*, vol. 9, no. 7, pp. 1–15, 2012.

[39] I. Poljanšek and M. Krajnc, "Characterization of phenol-formaldehyde prepolymer resins by in line FT-IR spectroscopy," *Acta Chim. Slov.*, vol. 52, no. 3, pp. 238–244, 2005.

[40] S. Jähnigen, E. Brendler, U. Böhme, G. Heide, and E. Kroke, "Silicophosphates containing SiO6octahedra-anhydrous synthesis under ambient conditions," *New J. Chem.*, vol. 38, no. 2, pp. 744–751, 2014.

[41] P. S. Parameswaran and E. T. Thachil, "Influence of ether linkages on the properties of resol phenolic resin," *Int. J. Polym. Mater. Polym. Biomater.*, vol. 56, no. 2, pp. 177–185, 2007.

[42] J. Brown and Z. Mathys, "Plasma surface modification of advanced organic fibres: Part V Part V Effects on themechanical properties of aramid/phenolic composites," *J. Mater. Sci.*, vol. 32, pp. 2599–2604, 1997.

[43] S. Feih, Z. Mathys, G. Mathys, A. G. Gibson, M. Robinson, and A. P. Mouritz, "Influence of water content on failure of phenolic composites in fire," *Polym. Degrad. Stab.*, vol. 93, no. 2, pp. 376–382, 2008.

[44] S. Aratama *et al.*, "Microscopic observation of voids and transverse crack initiation in CFRP laminates," *Adv. Compos. Mater.*, vol. 3046, pp. 1–16, 2016.

[45] R. Paskaramoorthy, S. Bugarin, and R. G. Reid, "Analysis of stress concentration

around a spheroidal cavity under asymmetric dynamic loading," *Int. J. Solids Struct.*, vol. 48, no. 14–15, pp. 2255–2263, 2011.

[46] G. Dale, M. Strawhorne, D. C. Sinclair, and J. S. Dean, "Finite element modeling on the effect of intra-granular porosity on the dielectric properties of BaTiO3 MLCCs," *J. Am. Ceram. Soc.*, vol. 101, no. 3, pp. 1211–1220, 2018.

[47] "COMSOL Multiphysics® Modeling Software." [Online]. Available: https://uk.comsol.com/. [Accessed: 18-Apr-2019].

[48] S. M. Arnold, P. L. Murthy, B. A. Bednarcyk, J. W. Lawson, and J. D. Monk, "Multiscale Modeling of Carbon / Phenolic Composite Thermal Protection Materials : Atomistic to Effective Properties," *NASA Tech. Memo. 219124*, no. July 2016, pp. 1–21, 2016.

Section 6.6: Supplementary Materials

Table S1. *The standard peak positions and the observed peaks of the resole phenol/formaldehyde resins.*

Functional group	Literature data of wavenumber, cm^{-1}	Observed wavenumber, cm^{-1}	Phenol/formaldehyde
OH stretching	3400	3352	Phenol/formaldehyde
in phase stretching vibration of -CH_2- alkane	2925	2912	Formaldehyde
out of phase stretching vibration of -CH_2- alkane	2850	2855	Formaldehyde
C = O stretch	1633	1630	Formaldehyde
C = C aromatic ring	1610	1612	Phenol
C = C aromatic ring	1517	1534	Phenol
C = C aromatic ring	1504	/	Phenol
C-H aliphatic	1480	1481	Phenol
-CH_2- deformation vibration	1460	/	
Scissoring vibration of -CH_2-	1450	1441	Formaldehyde
OH in plane	1390-1378	1356	Phenol/formaldehyde
asymmetric stretch of C-O	1237	1213	Phenol
C-O stretch	1153	1151	Phenol/formaldehyde
asymmetric stretching vibration of C – O-C aliphatic ether	1100	1100	Phenol/formaldehyde
C-O stretching of -CH_2OH	1045	1041	Phenol/formaldehyde
-C-OH	1020	1035	Phenol/formaldehyde
aliphatic hydroxyl	1000	1011	Phenol
1,2,4-substituted benzene ring	976	/	
CH out-of-plane, isolated H	885	885	Phenol
CH out-of-plane, para-substituted	835	818	
CH out of plane, ortho-substituted	760	755	Phenol
Adjacent 5H	694	687	Phenol/formaldehyde

Table S2. *Flexural properties of phenolic resin cured using long cure cycle without catalyst.*

Phenolic cured without catalyst	Flexural strength (MPa)	Flexural modulus (GPa)	Deflection (mm)
Sample 1	71.614	3.005	0.919
Sample 2	110.93	3.66	1.434
Sample 3	84.956	3.442	1.071
Sample 4	69.52	2.899	1.086
Sample 5	77.167	3.117	1.074
Sample 6	84.329	3.239	1.178
Sample 7	117.66	3.535	1.651

Table S3. *Flexural properties of phenolic resin cured with a fast action catalyst (phencat 10).*

Phenolic 10	Flexural strength (MPa)	Flexural modulus (GPa)	Deflection (mm)
Sample 1	70.045	3.036	1.334
Sample 2	58.061	1.804	1.117
Sample 3	90.84	2.045	1.713
Sample 4	62.028	2.533	1.214
Sample 5	55.843	2.237	0.999
Sample 6	79.882	2.615	1.514
Sample 7	64.163	1.98	1.088

Table S4. *Flexural properties of phenolic resin cured with a slow action catalyst (phencat 382)*

Phenolic 382	Flexural strength (MPa)	Flexural modulus (GPa)	Deflection (mm)
Sample 1	39.085	1.655	0.878
Sample 2	59.247	1.875	1.134
Sample 3	40.434	1.979	0.886
Sample 4	54.841	2.488	1.093
Sample 5	40.073	2.181	0.911
Sample 6	52.008	2.014	1.12
Sample 7	48.765	2.067	0.909

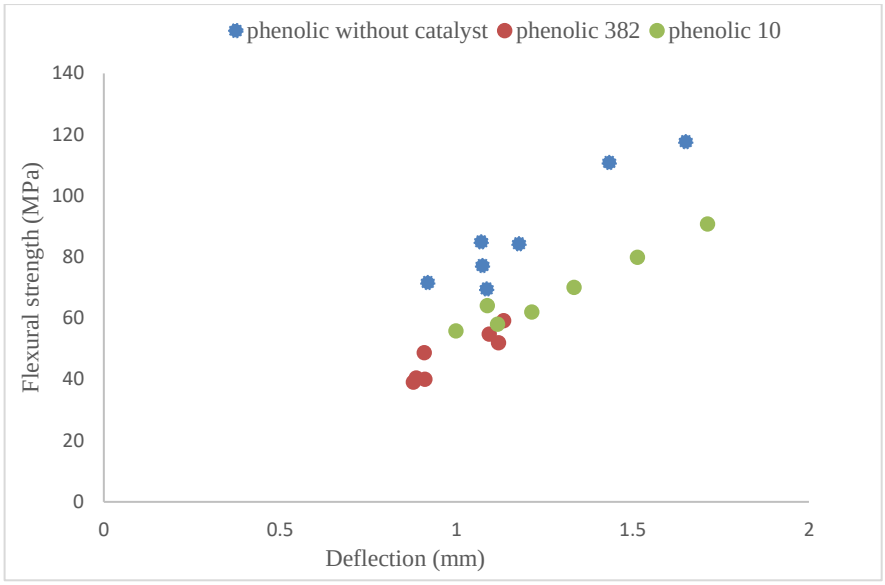

Figure S1. *Stress-strain values of all tested samples for each type of cured phenolic resin.*

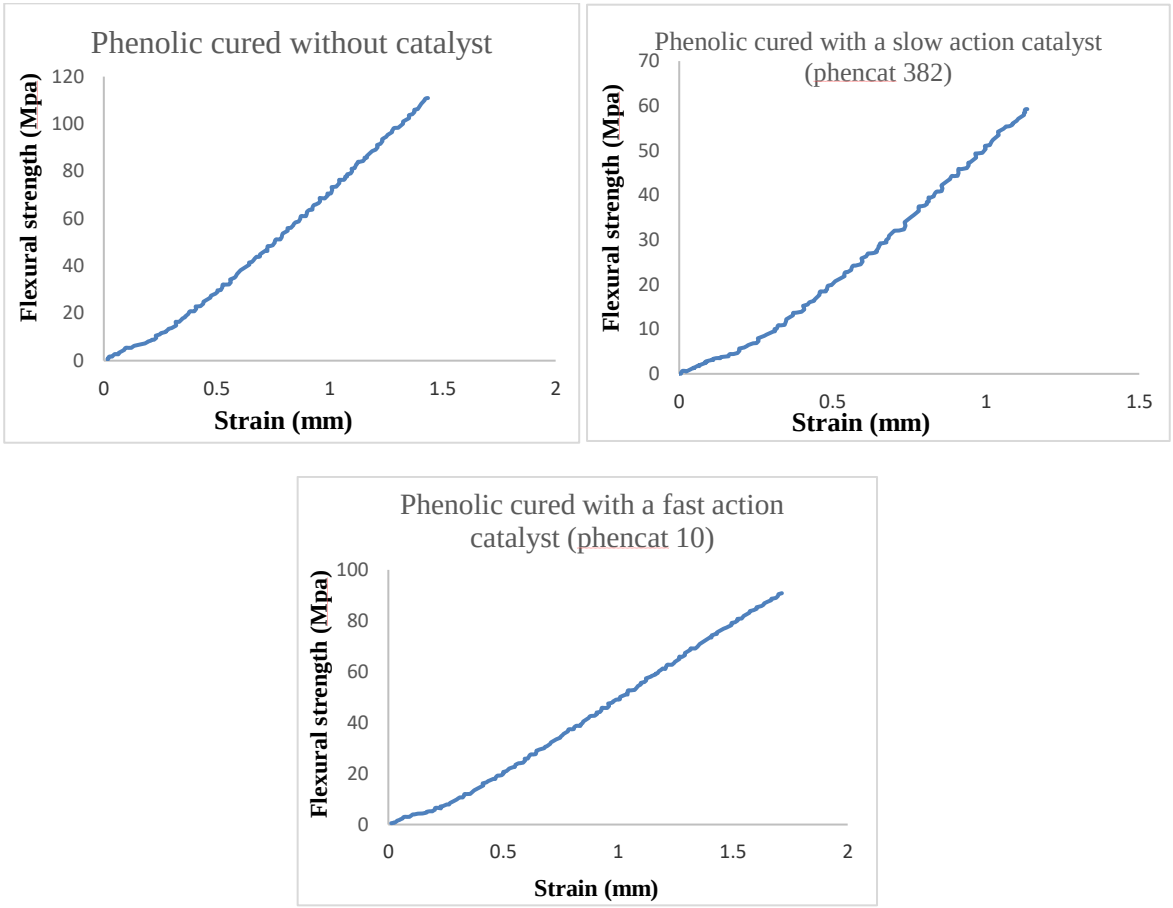

Figure S2. *Examples of the stress-strain curve for the three types of cured phenolic resin.*

Chapter 7: Interfacial bonding between ramie fibres and phenolic resins: effects of plasma treatment and cure cycle

Abstract: Natural fibres reinforced polymer composites offer many advantages such as availability, inexpensive, lightweight, and high specific mechanical properties. However, the applications of these materials are still limited due to the challenges in achieving good interfacial bonding between the fibres and matrix. This is highly influenced by the fibre surface characteristics and the polymer matrix properties. Therefore, in this study, the surface characteristics of ramie fibres were modified using low pressure plasma treatment in order to improve their interfacial bonding to the phenolic resins. Furthermore, the effects of using two different curing cycles (acid cure and thermal cure) on the properties of short ramie fibres-phenolic composites were also investigated. A new method for making mats of random short ramie fibres was developed and used for the fabrication of composites containing plasma treated fibres. The flexural properties of all composites were tested and the obtained fracture surfaces were investigated using LV-SEM. The results indicated clear effects for the plasma treatment and cure cycle conditions on the fibre-matrix interfacial bonding, and consequently the flexural properties of the composites.

Section 7.1: Introduction

The use of natural plant fibres such as ramie, flax, jute, hemp, kenaf, and sisal as reinforcements in the polymer composites has recently received great attention in various engineering applications. This is due to their excellent mechanical characteristics such as flexibility, high toughness, high specific modulus, and specific strength as well as their low cost, low density, recyclability, and renewability [1]–[8]. Such properties make plant fibre composites one of the high-performance group of materials with both economic and environmental benefits [9]. However, the properties and performance of these materials are highly influenced by the properties of the individual components (fibres and matrix) and

their surface adhesion properties as well as the method of composite fabrication [7][10]–[12].

Among natural plant fibres, ramie fibres are widely used as a reinforcement in polymer composites due to its favourable properties such as high crystallinity, commercial availability [13]–[15], and being one of the longest and strongest fine textile fibres [16][17]. Nonetheless, ramie fibres present some disadvantages such as poor wettability, incompatibility with some types of polymer matrices, and low moisture resistance [9]. However, it is possible to overcome some of these challenges via surface modification and make fibres more compatible with some polymer matrices [9][10]. In our previous study, it was found that the 2 min of low pressure plasma treatment of ramie fibres can resulted in a nanoscale surface roughness without affecting or changing the fibre bulk properties [18]. Such results are expected to increase the fibre surface area and hence better fibre-matrix interfacial bonding. Therefore, here we investigated the effects of plasma treatment on the fibre-matrix interfacial bonding in the system of random short ramie fibres-phenolic resin composites before and after plasma treatment.

In addition, the use of thermoset phenolic resin as a matrix for natural plant fibres, as in this study, the problem of lack of adhesion between the fibre and matrix can be minimised. This is because some degree of interaction is expected to exist between the hydrophilic ramie fibres and polar hydroxyl groups present in the structure of phenolic resins [19][20]. This factor can be considered as an advantage that phenolic resin possesses if compared to the hydrophobic thermoplastic matrices [21]. Moreover, composites based on phenolic resins as a matrix yield low levels of combustion products and smoke under both smouldering and flaming fire conditions and are superior in terms of other flammability properties to epoxy, polyester, and vinyl ester-based composites [22][23]. However, the curing process of phenolic resin is complex and usually involves several types of reactions. One of the main

issues is the generation of water and formaldehyde as by-products of the crosslinking reaction of the phenolic resin with the consequent formation of voids [11][24]–[27]. The curing conditions (cure cycle) are very important in controlling the voids content, size, and distribution in the final cured resin. In an earlier study, we found that the use of short cure cycle (3-4 hrs) with the addition of fast action acid catalyst (phencat 10), a homogenous voids size and distribution can be achieved in the final cured resin. On the other hand, a microvoids free phenolic resin was achieved with the use of long cure cycle (4 days) without the addition of curing agent [28]. Thus, in this work, we investigated the effects of the above two cure cycles on the microstructural and mechanical properties of random short ramie fibres reinforced phenolic resin composites.

Finally, the process of mixing short fibres into the thermosetting resins has generally been based on mechanical stirring or blending, a process which has the tendency to cause fibre damage and fibre agglomeration, as well as the high possibility of formation air-bubbles [29]. To overcome this problem, we reported a method in which the effect of plasma treatment can also be utilised to hold the short ramie fibres together as a mat after compacting them.

Therefore, in this study, the untreated and plasma treated random short ramie fibres mats reinforced phenolic thermoset matrix composites were fabricated. The effects of the plasma treatment on the interfacial bonding between fibres and matrix was investigated. The structural and mechanical properties of the prepared composites were optimised via the use of two different curing cycles. Low Voltage Scanning Electron Microscopy (LV-SEM) was used to observe the structural properties of the prepared composites. Flexural test was also performed for all different prepared composites, in order to find a composite fabrication procedure that leads to optimise the mechanical properties.

Section 7.2: Experimental Methods

Section 7.2.1: Materials

Ramie fibres (Boehmeria nivea) used as a reinforcement were supplied by Wild Fibres store, UK and used as received for the experiments. The polymer matrix selected for the fabrication of fibre composites was resole commercial phenolic resin (Cellobond J2027X) and kindly supplied by Caleb Technical Products Ltd., UK. The curing agent used was phencat 10 (fast action acid catalyst) which also supplied by Caleb Technical Products Ltd., UK.

Section 7.2.2: Low pressure plasma surface treatment

Low pressure plasma surface treatment was performed using Diener Electronic Zepto plasma surface cleaner with 40 kHz power supply frequency and chamber size of 2.6 Litre (borosilicate glass cylindrical chamber). The fibres were first cut and prepared into a length of about 8-10 mm. The fibres were then placed inside the plasma chamber and the chamber was evacuated to 0.1 mbar. The ambient air was used as a process gas. Plasma was generated at power of 100 W and a chamber pressure of 0.3 mbar. Ramie fibres were treated for 2 min in two different steps (see Section 7.2.3).

Section 7.2.3: Fabrication of composites

Generally, polymer thermoset composites are fabricated using techniques such as hand layup, hot press, pre-preg, resin transfer, injection moulding, casting, filament winding for continuous fibres, and sheet moulding (SMC) for short fibres [30]. In this study, untreated and plasma treated random short ramie fibres were used for reinforcing the phenolic composites. In the case of using untreated fibres, it was very difficult to make mats of short ramie fibres due to the poor compatibility between the fibres itself. Therefore, the untreated short ramie fibres were just laid down in the PTFE mould (with dimensions of 12.7 mm wide×56 mm long×1.6 mm thick) and then a load was place on it manually for 5 min without any further movement to the fibres. Whereas in the case of using plasma treated fibres, the

mats were prepared more easily and as follows. The 1 minute plasma treated fibres was first placed in the PTFE mould and then a load was placed on it manually for 5 min to compact the mat (Figure 7-1). After that, the prepared mats were plasma treated for the second minute and then placed again in the PTFE mould. Thereafter, two types of resole phenolic resins were prepared, considering the ability of resole phenolic resin to be cured either with the use of curing agent (short cure cycle (4 hrs)) or with the application of heat only, using long cure cycle (4 days) [28]. In the case of using curing agent, fast action acid catalyst was used with a mixing ratio of 5 wt% of the resin. The prepared resins were then poured on the already prepared mats and then placed in the autoclave to be cured using the two different curing cycles depending on the resin type. The used curing cycles were elsewhere reported [28]. We will refer to this as composite- acid cured and composite thermal cured. The content of ramie fibres for each fabricated composites was 10%, 15%, and 20 % by weight.

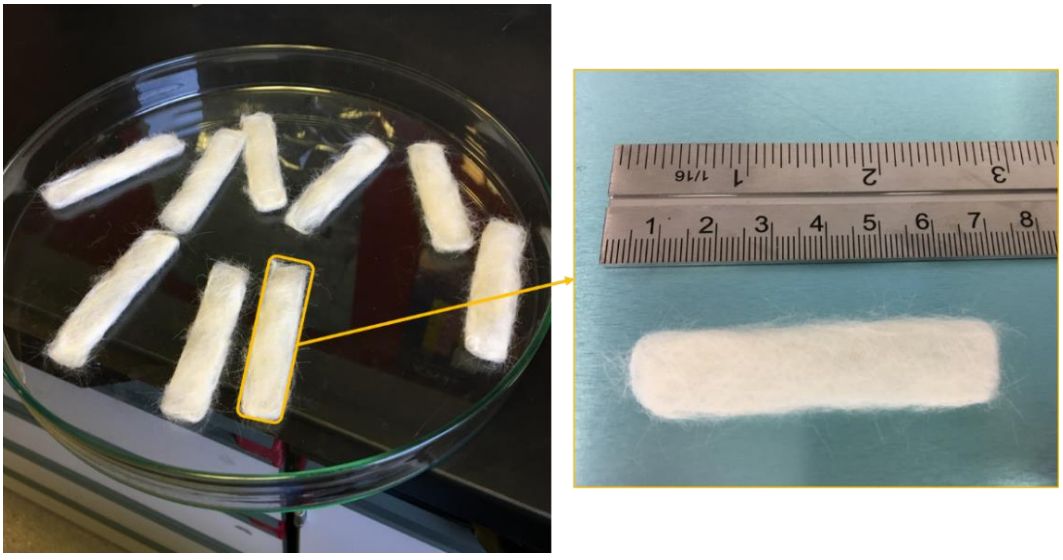

Figure 7-1: *Mats of plasma treated random short ramie fibres.*

Section 7.2.4: Scanning electron microscopy

Fracture surface morphology of the composites after flexural test was examined using low voltage Scanning Electron Microscopy (FEI Nova Nano SEM 450). Low accelerating voltage (1 kV) was used to avoid sample surface charging and damage with typical vacuum

pressure of 10^{-5} mbar, and a working distance of about 4mm. Secondary electron images were collected using two detectors: Everhart-Thornley Detector (ETD) for low magnification images and Through Lens Detector (TLD) to obtain high magnification images.

Section 7.2.5: Flexural properties

The flexural properties of the composites were determined using a Lloyd TA500 tensometer. The test was conducted according to the ASTM D790 at a crosshead speeds of 2.0 mm/min. The tests were performed at room temperature (22 ± 3 °C). The ultimate bending results (strength and modulus) for each composite were calculated as an average of seven specimens per test condition.

Section 7.3: Results and discussion

Section 7.3.1: Fibre distribution in composites

An overview of LV-SEM micrographs obtained from flexural fractured surfaces of untreated and plasma treated short ramie fibres reinforced phenolic composites are shown in Figure 7-2. These micrographs show some information about the ramie fibre distribution in the phenolic resin composites. In both samples, untreated (Figure 7-2a) and plasma treated fibre composites (Figure 7-2b) the ramie fibres are well dispersed in the resin and there are no signs of fibres agglomerations. This indicates that the method of composites fabrication which was based on making mats of short fibres have successfully employed.

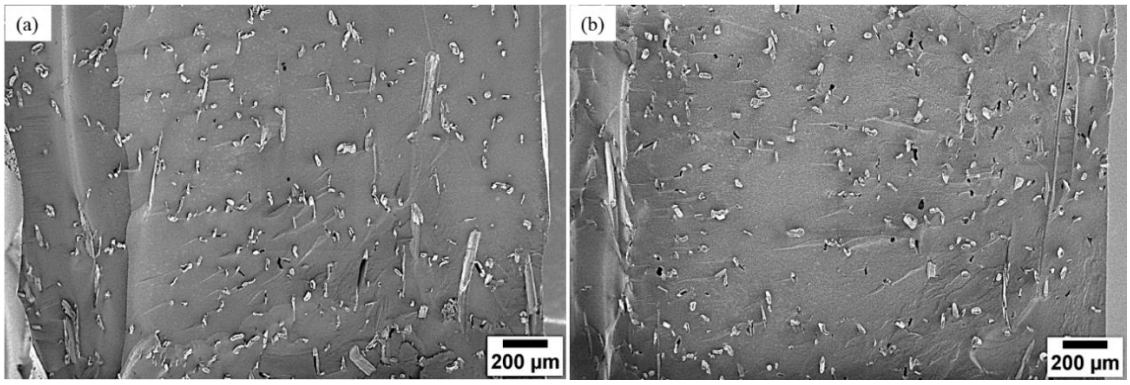

Figure 7-2: *Overview LV-SEM micrographs of the flexural fractured surfaces of (a) untreated short-ramie-fibres-phenolic resin composite and (b) plasma treated short-ramie fibres-phenolic resin composite.*

Section 7.3.2: Fibre-matrix interface morphology-acid cured composites

The fibre-matrix interfacial bonding is of greater importance in short fibre composites than in continuous fibre composites. This is partly due to the smaller volumes of the fibre in short fibre composites than those in continuous fibre composites and also due to the fibre critical lengths are usually of the same order of magnitude as the short fibre lengths. This means small changes in the interfacial bonding between fibres and matrix effect the fibre critical length, and consequently the effectiveness of the reinforcement (short fibres) quite dramatically [31].

Therefore, a detailed view of the fibre-matrix interface morphology of the untreated and plasma treated fibre-phenolic composites, cured using short cure cycle with the addition of fast action acid catalyst are investigated and presented in Figure 7-3. In Figure 7-3a (untreated fibre), dense and homogenous coverage of the phenolic fracture surface with spherical features with an average diameter of 0.52±0.15 µm were observed. These features can be attributed to the trapped water present as result of the complex polymerisation process including the release of formaldehyde and water as by-products. With the use of fast action acid catalyst, the crosslinking rate of the phenol and formaldehyde is relatively fast, therefore, the generated by-products will not be able to be released or diffuse, resulting in a homogenous distribution of voids in the final cured resin [28]. A higher magnification LV-

SEM image of the fibre-matrix interface (Figure 7-3b) also reveals microvoids along the fibre-matrix interface. Furthermore, these microvoids were locally varied around the fibre, leading to localised void free zones as shown in Figure 7-3a and b. Presumably, this is due to the inhomogeneous coverage of fibres by waxes and pectins. Those could block the water diffusion into the fibres locally. In addition, Figure 7-3c shows an unfilled fibre lumen in the composites which is another feature that increases the number of defects in the composites. The unfiled lumen could be due to the poor interaction between the fibres and matrix and or due to the increases in the viscosity of resin that is caused by the addition of fast action acid catalyst. The viscosity of the resin is visibly increased after the addition of fast action acid catalyst. Thus, the interdiffusion of phenolic resin into the untreated ramie fibres might be reduced.

However, in the case of using plasma treated fibre, the microvoids along the fibre-matrix interface are larger compared to those of untreated fibre as shown in Figure 7-3d. Moreover, plasma treated fibres tend to be surrounded by continuous void free zones followed by a ring of large voids and then a homogenous voids size distribution (Figure 7-3e). To further confirm this, a histogram of the voids diameter distribution around the untreated and plasma treated fibre composites (Figure 7-4a and d) were plotted in Figure 7-4c and f, which were derived from the binary images in Figure 7-4b and e. It can be clearly seen a very broad size distribution of voids with an average diameter of 1.13±0.3 μm around the plasma treated fibre (Figure 7-4f). In contrast, in the case of using untreated fibres, the histogram (Figure 7-4c) shows a more homogenous voids size distribution around the fibre with a smaller average diameter (0.64±0.2 μm) than in the case of using plasma treated fibres. This could be attributed to the differences in the surface chemistry of the fibres after plasma treatment. For instance, the FTIR analysis in our previous study showed that the absorbed water in the crystalline cellulose of ramie fibres was decreased gradually with plasma treatment [18].

This was attributed to the temperature effect of the plasma during the treatment and also to the bond cleavage with plasma to form free radicals [32][33]. This could lead to dryer fibres as the result of plasma treatment that are able to attract and interact with more water from the resin. Following the assumption that the water within the phenolic resins is primarily free water (not bounded water) [34], therefore, the generated by-products (predominate water) in the phenolic resin during the crosslinking could be assumed as free water that can diffuse and interact with other water molecules present on the fibre surface.

Therefore, the observations in Figure 7-3 could be explained as resulting from the water generated as by-products in the phenolic resin during crosslinking and that was attracted by the dry fibres obtained by plasma treatment. Some of this water was absorbed by the fibre and some coalesced and form large voids in the fibre-matrix interface. This scenario is also consistent with the presence of a distinct void free zone around the fibre. Beyond the voids free zones, the generated water coalesced and because of the fast crosslinking rate they could not diffuse into the fibre before the gel point is reached, leading to broad voids size distribution in this area. Furthermore, the void free zones might also prevent the diffusion of the voids into the fibres because of the high density of this area. This is in contrast, to the voids in the case of using untreated fibres, voids were more homogenously distributed around the fibre, and no distinct continuous void free zone around the fibre is observed. This could be attributed to the higher level of water in the untreated fibres that could only attract and interact with the water close by and also due to the inhomogeneous coverage of ramie fibre by waxes and pectins.

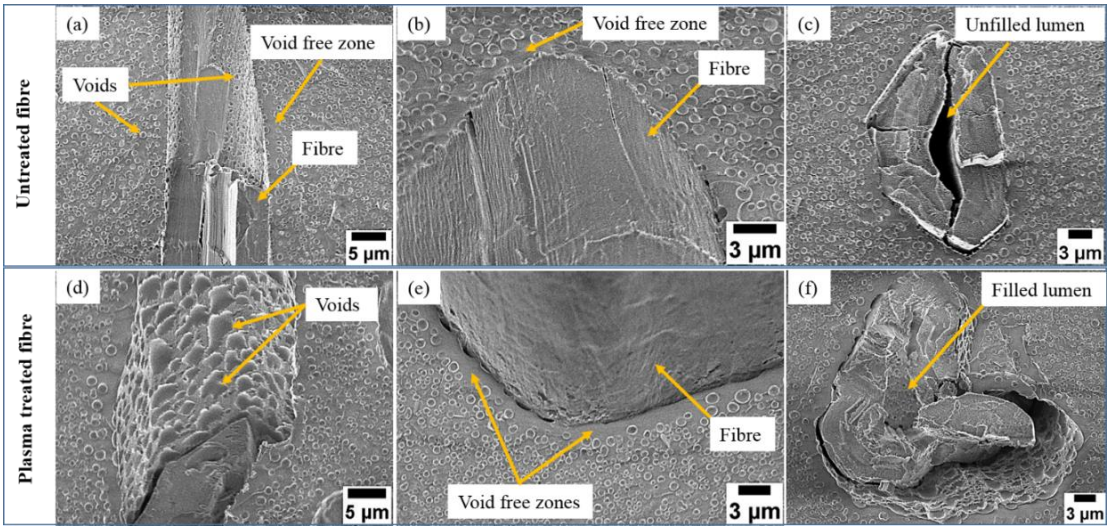

Figure 7-3: *LV-SEM micrographs of the fibre-matrix interface of (a) (b) (c) untreated ramie fibre-phenolic resin composites and (d) (e) (f) 2 min plasma treated ramie fibres-phenolic resin composites at different magnifications. The composites were cured using short cure cycle.*

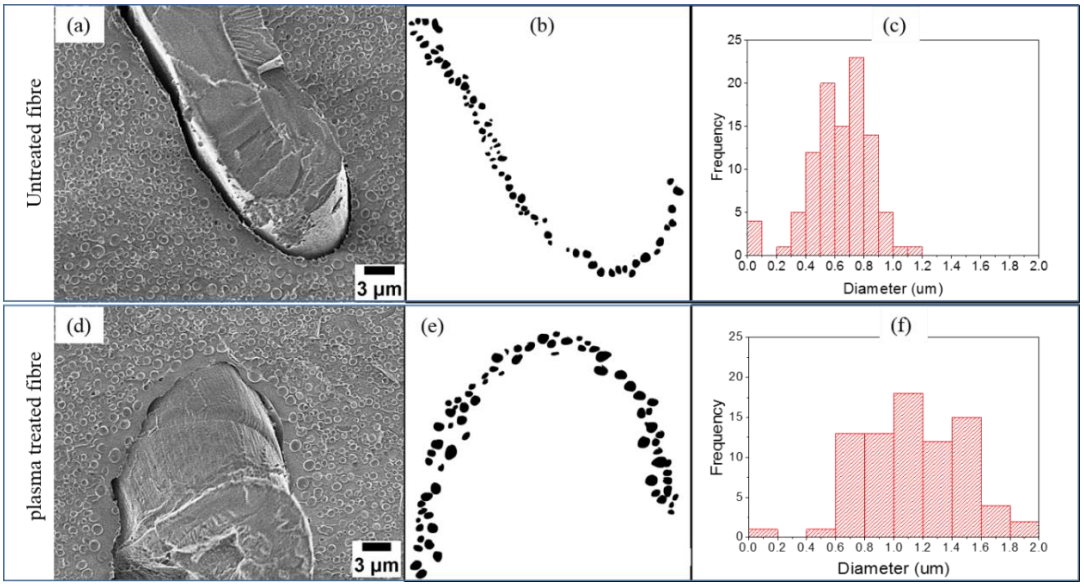

Figure 7-4: *LV-SEM micrographs of the fibre-matrix interface of (a) (b) (c) untreated ramie fibre-phenolic resin composites and (d) (e) (f) 2 min plasma treated ramie fibres-phenolic resin composites at different magnifications. The composites were cured using short cure cycle.*

Section 7.3.3: Fibre-matrix interface morphology-thermal cured composites

In general, three different zones can be defined for flexural fractured surfaces, namely compressive, neutral, and tensile zone. When the sample is subjected to a bending load, a concave upward curvature will be developed. This leads to compression stresses at the top of the sample while a tensile stresses will be generated with the lower region. The neutral

zone is the transition zone between the compressive and tensile zones [35][36]. For a reliable comparison of the interfacial bonding between the untreated and plasma treated fibre composite, all the LV-SEM micrographs in this study were collected from the tensile approaching the neutral zone and are shown in Figure 7-5. Unlike the structure of the phenolic cured using short cure cycle (Figure 7-3a), a homogenous fracture surface with free of microvoids was observed for the phenolic resin cured using a long cure cycle as shown in Figure 7-5. This was attributed to the time available for the water vapour to be released before the gel point of the resin is reached [28]. If this is long enough, as in the case of using long cure cycle (4 days), the formation of microvoids in the cured resin can be prevented.

In terms of the fibre-matrix interfacial bonding, the LV-SEM micrographs of the untreated fibre composites showed poor interfacial adhesion between the untreated ramie fibre and phenolic resin as shown in Figure 7-5a-c. The fibres are clearly debonded and pulled out from the resin (Figure 7-5a and b) with a noticeable gap between the fibre and matrix. In addition, the fibre surface shows very few signs of adhering polymer as shown in Figure 7-5b and c (indicated by arrows). This indicates the poor interaction between fibre and matrix which can be attributed to the poor fibre surface adhesion properties.

However, in the case of using plasma treated fibres (Figure 7-5d-f), the fibres are broken off near the matrix surface with a very short fibre pull out. Moreover, it can be clearly seen in Figure 7-5d and e, the fibre-matrix interface is almost continuous and the fibre surface seems to be totally covered by the resin. This is likely to play an important role with regards to mechanical properties of the composite (see Section 7.3.4) as the degree of adhesion between the fibres and matrix govern load transfer between the composite constituents. Further differences between the untreated and plasma treated fibre is that the fibre lumen shown in Figure 7-5f is clearly filled by the resin in the case of plasma treated fibre which increase the homogeneity of the composite.

All the above can be attributed to the changes in the surface morphology and surface chemistry of the fibres before and after plasma treatment. In terms of the fibre surface morphology, it has been observed that the surface of the untreated ramie fibre was smooth and almost homogenous on the nanoscale [18]. This was attributed to the primary amorphous layer of ramie fibres that consists of waxes, pectin, and proteinaceous materials [37]. This is in contrast, to the plasma treated fibres, the 2 min of low pressure plasma treatment of ramie fibres showed rougher surface with greater exposure of crystalline cellulose microfibrils in comparison to the untreated fibre [18]. Such changes are expected to increase the fibre surface interfacial area and also improve the mechanical bonding between the fibre and matrix. In terms of the chemical changes, it has been proven that the low pressure plasma treatment was effective in removing the non-cellulosic compounds such as amorphous hemicellulose and waxes from the surface of ramie fibres after 2 min of treatment [18]. This could increase the surface reactivity of the fibres and consequently improve the chemical bonding between the fibres and matrix.

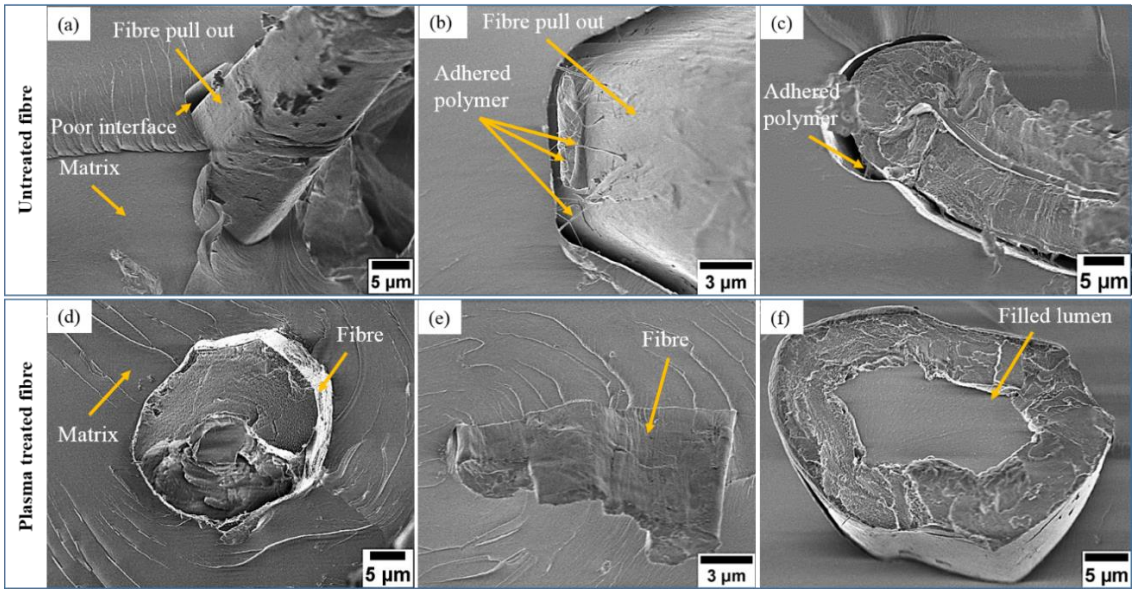

Figure 7-5: *LV-SEM micrographs of the fibre-matrix interface of (a) (b) (c) untreated ramie fibre-phenolic resin composites and (d) (e) (f) 2 min plasma treated ramie fibres-phenolic resin composites at different magnifications. The composites were cured using long cure cycle.*

Section 7.3.4: Flexural properties

The flexural properties (modulus and strength) of the pure phenolic and its composites (short ramie fibres-phenolic resin composites) produced using short cure cycle (acid cured) and long cure cycle (thermal cured) are presented in Figure 7-6. The average flexural modulus of pure phenolic resin (acid cured) was 2.3 GPa. With the use of plasma treated ramie fibres, the average flexural modulus of the composite was linearly increased with increasing the fibre content (Figure 7-6a). This is because ramie fibres are very stiff (Young's modulus of 31 GPa) [18] compared to phenolic resin (flexural modulus of 2.3 GPa). However, the composite based on 15 wt% untreated fibres shows a reduction in the average flexural modulus by approximately 12%, compared to those of 15 wt% plasma treated composites as shown in Figure 7-6a. This indicates the better incorporation of the plasma treated ramie fibres into phenolic resin than those of untreated fibres.

In terms of the flexural strength of the acid cured composites, the plasma treated fibre composite showed higher flexural strength than that of untreated fibre composite. This could be due to the continuous void free zone around the plasma treated fibres, as observed by the LV-SEM in Figure 7-3e. Thus, the stress concentration points around the plasma treated fibres were less than in the case of untreated fibres, and consequently the higher flexural strength for plasma treated fibre composites than those of untreated fibre composites (Figure 7-6b). However, both materials (untreated and plasma treated fibre composites with 15 wt% fibre content) show clear decreasing in the strength compared to that of pure phenolic resin (Figure 7-6b). This is consistent with other work on natural fibre-phenolic composites [38]. It is well known that the fibre-matrix interface plays an important role in determining the final mechanical properties of the composites, as transferring the stress between the fibre and matrix occurs through the interface region. This is mainly dependent on the degree of interfacial adhesion between fibres and matrix. The maximum stress level can be maintained

across the interface without disruption if high interfacial strength is achieved [39]. However, the LV-SEM micrographs in Section 7.3.2 (Figure 7-3) showed that the interfacial bonding between the fibres and matrix was very poor as well as the presence of microvoids along the interface for both materials (untreated and plasma treaded fibre composites). Furthermore, unfilled lumen was clearly observed in some samples, resulting in a more defects in the final composites structure. The presence of these defects in the composites could act as a stress concentration points in the polymer matrix, and consequently crack initiation, fibre-matrix debonding and finally composite failure [40]. All of this could explain the reason why the acid cured composites showed lower flexural strength than the pure phenolic resin.

In contrast, the flexural properties (modulus and strength) of the thermal cured composites (Figure 7-6c and d) showed a better trend compared to those of acid cured composites. For instance, the average flexural modulus of the pure phenolic resin (thermal cured) was 3.2 GPa (Figure 7-6a). This was increased to 4.9 GPa, when 15 wt% of plasma treated fibres was added to phenolic resin which indicate an improvement of about 34% of the pure phenolic resin (thermal cured). This is in contrast to the materials produced using short cure cycle (acid cured) with the use of 15 wt% fibre, the improvement in the modulus was only 17% of the pure phenolic (acid cured). More importantly, unlike in the case of using short cure cycle, the flexural strength of the composite materials produced using long cure cycle was maintained in the same range of the flexural strength of the pure phenolic resin (thermal cured) as shown in Figure 7-6d.

All the above can be attributed to the resin characteristics. As observed above (Section 7.3.2), the formation of microvoids in the cured resin in the case of using short cure cycle were along fibre-matrix interface, resulted in a very poor interfacial bonding. In addition, in the case of using plasma treated fibres, a non-homogenous distribution of the microvoids was observed around the fibres. It has been shown in our previous study, the non-homogenous

distribution of the micrvoids in the cured resin resulted in a reduction in the mechanical properties compared to those with a homogenous microvoids distribution [28]. This is in contrast the composites produced using long cure cycle showed void free structure with a better interfacial bonding between the fibre and matrix than those of composites produced using short cure cycle. Thus, the flexural properties of thermal cured phenolic composites were higher than those of acid cured phenolic composites.

However, it is also important to point out that in the case of using a long cure cycle, the flexural modulus and flexural strength of the plasma treated fibre composites were higher than those of untreated fibre composites (Figure 7-6c and d). As mentioned above, the mechanical properties of the final composites are highly influenced by the degree of the interfacial bonding between the fibre and matrix. In general, the interfacial bonding between natural fibres and polymer matrices is effected by the mechanical interlocking, chemical bonding, and molecular attractive forces between the two components [39]. The presence of the non-cellulosic compounds (e.g. waxes and pectins) on the surface of untreated ramie fibres could act as a barrier for the mechanical/chemical interlocking between the ramie fibres and phenolic resin. As a result of this, the interfacial bonding between ramie fibres and phenolic resin was very weak, as indicated by the LV-SEM observations in Figure 7-5a-c. Thus, the stress transfer between the fibre and matrix was inefficient in the case of using untreated ramie fibres, and consequently the early failure of the composites. This is in contrast the interfacial bonding between ramie fibres and phenolic resin was much better in the case of using plasma treated fibres than that of untreated fibre (indicated by the LV-SEM micrographs in Figure 7-5d-f). Thus, the stress was sufficiently transferred between the fibres and matrix through the interface, resulting in a higher flexural properties. Therefore, the differences in the flexural properties between the two materials (untreated and plasma treated fibre composites) can be attributed to the effects of the plasma treatment on the

surface morphology/chemistry of ramie fibres, and consequently the fibre-matrix interfacial bonding.

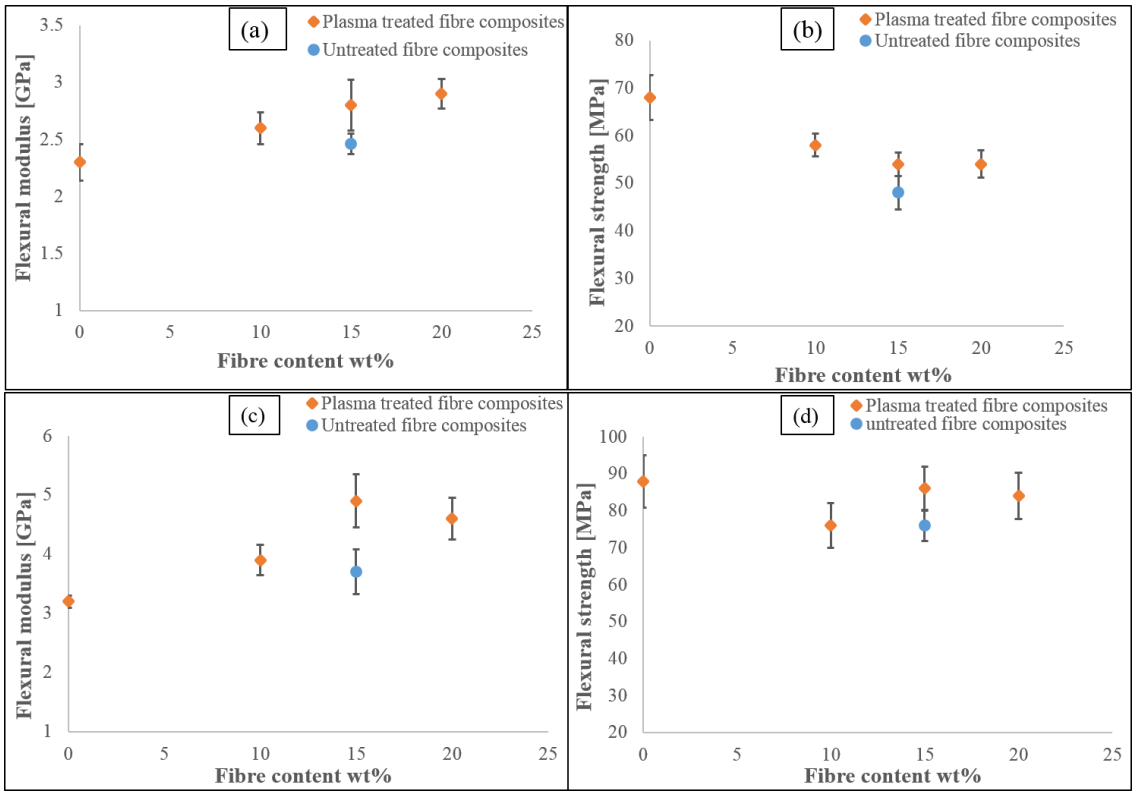

Figure 7-6: *The flexural properties of the untreated and plasma treated short-ramie-fibres-phenolic composites as a function of fibre content: (a) and (b) flexural modulus and flexural strength respectively of acid cured composites, (c) and (d) flexural modulus and flexural strength respectively of thermal cured composites.*

Section 7.4: Conclusions

Mats of random short ramie fibres were successfully fabricated utilising the effects of plasma treatment in improving the compatibility between the fibres itself. Furthermore, in the case of using plasma treated fibres in reinforcing the phenolic resin composite, the Young's modulus was clearly improved in both composites (acid cured and thermal cured). However, this is not the case in terms of the flexural strength for both composites. It has been shown that the flexural strength was gradually decreased for the plasma treated fibre composites (acid cured) whereas in the case of thermal cured composite the flexural strength was maintained in the range of the pure phenolic strength. This was attributed to the formation

of voids along the fibre-matrix interface in the case of acid cured composites. Therefore, it can be concluded that plasma treatment is more effective when used in combination with a thermal curing.

Section 7.5: References

[1] L. Yan, "Effect of alkali treatment on vibration characteristics and mechanical properties of natural fabric reinforced composites," *J. Reinf. Plast. Compos.*, vol. 31, no. 13, pp. 887–896, 2012.

[2] H. Alamri and I. M. Low, "Microstructural, Mechanical, and Thermal Characteristics of Recycled Cellulose Fiber-Halloysite-Epoxy Hybrid Nanocomposites," *Polym. Compos.*, pp. 589–600, 2012.

[3] J. D. Megiatto, E. C. Ramires, and E. Frollini, "Phenolic matrices and sisal fibers modified with hydroxy terminated polybutadiene rubber: Impact strength, water absorption, and morphological aspects of thermosets and composites," *Ind. Crops Prod.*, vol. 31, no. 1, pp. 178–184, 2010.

[4] M. Haq, R. Burgueño, A. K. Mohanty, and M. Misra, "Hybrid bio-based composites from blends of unsaturated polyester and soybean oil reinforced with nanoclay and natural fibers," *Compos. Sci. Technol.*, vol. 68, no. 15–16, pp. 3344–3351, 2008.

[5] M. M. Kabir, H. Wang, K. T. Lau, and F. Cardona, "Chemical treatments on plant-based natural fibre reinforced polymer composites: An overview," *Compos. Part B*, vol. 43, no. 7, pp. 2883–2892, 2012.

[6] Q. T. H. Shubhra *et al.*, "Characterization of plant and animal based natural fibers reinforced polypropylene composites and their comparative study," *Fibers Polym.*, vol. 11, no. 5, pp. 725–731, 2010.

[7] S. Marais *et al.*, "Unsaturated polyester composites reinforced with flax fibers: Effect of cold plasma and autoclave treatments on mechanical and permeation properties," *Compos. Part A Appl. Sci. Manuf.*, vol. 36, no. 7, pp. 975–986, 2005.

[8] D. M. Matoke, G. M.; Owido, S.F.; Nyaanga, "Effect of Production Methods and Material Ratios on Physical Properties of the Composites," *Am. Int. J. Contemp. Res.*,

vol. 2, no. 2, pp. 208–213, 2012.

[9] Y. Li, S. Manolache, Y. Qiu, and M. Sarmadi, “Effect of atmospheric pressure plasma treatment condition on adhesion of ramie fibers to polypropylene for composite,” *Appl. Surf. Sci.*, vol. 364, pp. 294–301, 2016.

[10] E. Bozaci *et al.*, “Effects of the atmospheric plasma treatments on surface and mechanical properties of flax fiber and adhesion between fiber-matrix for composite materials,” *Compos. Part B Eng.*, vol. 45, no. 1, pp. 565–572, 2013.

[11] J. M. Laza, J. L. Vilas, M. Rodriguez, M. T. Garay, F. Mijangos, and L. M. Leon, “Analysis of the crosslinking process of a phenolic resin by thermal scanning rheometry,” *J. Appl. Polym. Sci.*, vol. 83, pp. 57–65, 2002.

[12] A. Ticoalu, T. Aravinthan, and F. Cardona, “A review of current development in natural fiber composites for structural and infrastructure applications,” in *Southern Region Engineering Conference*, 2010, no. November, pp. 1–5.

[13] X. Liu and L. Cheng, “Influence of plasma treatment on properties of ramie fiber and the reinforced composites,” *J. Text. Inst.*, vol. 31, no. 15, pp. 1723–1734, 2017.

[14] Q. Zhang, Y. Jiang, L. Yao, Q. Jiang, and Y. Qiu, “Hydrophobic surface modification of ramie fibers by plasma-induced addition polymerization of propylene,” *J. Adhes. Sci. Technol.*, vol. 29, no. 8, pp. 691–704, 2015.

[15] C. Xu, Y. Gu, Z. Yang, M. Li, Y. Li, and Z. Zhang, “Mechanical properties of surface-treated ramie fiber fabric/epoxy resin composite fabricated by vacuum-assisted resin infusion molding with hot compaction,” *J. Compos. Mater.*, vol. 50, no. 9, pp. 1189–1198, 2016.

[16] G. Koronis, A. Silva, and A. P. Soares Dias, “Development of green composites reinforced with ramie fabrics: Effect of aging on mechanical properties of coated and uncoated specimens,” *Fibers Polym.*, vol. 15, no. 12, pp. 2618–2624, 2014.

[17] S. N. Pandey, “Ramie fibre: Part II. Physical fibre properties. A critical appreciation of recent developments,” *Text. Prog.*, vol. 39, no. 4, pp. 189–268, 2007.

[18] S. F. Hamad, N. Stehling, S. A. Hayes, J. P. Foreman, and C. Rodenburg, “Exploiting Plasma Exposed, Natural Surface Nanostructures in Ramie Fibers for Polymer

Composite Applications," *Materials (Basel).*, vol. 12, pp. 1–15, 2019.

[19] J. D. Megiatto, C. G. Silva, E. C. Ramires, and E. Frollini, "Thermoset matrix reinforced with sisal fibers: Effect of the cure cycle on the properties of the biobased composite," *Polym. Test.*, vol. 28, no. 8, pp. 793–800, 2009.

[20] J. D. Megiatto, F. B. Oliveira, D. S. Rosa, C. Gardrat, A. Castellan, and E. Frollini, "Renewable resources as reinforcement of polymeric matrices: Composites based on phenolic thermosets and chemically modified sisal fibers," *Macromol. Biosci.*, vol. 7, no. 9–10, pp. 1121–1131, 2007.

[21] J. D. Megiatto, C. G. Silva, D. S. Rosa, and E. Frollini, "Sisal chemically modified with lignins: Correlation between fibers and phenolic composites properties," *Polym. Degrad. Stab.*, vol. 93, no. 6, pp. 1109–1121, 2008.

[22] J. Brown and Z. Mathys, "Plasma surface modification of advanced organic fibres: Part V Part V Effects on themechanical properties of aramid/phenolic composites," *J. Mater. Sci.*, vol. 32, pp. 2599–2604, 1997.

[23] E. C. Ramires and E. Frollini, "Tannin-phenolic resins: Synthesis, characterization, and application as matrix in biobased composites reinforced with sisal fibers," *Compos. Part B*, vol. 43, no. 7, pp. 2851–2860, 2012.

[24] M. Asim, N. Saba, M. Jawaid, M. Nasir, M. Pervaiz, and O. Y. Alothman, "A review on Phenolic resin and its Composites," *Curr. Anal. Chem.*, vol. 14, pp. 1–13, 2018.

[25] J. C. Munoz, H. Ku, F. Cardona, and D. Rogers, "Effects of catalysts and post-curing conditions in the polymer network of epoxy and phenolic resins: Preliminary results," *J. Mater. Process. Technol.*, vol. 202, no. 1–3, pp. 486–492, 2008.

[26] H. S. L. Ku, F. Cardona, M. Trada, and G. Vigier, "Flexural properties of sawdust reinforced phenolic composites: Pilot study," *J. Appl. Polym. Sci.*, vol. 114, no. 3, pp. 1927–1934, 2009.

[27] C. Kaynak and C. C. Tasan, "Effects of production parameters on the structure of resol type phenolic resin/layered silicate nanocomposites," *Eur. Polym. J.*, vol. 42, no. 8, pp. 1908–1921, 2006.

[28] S. F. Hamad *et al.*, "Optimizing size and distribution of voids in phenolic resins

through the choice of catalyst types," *J. Appl. Polym. Sci.*, vol. 48249, pp. 1–10, 2019.

[29] I. M. Low, J. Somers, H. S. Kho, I. J. Davies, and B. A. Latella, "Fabrication and properties of recycled cellulose fibre-reinforced epoxy composites," *Compos. Interfaces*, vol. 16, no. 7–9, pp. 659–669, 2009.

[30] T. C. Fong, N. Saba, C. K. Liew, R. De Silva, M. E. Hoque, and K. L. Goh, "Yarn Flax Fibres for Polymer-Coated Sutures and Hand Layup Polymer Composite Laminates," in *Manufacturing of natural fibre reinforced polymer composites*, M. S. Salit, M. Jawaid, N. Bin Yusoff, and M. E. Hoque, Eds. Cham: Springer International Publishing, 2015, pp. 155–175.

[31] M. J. Carling, "Fracture Mechanics of Short Fibre Composites," Imperial College of Science and Technology, 1988.

[32] M. M. Morshed, M. M. Alam, and S. M. Daniels, "Plasma treatment of natural jute fibre by RIE 80 plus plasma tool," *Plasma Sci. Technol.*, vol. 12, no. 3, pp. 325–329, 2010.

[33] E. Sinha, "Effect of cold plasma treatment on macromolecular structure, thermal and mechanical behavior of jute fiber," *J. Ind. Text.*, vol. 38, no. 4, pp. 317–339, 2009.

[34] R. M. Sullivan, E. Stokes, and E. H. Baker, "Effect of Water on the Thermo-Mechanical Behavior of Carbon Cloth Phenolic," *NASA/TM*, pp. 1–13, 2011.

[35] R. Roy, B. K. Sarkar, and N. R. Bose, "Effects of moisture on the mechanical properties of glass fibre reinforced vinylester resin composites," *Bull. Mater. Sci.*, vol. 24, no. 1, pp. 87–94, 2001.

[36] A. Khadimallah, M. W. Bird, and K. W. White, "Prediction of tensile power law creep constants from compression and bend data for ZrB 2 –20 vol% SiC composites at 1800 °C," *J. Adv. Ceram.*, vol. 6, no. 4, pp. 304–311, 2017.

[37] H. Y. Choi and J. S. Lee, "Effects of surface treatment of ramie fibers in a ramie/poly(lactic acid) composite," *Fibers Polym.*, vol. 13, no. 2, pp. 217–223, 2012.

[38] E. Rojo, M. Oliet, M. V. Alonso, B. Saz-Orozco, and F. Rodriguez, "Mechanical and Interfacial Properties of Phenolic Composites Reinforced With Treated Cellulose Fibers," *Polym. Eng. Sci.*, pp. 2228–2238, 2014.

[39] Y. Zhou, M. Fan, and L. Chen, “Interface and bonding mechanisms of plant fibre composites: An overview,” *Compos. Part B Eng.*, vol. 101, pp. 31–45, 2016.

[40] M. A. Sawpan, K. L. Pickering, and A. Fernyhough, “Flexural properties of hemp fibre reinforced polylactide and unsaturated polyester composites,” *Compos. Part A Appl. Sci. Manuf.*, vol. 43, no. 3, pp. 519–526, 2012.

Chapter 8: Conclusions and future work

Section 8.1: Conclusions

In this thesis, short-plant-fibres reinforced polymer composites were fabricated. For this purpose, the microstructure of flax, jute, sisal, and ramie plant fibres was observed using LV-SEM. Ramie fibres among these fibres are characterised by the high crystallinity and commercial availability, therefore, it has been chosen to be used as a reinforcement for the composite in this project. The surface characteristics of ramie fibres were modified by low pressure plasma treatment in order to improve the fibre surface adhesion properties. In terms of polymer matrix, resole type phenolic resin was used. The conclusions that can be derived from all the above are as following:

1- The mechanical properties of the plant fibres are highly influenced by their microstructural properties and thus variations in the properties are mostly due to the structural variations. Further variations might be due to errors arising from testing techniques such as the method of cross-sectional area measurements. This can be minimized by measuring the true cross-sectional area using the LV-SEM images of the tensile fractured surfaces.

2- Low pressure plasma treatment was successfully used to create nanoscale surface structures for ramie fibres. These nanostructures were identified to be crystalline cellulose microfibrils (10-40 nm in diameter). The optimum time to expose these microfibrils without affecting the fibre strength and modulus was found to be 2 min of plasma treatment. The exposing of these microfibrils resulted in a nanoscale surface roughness which increases the surface area and led to better surface wettability with phenolic resin.

3- The mechanical properties of the resole type phenolic resin can be compromised by voids. However, the conventional approach is to minimize or to avoid the void

content in the resin but the LV-SEM combined with the finite element modelling in this study show that the size and spatial distribution of the voids in the cured resin are of great importance in determining the mechanical properties of the phenolic resin. It has been found that for the similar void content, achieving a homogenous void size and distribution is critical.

4- Finally, short-ramie-fibres reinforced phenolic resin composites were successfully fabricated using a method which was based on making mats of short fibres. A good degree of dispersion and uniform distribution of the short fibres in the resin was achieved. In terms of the mechanical properties, the flexural Young's modulus has clearly increased for both composites (acid cured and thermal cured) with the addition of plasma treated fibre. In the case of flexural strength, the thermal cured samples maintain the flexural strength with the addition of plasma treated fibres whereas acid cured samples show reduced strength due to the formation of voids along the fibre-matrix interface. Therefore, it can be concluded that the plasma treatment is more beneficial when thermal curing is used.

Section 8.2: Future work

In this study, the effects of the low pressure plasma treatments on the surface morphology of ramie fibres and their influence on the structural and mechanical properties of the short-ramie-fibres-phenolic resin composites was investigated and discussed. However, some further work is required and as follows:

1- In this research, low pressure plasma treatment has been used to modify the surface characteristics of ramie fibres, however, the atmospheric plasma treatment could also be considered.

2- The 2 min of plasma treatment was the optimum time for exposing the cellulose microfibrils without affecting the fibre mechanical properties, however, this might

not be the optimum time for a good fibre-matrix interface. Therefore, different plasma durations should be considered in order to optimise the fibre-matrix interface.

3- This project has only focused on using short ramie fibres as a reinforcement, therefore, it is suggested studying the effects of fibre length on the properties of ramie fibre-phenolic resin composites.

4- Mats of plasma treated short-ramie-fibres were successfully prepared, therefore, it is highly recommended to apply the same method on different plant fibres such as jute, hemp, flax, and nettle.

5- In this study, the size and distribution of the voids in the cured phenolic resins were optimised through the choice of catalyst type and it has been shown that the size and spatial distribution of the voids are of great importance in determining the final mechanical properties of the cured resin. A study how this translates to phenolic foams could be carried out.

6- This study aimed to synthesis environmentally friendly composites reinforced by natural plant fibres, however, the use of phenolic resins as a polymer matrix resulted in a not fully green composites. Therefore, it is highly recommended to replace the phenol by a biobased materials.

7- Finally, the structural and mechanical properties of the short-ramie-fibre-phenolic resin composites were investigated in this study. However, investigating other properties such as thermal properties are also recommended.